CHALMERS
UNIVERSITY OF TECHNOLOGY

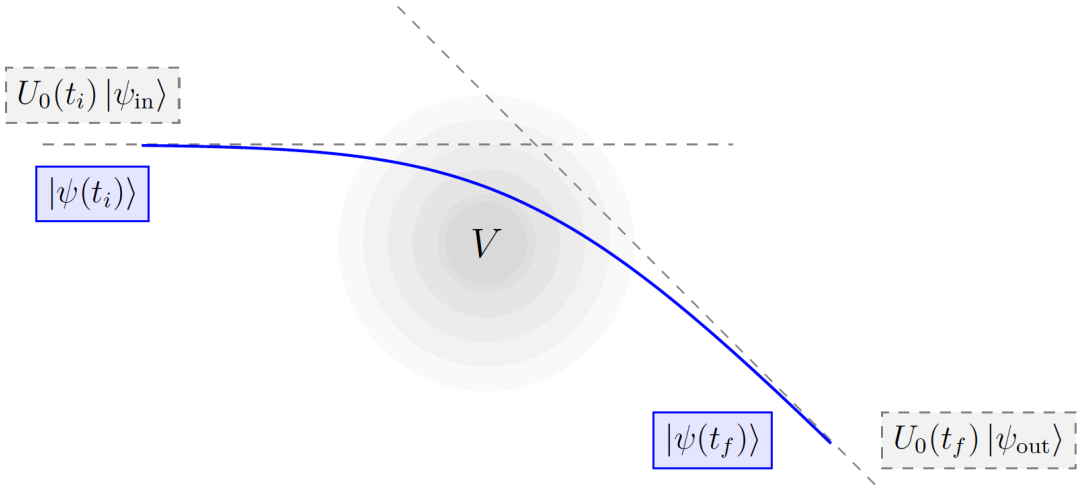

Renormalization of Chiral Effective Field Theory in the Nucleon-Nucleon Sector

Bayesian Inference of Low-Energy Constants in Modified Weinberg Power Counting

Master's thesis in Physics

OLIVER THIM

DEPARTMENT OF PHYSICS
CHALMERS UNIVERSITY OF TECHNOLOGY
Gothenburg, Sweden 2021
www.chalmers.se

Master's thesis 2021

Renormalization of Chiral Effective Field Theory in the Nucleon-Nucleon Sector

Bayesian Inference of Low-Energy Constants in Modified Weinberg Power Counting

Oliver Thim

CHALMERS
UNIVERSITY OF TECHNOLOGY

Department of Physics
Division of Subatomic, High Energy and Plasma Physics
Theoretical Subatomic Physics
Chalmers University of Technology
Gothenburg, Sweden 2021

Renormalization of Chiral Effective Field Theory in the Nucleon-Nucleon Sector
Bayesian Inference of Low-Energy Constants in Modified Weinberg Power Counting
Oliver Thim

© Oliver Thim, 2021.

Supervisor: Christian Forssén, Department of Physics
Examiner: Christian Forssén, Department of Physics

Master's Thesis 2021
Department of Physics
Division of Subatomic, High Energy and Plasma Physics
Theoretical Subatomic Physics
Chalmers University of Technology
SE-412 96 Gothenburg
Telephone: +46 31 772 1000

Cover: An illustration of quantum-mechanical scattering and asymptotically free states. The quantum state $|\psi(t)\rangle$ (blue solid line) of the system approaches asymptotic quantum states, $U_0(t_i)\,|\psi_{\text{in}}\rangle$ and $U_0(t_f)\,|\psi_{\text{out}}\rangle$ (grey dashed lines) for early- and late times t_i, t_f. For times where $|\psi(t)\rangle$ is far away from the range of the potential the evolution resemble the evolution of the free Hamiltonian. For more information, see Fig. 4.1 in Chapter 4.

Typeset in LaTeX
Printed by Chalmers Reproservice
Gothenburg, Sweden 2021

Renormalization of Chiral Effective Field Theory in the Nucleon-Nucleon Sector
Bayesian Inference of Low-Energy Constants in Modified Weinberg Power Counting
Oliver Thim
Department of Physics
Chalmers University of Technology

Abstract

The calculation of nuclear properties from QCD, the underlying theory of the strong nuclear force, is still an open problem in physics. Effective field theories provide a possible solution by describing nuclei in terms of effective degrees of freedom; neutrons, protons, and pions. The effective description comes at a cost, namely undetermined parameters known as low-energy constants (LECs), that need to be fixed by experimental data. Furthermore, while renormalization-group (RG) invariance of predictions is a field-theoretic requirement, it is known that interaction potentials constructed with Weinberg power counting (WPC) are not RG invariant at leading order.

The purpose of this thesis is to study a leading order *modified* Weinberg power counting potential, with additional counter terms and their associated LECs promoted to leading order. We show that the modified potential gives RG invariant predictions of nucleon-nucleon scattering phase shifts in partial waves that are otherwise problematic in WPC. Moreover, Bayesian inference is used to determine LECs from measured total scattering cross sections, which allows to account for both experimental and model uncertainties. RG-invariant predictions of scattering cross sections are demonstrated using the obtained posterior distributions of LECs. In conclusion, we find that the modified potential performs better, producing RG-invariant results for phase shifts and cross sections. We also show that total scattering cross sections do not impose very hard constraints on all LECs which calls for the inclusion of more experimental data in the inference.

Keywords: nuclear physics, χEFT, renormalization, neutron-proton scattering, Bayesian inference, LECs, power counting, modified Weinberg power counting

Acknowledgements

First and foremost I want to thank my supervisor Prof. Christian Forssén for all the guidance and help which made this project possible to complete. Furthermore, I want to thank all the members of the Theoretical Subatomic Physics group, and in particular Prof. Andreas Ekström, Sean Miller, Dr. Chieh-Jen Yang and Isak Svensson for many helpful discussions. Last, I want to thank Alma for always being there for me in moments when I need it.

Oliver Thim, Gothenburg, June 2021

Table of Contents

1

Introduction

The goal of physics, and science in general, is to combine experimental observations and theoretical models to increase the understanding of the world and phenomena around us. Nuclear physics is a sub-field that studies properties of atomic nuclei, such as their binding energies, how their constituents interact via the nuclear forces, and their properties as quantum-mechanical many-body systems. Having a good understanding of atomic nuclei is not only of academic interest that, for example, could help explore questions in the fields of particle physics, astrophysics, and cosmology. It is also important for various practical applications such as nuclear reactors, medical physics, and materials science.

Finding an accurate description of the strong nuclear force has been a challenge in physics since the first description by Yukawa [1], and is one of the long-standing unsolved problems in theoretical physics. Since Yukawa's model in the '30s—describing the nuclear fore as arising from the exchange of a massive boson—there has been an enormous theoretical development, alongside experimental advancements [2]. Over the years, many accurate phenomenological models have been developed, see e.g. Ref. [3].

During the later half of the 20th century, the theory of quantum fields—Quantum Field Theory (QFT)—was used to develop models of fundamental particle interactions with enormous success. This led to what is now called the standard model (SM) of particle physics, which describes all observed forces in nature (except gravity) with unprecedented success. The part of the standard model describing the strong force, involving quarks and gluons, is Quantum Chromodynamics (QCD) which was formulated in the '80s [4]. Since QCD is believed to be the underlying theory governing the behavior of nuclear physics, it has been a long-standing goal to compute nuclear properties from this underlying fundamental theory.

Unfortunately it turns out that it is hard to describe nuclear properties using QCD. The coupling constant becomes very large at nuclear energy scales $\sim$ MeV, which means that perturbative calculations are not applicable. Lattice QCD is an approach to deal with this problem by doing the non-perturbative calculations numerically by brute force on a discretized space-time lattice. However, the successes so far for predicting nuclear properties and forces are limited [5]. In the '90s Weinberg in-

troduced, and pioneered, the approach of using effective field theories (EFT) to describe the low-energy effective behavior of QCD, applicable at energy scales relevant to nuclear physics, see Refs [6]–[8]. The key to formulating a theory that can hope to be perturbative is to use other degrees of freedom, namely nucleons and mesons—which appear as relevant bound states at nuclear energy scales. However, the effective description comes at a cost, namely undetermined parameters known as low-energy constants (LECs), that need to be fixed by experimental data.

An EFT has a connection to the underlying theory (in this case QCD) via symmetries and broken symmetries—which constrain the allowed interactions. Such connections are not present in phenomenological models. Since the relevant symmetry is the *chiral* symmetry of low-energy (massless) QCD, the effective field theory is called chiral EFT (χEFT). This theory is perturbative in the nuclear energy regime, and the infinite number of interaction terms allowed by the symmetries can be ordered by importance via a so-called *power counting*. Effectively this yields a finite number of relevant interaction terms at a given order in the power counting. Weinberg introduced a power counting which is referred to as Weinberg power counting (WPC) [6], which is widely used.

In χEFT, a phenomena called *infrared enhancement* arises due to a large nucleon mass. This requires a non-perturbative resummation of certain irreducible Feynman diagrams, containing nucleon-nucleon intermediate states, to obtain nuclear scattering amplitudes. However, the resummation causes some problems. The counterterms present at a given order in the power counting are not necessarily enough to properly renormalize the resummed amplitude, which can lead to results that are not invariant under the renormalization group (RG) flow. This is indeed found to be the case; see Ref. [9]. To fix the problem of non-RG-invariant amplitudes, Nogga et al. [9] proposed to promote certain counterterms—appearing at higher-order in WPC—to lower orders, with the hope of getting RG invariant results. This power counting is sometimes referred to as modified WPC (MWPC). MWPC has been studied, e.g., in Refs. [9], [10], where the focus has been on inferring LECs from scattering phase shifts. What has not been done is to use Bayesian inference to determine LECs with proper uncertainty quantification in MWPC.

This thesis will study leading order χEFT in Weinberg- and modified Weinberg power counting—in particular the RG behavior and the inference of LECs. The purpose of the thesis is to study the following questions:

1. How is a leading order χEFT Lagrangian constructed from QCD?

2. How do leading order MWPC nucleon-nucleon potentials perform at predicting RG-invariant phase shifts for neutron-proton (np) scattering, compared to leading order WPC?

3. How well can the LECs of a MWPC nucleon-nucleon potential be determined using Bayesian inference from total np scattering cross sections? To which

degree do the inferred LECs produce RG invariant predictions of np cross sections?

The target audience for this thesis is second-year master's students in physics with a theoretical orientation. The text assumes; familiarity with the basics of QFT, a good understanding of quantum mechanics as well as a basic knowledge of nuclear and particle physics.

The thesis is organized in two main parts as follows. In Part I, relevant theory is presented and question (1) is addressed. Relevant concepts of QFT are introduced in Chapter 2, followed by χEFT in Chapter 3 and quantum-mechanical scattering theory in Chapter 4. Part II of the thesis describes the methods and results regarding questions (2) and (3). In Chapter 5 np scattering phase shifts in WPC and MWPC are studied, and a Bayesian inference of LECs in MWPC is performed in Chapter 6. Results are summarized and conclusions are made in Chapter 7. For reference, some commonly used abbreviations are summarized in Table 1.1. Natural units ($c = \hbar = 1$) are used throughout the thesis while other conventions are summarized in Appendix A.

Table 1.1: Frequently used abbreviations.

Abbreviation	Meaning
χEFT	Chiral Effective Field Theory
χPT	Chiral Perturbation Theory
cm	center-of-mass
DoB	degree-of-belief
EFT	Effective Field Theory
LO	leading order
LS	Lippman Schwinger
MCMC	Markov Chain Monte Carlo
MWPC	modified Weinberg power counting
np	neutron-proton
NN	nucleon-nucleon
pdf	probability density function
QFT	Quantum Field Theory
QCD	Quantum Chromodynamics
rel	relative
RG	Renormalization group
SSB	Spontaneous Symmetry Breaking
WPC	Weinberg power counting

Part I

Theory

2

Quantum Field Theory

Quantum Field Theory (QFT) is the framework in which the standard model of particle physics is formulated, and is a product of combining quantum mechanics and special relativity. The part of the standard model describing the strong nuclear force is Quantum Chromodynamics (QCD), and is the main part of interest for nuclear physicists as well as this thesis. As stated before, the reader is assumed to have some knowledge of QFT, corresponding to an introductory course. This mainly includes treating canonical quantization of the scalar field and the Dirac field, as well as how to compute matrix elements of an interacting theory using Feynman diagrams. These parts roughly corresponds to Chapters 1-4 and parts of Chapter 5 in Ref. [11].

This chapter starts with an introduction to QCD starting from the well-known theory of Quantum Electrodynamics (QED). Furthermore, some important QFT concepts are introduced to give a solid ground to understand *effective field theories*, that is the subject of Chapter 3. These concepts are: *the path integral formulation*, *renormalization* and *spontaneous symmetry breaking*. For a more thorough introduction the reader can consult any introductory QFT textbook. The material in this chapter in mainly built on Ref. [11].

2.1 Gauge Theories and QED

Before diving into QCD, it is worth taking a step back and looking into the more familiar theory of QED describing the interactions between leptons and photons. The QED Lagrangian reads,

$$\mathcal{L}_{\text{QED}} = \sum_{f=e,\mu,\tau} \bar{\psi}_f \left(i\gamma^\mu \partial_\mu - m_f \right) \psi_f - \frac{1}{4} F_{\mu\nu} F^{\mu\nu} - e\bar{\psi}_f \gamma^\mu \psi_f A_\mu, \tag{2.1}$$

where the sum is over the lepton flavors e, μ and τ with corresponding mass denoted by m_f. The lepton Dirac fields are denoted by ψ_f, the photon field by A_μ and e is the electromagnetic coupling. $F_{\mu\nu}$ is the field strength tensor defined by [11]

$$F_{\mu\nu} \equiv \partial_\mu A_\nu - \partial_\nu A_\mu. \tag{2.2}$$

The *gamma matrices*, γ^μ, satisfy the Clifford algebra $\{\gamma^\mu, \gamma^\nu\} = 2g^{\mu\nu}\mathrm{id}$, where id is the identity in Dirac spinor space[1].

At first glance this Lagrangian may seem rather arbitrary. Two interesting questions that can arise are why the interaction term,

$$\mathcal{L}_{\text{int}} = -e\bar{\psi}_f \gamma^\mu \psi_f A_\mu, \tag{2.3}$$

has this particular form, and if there can be higher order interaction terms. These questions are very interesting and fortunately have rather good answers. In fact, both these questions are key in understanding the general structure of so called *gauge theories* and will be answered during this chapter.

There are some postulates that govern the procedure for how relativistic QFT Lagrangians are constructed, which heavily constrain possible terms. The validity of this procedure is of course nothing one can prove, but rests on the empirical facts that these theories turn out to work *really* well describing observed phenomena in nature [12]. Apart from the rather obvious postulate that Lagrangians should be Lorentz scalars, that is, invariant under Lorentz transformations, a concept called *gauge invariance* has proven very helpful. A theory with gauge invariance is called a *gauge theory* and has the additional postulate that the Lagrangian should be gauge invariant.

Gauge invariance is similar to Lorentz invariance. In the same way that all constituents, parameters and fields, have a particular transformation properties under the Lorentz group, for example

$$m_f \mapsto m_f' = m_f, \text{ (Lorentz scalar) } A_\mu \mapsto A_\mu' = \Lambda_\mu{}^\nu A_\nu, \text{ (Lorentz vector)}, \tag{2.4}$$

the matter fields get a postulated transformation property under a *gauge group*, G; $\psi_f \overset{G}{\mapsto} \psi_f'$. The principle of gauge invariance then requires the Lagrangian to be invariant under a gauge transformation. More specifically, the equations of motion need to be invariant, so the Lagrangian is allowed to change up to a total derivative $\mathcal{L} \overset{G}{\mapsto} \mathcal{L} + \partial_\mu K^\mu$.

The special thing about the gauge transformations is that they are *local*, that is, the group elements depends on the spacetime coordinate, x^μ. As an example, take QED with only one flavor of leptons, e.g. electrons ψ_e, where the e subscript is dropped from now on. For QED the gauge group is $G = U(1)$ and the local gauge transformation of the matter field, ψ, is given by

$$\psi(x) \overset{G}{\mapsto} \psi'(x) = e^{i\alpha(x)}\psi(x), \tag{2.5}$$

where $\alpha(x)$ is a real, spacetime-dependent phase. The QED Lagrangian is invariant under the transformation in Eq. (2.5) provided that A_μ transforms as

$$A_\mu \overset{G}{\mapsto} A_\mu' = A_\mu - \frac{1}{e}\partial_\mu \alpha(x), \tag{2.6}$$

[1]For some more information about the gamma matrices see Appendix A

which is the familiar gauge invariance of the electromagnetic vector potential.

One can invent a procedure that can be used to derive the QED Lagrangian starting from the free Lagrangian for the electron field ψ,

$$\mathcal{L}_{\text{free}} = \bar{\psi}\left(i\gamma^{\mu}\partial_{\mu} - m\right)\psi. \tag{2.7}$$

The reason why such a procedure is useful is because it can give guidance about how to construct more general gauge theories. By staring with the free Lagrangian in Eq. (2.7) and postulating $G = U(1)$ gauge invariance (see. Eq. (2.5)) one can *derive* the existence of a vector field A_{μ} that transforms according to Eq. (2.6) and gives rise to the interaction term in Eq. (2.3). The term $-\frac{1}{4}F_{\mu\nu}F^{\mu\nu}$ is constructed as the *simplest* Lorentz- and gauge invariant term involving A_{μ}.

In summary, start with a free Lagrangian of the matter fields and postulate a transformation under some gauge group, G. This gives interactions between the matter fields and, possibly multiple, vector fields. Finally, construct the simplest free Lagrangian involving only the vector fields that emerged in the former step.

QED is sometimes called an *abelian* gauge theory, since the gauge group $U(1)$ is an abelian group and hence a gauge theory based on a non-abelian group is called a non-abelian gauge theory. For more details the reader is referred to Chapter 15 in Ref. [11].

2.2 QCD—the Gauge Theory of Strong Interactions

Having studied QED in the last section the attention is now turned to QCD, the theory of strong interactions. Using the procedure outlined in the last paragraphs in the previous section about the construction of a general gauge theory, QCD can be understood as a direct generalization of QED. Of course, this recipe-like construction of theories is not in any way how the theories were first discovered[2], but serves a purpose for understanding the characteristics of the theories. The other purpose of presenting the general ideas of the construction of QCD is that the same principles will be used when constructing a low-energy effective field theory of nucleons and pions in Chapter 3.

The first step is to specify the matter fields and a gauge group. The matter content of QCD is spin $\frac{1}{2}$ quarks which are described by Dirac spinors. The gauge group for the quarks is $SU(3)_c$, where the subscript c stands for *color*, which is the name for the gauge degrees of freedom in QCD. The action of the gauge group transforms the fields, which is achieved by letting the fields transform in some representation of the gauge group. The choice is to have the fields transforming in the *fundamental representation* of $SU(3)_c$ [11]. The fundamental representation[3] is the representation

[2]For a historical overview of QCD see Ref. [4].
[3]Also called *defining representation*

that defines the group. $SU(3)$ is, as familiar, the group of unitary 3×3 matrices that have determinant $+1$. Hence, these matrices act on a complex three dimensional vector space $\mathbb{W}$ called *color space*.

Let $\mathbb{D}$ denote the space of Dirac fermion fields. The quark fields for each flavor $f \in \{u, d, c, s, t, b\}$ is formally an element of the tensor product of $\mathbb{D}$ and $\mathbb{W}$; $\psi_f \in \mathbb{D}\otimes\mathbb{W}$. A conventional and convenient way to represent ψ_f is as a vector in color space, $\mathbb{W}$,

$$\psi_f = \begin{pmatrix} \psi_{f,r} \\ \psi_{f,g} \\ \psi_{f,b} \end{pmatrix}, \ \psi_{f,i} \in \mathbb{D}, \ i = r, g, b. \tag{2.8}$$

This is of course equivalent to choosing a basis in $\mathbb{W}$. The color names, red (r), green (g) and blue (b) are purely conventional [11]. An important note is that the gauge degrees of freedom of ψ in $\mathbb{W}$ are not physical degrees of freedom, but can be seen as auxiliary degrees of freedom introduced by the gauge-theory scheme. It is the color components that the gauge group acts on, and this is conveniently described in the index notation introduced in Eq. (2.8).

A group element in the fundamental representation of $SU(3)$, which is allowed to depend on x^μ, is denoted $w(x) : \mathbb{W} \to \mathbb{W}$. By using the generators of the *Lie algrbra* T^a, $a = 1, ..., 8$ in the fundamental representation, called the *Gell-Mann matrices*, $w(x)$ can be written as

$$w(x) = \exp\left[i\alpha^a(x)T^a\right]. \tag{2.9}$$

$\alpha^a(x)$ are real parameters that depend on x^μ [11]. The gauge transformation can be written in terms of color indices as

$$\psi_i(x) \mapsto \psi_i'(x) = w_{ij}(x)\psi_j(x) = \exp\left[i\alpha^a(x)T^a_{ij}\right]\psi_j(x), \tag{2.10}$$

where $i, j \in \{r, g, b\}$ and the flavor index f on ψ is suppressed.

The fact that the group elements $w_{ij}(x)$ can depend on x^μ, is the source of needing to introduce interactions of the fields ψ_i with vector fields A^a_μ, $a = 1, \ldots, 8$ to make sure derivatives of ψ_i have well-defined gauge-transformation properties. A *covariant derivative* D_μ, that makes $D_\mu\psi_i$ transform as ψ_i under gauge transformations, needs to be constructed. By introducing a so called compensator field $U_{ij}(x, y)$ that transforms as

$$U(x, y) \mapsto w(x)U(x, y)w^\dagger(y), \tag{2.11}$$

the derivative D_μ can be defined as

$$D_\mu\psi_i(x) \equiv \lim_{\epsilon^\mu\to0} \frac{\psi_i(x+\epsilon) - U(x+\epsilon, x)\psi_i(x)}{\epsilon^\mu}. \tag{2.12}$$

By Taylor expanding U, with the first order expansion coefficients, A^a_μ, it can be shown that the covariant derivative takes the form

$$D_\mu = \partial_\mu - igA^a_\mu T^a, \tag{2.13}$$

where g is the *strong coupling constant* and T^a are the Gell-Mann matrices [11]. It can also be shown that the covariant derivative of ψ transforms as

$$D_\mu \psi_i(x) \mapsto \exp\left[i\alpha^a(x) T^a_{ij}\right] D_\mu \psi_j(x). \tag{2.14}$$

Starting from the free Lagrangian for the quarks,

$$\mathcal{L}_{\text{free}} = \sum_f \bar{\psi}_f \left(i\gamma^\mu \partial_\mu - m_f\right) \psi_f, \tag{2.15}$$

it is seen that gauge invariance is spoiled since $\partial_\mu \psi_f$ do not transform in the correct way. To fix it, let $\partial_\mu \to D_\mu$, which introduces an interaction term similar to the one in QED by expanding Eq. (2.13). In analogy with QED one can define a field strength tensor for the vector fields A^a_μ introduced by the covariant derivative as

$$F^a_{\mu\nu} \equiv \partial_\mu A^a_\nu - \partial_\nu A^a_\mu + g f^{abc} A^b_\mu A^c_\nu, \tag{2.16}$$

where f^{abc} are the *structure constants* of the Lie algebra of $SU(3)$ appearing in the commutation relations of the generators [11]

$$[T^a, T^b] = i f^{abc} T^c. \tag{2.17}$$

The simplest possible Lorentz- and gauge invariant term that can be built from $F^a_{\mu\nu}$ is $-\frac{1}{4} F^a_{\mu\nu} F^{\mu\nu}_a$ which is added to get the full QCD Lagrangian

$$\mathcal{L}_{\text{QCD}} = \sum_f \bar{\psi}_f (i \not{D} - m_f) \psi_f - \frac{1}{4} F^a_{\mu\nu} F^{\mu\nu}_a. \tag{2.18}$$

It is actually possible to construct an infinite number of Lorentz- and gauge invariant terms involving more fields, for example:

$$(\bar{\psi}_f \psi_f)^2, \tag{2.19}$$
$$(F^a_{\mu\nu} F^{\mu\nu}_a)^2, \tag{2.20}$$
$$(\bar{\psi}_f \not{D} \psi_f)^2, \tag{2.21}$$

and so on. The requirement that the theory should be *renormalizable*, which implies that the operators in each term must have mass dimension ≤ 4, excludes these terms. The *mass dimensions* of the fields ψ_f and A^a_μ are calculated using that the action, S, is dimensionless in natural units $\hbar = c = 1$. Since

$$S = \int d^4x \; \mathcal{L}, \quad [S] = \mathrm{M}^0, \tag{2.22}$$

and dimension of length is the inverse dimension of mass giving $[d^4x] = \mathrm{M}^{-4}$, the mass dimension the Lagrangian is $[\mathcal{L}] = \mathrm{M}^4$. Examining the kinetic terms for ψ_f and A^a_μ gives the mass dimensions $[\psi_f] = \mathrm{M}^{3/2}$ and $[A^a_\mu] = \mathrm{M}$. By constructing all possible Lorentz- and gauge invariant combinations of the fields ψ_f and A^a_μ it can be shown that the terms appearing in $\mathcal{L}_{\text{QCD}}$ are the only ones with mass dimension ≤ 4 [11]. The issue of renormalization will be discussed more in Section 2.4, and is an important aspect in QFT.

2.3 The Path Integral Formulation

A very powerful tool in quantum mechanics, and QFT in particular, is the so called path integral formulation first proposed by Feynman in 1948 [13]. In this approach to quantum mechanics, as opposed to canonical quantization, one starts with an ansatz for correlation functions, or transitions amplitudes, which is a generalization of the classical action principle. The great advantage with this approach is that one can go from a Lagrangian to correlation functions, also called Green's functions, much easier than in the framework of canonical quantization. It is also easier to analyze *symmetries*, *renormalization* and *effective field theories* in this formulation, which will be discussed later in the thesis. The material in this section will mostly follow Ref. [11].

2.3.1 Derivation and the Generating Functional

In quantum mechanics the unitary *time evolution operator* in position space is defined by

$$U(x_a, x_b; T) \equiv \langle x_b | e^{-iHT} | x_a \rangle \,, \tag{2.23}$$

which satisfies the *Schrödinger equation*

$$i\frac{\partial}{\partial T} U(x_a, x_b; T) = H U(x_a, x_b; T). \tag{2.24}$$

The time evolution operator measures the probability amplitude of the initial state $|x_a\rangle$ to evolve into $|x_b\rangle$ in time T for a system with Hamiltonian H. Motivated by the superposition principle and the double slit experiment, an ansatz for U was proposed [13], that includes summing over possible classical paths the system can move from state $|x_a\rangle$ to $|x_b\rangle$. This sum is formally a *functional integral* and reads

$$U(x_a, x_b; T) \equiv \int \mathcal{D}x(t)\ e^{iS[x(t)]}, \tag{2.25}$$

where $S[x(t)]$ is the classical action corresponding to the Hamiltonian H. $\mathcal{D}x(t)$ is the so-called *functional measure* which represents that the functional $e^{iS[x(t)]}$ is integrated over all possible paths $x(t)$ from x_a to x_b. The functional measure can be defined by discretizing the integral in time-steps $0 = t_0 < t_1 < ... < t_n = T$. By letting $\Delta t \equiv t_{i+1} - t_i$ go to zero, one can show that this ansatz for U indeed satisfies the Schrödinger equation. For details see Chapter 9 in Ref. [11].

The path integral formulation can be generalized from quantum mechanics to QFT, where one instead considers the evolution of a given *field configuration* $\phi_a(x)$ to another, $\phi_b(x)$, by the Hamiltonian of the field theory. A scalar field, $\phi(x)$, is used here to illustrate the procedure, and the generalization is straight forward to spinor fields and vector fields [11]. The generalization of Eq. (2.25) to QFT reads

$$\langle \phi_b(x^0 = T, \boldsymbol{x}) | e^{-iHT} | \phi_a(x^0 = 0, \boldsymbol{x}) \rangle = \int \mathcal{D}\phi\ \exp\left(i \int_0^T d^4x\ \mathcal{L} \right) \tag{2.26}$$

where the functional integration is over field configurations $\mathcal{D}\phi$.

The main goal of QFT is however to compute scattering amplitudes, and for that purpose the correlator in Eq. (2.26) is not that helpful. The important correlation functions to compute are of the form

$$\langle \Omega | \mathcal{T}\{\phi(x)\phi(y)\} | \Omega \rangle \,, \tag{2.27}$$

where $\mathcal{T}$ is the time-ordering operator, and $|\Omega\rangle$ is the vacuum of the full interacting theory. Correlation functions, also called *Green's functions*, can be generalized to arbitrary many fields,

$$G^{(n)}(x_1, ..., x_n) \equiv \langle \Omega | \mathcal{T}\{\phi(x_1) \dots \phi(x_n)\} | \Omega \rangle \,. \tag{2.28}$$

One can show that these Green's functions can be related to the definition in Eq. (2.26) and they can be expressed in terms of path integrals as [11]

$$G^{(n)}(x_1, ..., x_n) = \lim_{T \to \infty(1-i\epsilon)} \frac{\int \mathcal{D}\phi \ \phi(x_1) \dots \phi(x_n) \exp\left(i \int_{-T}^{T} d^4x \ \mathcal{L}\right)}{\int \mathcal{D}\phi \ \exp\left(i \int_{-T}^{T} d^4x \ \mathcal{L}\right)} \tag{2.29}$$

where the $-i\epsilon$ has the same role as in Feynman propagators. The T limit is usually omitted.

A useful object called *generating functional* is defined as

$$Z[J] \equiv \int \mathcal{D}\phi \ \exp\left[i \int d^4x [\mathcal{L}(\phi) + J(x)\phi(x)]\right], \tag{2.30}$$

which is a functional of $J(x)$ and $J(x)\phi(x)$ is called a *source term*. Using *functional derivatives*[4], $\frac{\delta}{\delta J(x)}$, and Eq. (2.29) one can show that the n-point Green's functions can be obtained from the generating functional as

$$G^{(n)}(x_1, ..., x_n) = Z[J]^{-1} \left(-i\frac{\delta}{\delta J(x_1)}\right) \dots \left(-i\frac{\delta}{\delta J(x_n)}\right) Z[J]\Big|_{J=0}. \tag{2.31}$$

This relation shows the power of the path integral formalism in its full glory. It is a direct connection between the Lagrangian of the theory, $\mathcal{L}(\phi)$, and the time ordered correlation functions $G^{(n)}$, which relates to observables. The generating functional is an object that, in analogy with the partition function in statistical mechanics, encodes *all* information of the theory in the sense that all possible correlation functions can be computed from it. This formalism will now be used to discuss the role of *symmetries* in the theory and how symmetries of the Lagrangian will affect symmetries of Green's functions $G^{(n)}$.

2.3.2 Symmetries in the Path Integral Formulation

In the path integral formulation the Green's functions, $G^{(n)}$, are encoded in the generating functional $Z[J]$, see Eq. (2.31). This makes it manifest that field transformations $\phi \mapsto \phi'$ leaving $\mathcal{L}$ invariant, i.e. $\mathcal{L}(\phi) = \mathcal{L}(\phi')$, will be a symmetry of

[4]See eg. [11]

the generating functional, and hence produce the same Green's functions $G^{(n)}$ and quantum dynamics[5].

Recall that in the classical theory a *symmetry* is a field transformation $\phi(x) \mapsto \phi'(x)$ that leaves the equations of motion in variant, which is equivalent to the Lagrangian being invariant up to a total divergence term

$$\mathcal{L}(\phi) \mapsto \mathcal{L}(\phi') + \partial_\mu K^\mu. \tag{2.32}$$

An equivalent formulation is that the action is invariant $S[\phi] = S[\phi']$, since a total divergence term vanish if the fields are assumed to decay rapidly towards infinity. *Noether's theorem* states that to every such symmetry there exists a conserved current $j^\mu(x)$ satisfying $\partial_\mu j^\mu = 0$. A crucial step in deriving this conservation law is to use the *Euler-Lagrange equations* derived from the Lagrangian. In the quantum theory the Euler-Lagrange equations can not be assumed to hold for the fields. In the path integral formulation, the quantization is achieved by integrating over *all possible* classical field configurations. It is thus clear that the classical derivation does not hold [14].

The analogue to Noether's theorem in the quantum theory can be derived using the generating functional, and in the same spirit as in the classical case subject the fields to a symmetry transformation. Exactly as in the classical case where a symmetry is a transformation that leaves the equations of motion invariant, which is equivalent to $S[\phi] = S[\phi']$, a symmetry of the quantum theory is a symmetry of the *quantum dynamics*, that is, a symmetry of the Green's functions $G^{(n)}$. From Eq. (2.31) it is manifest that a transformation that satisfies $S[\phi] = S[\phi']$ leaves the Green's functions unchanged, and is thus a symmetry of the quantum theory[6].

Assume that the infinitesimal transformation

$$\phi(x) \mapsto \phi(x) + i\alpha^a T^a \phi(x) \tag{2.33}$$

is a symmetry of the action, where α^a is infinitesimal and T^a are generators some Lie group. This is equivalent to

$$\mathcal{L}(\phi) \mapsto \mathcal{L}(\phi) + \alpha^a \partial_\mu K^{\mu,a}. \tag{2.34}$$

The trick is now to promote the parameters α^a to functions $\alpha^a(x)$. By considering a variable change in the generating functional, given by the infinitesimal symmetry transformation in Eq. (2.33) where $\alpha^a \to \alpha^a(x)$, one can derive the relation

$$\langle \partial_\mu j^\mu \rangle = 0, \tag{2.35}$$

where

$$j^\mu = \frac{\partial \mathcal{L}}{\partial(\partial_\mu \phi)} i T^a \phi - K^\mu \tag{2.36}$$

[5]There are subtleties related to so called *quantum anomalies*. The statement that the generating functional is invariant provided that the Lagrangian is invariant implicitly assumes the measure is invariant $\mathcal{D}\phi = \mathcal{D}\phi'$, which in some special cases are not true, see Chapter 19 in Ref. [11].

[6]Again, with the caveat that there is no quantum anomaly, see Chapter 19 in Ref. [11]

is the usual Noether current and $\langle\cdot\rangle$ denotes the vacuum expectation value.

One can also obtain a more general equation with insertions of a number of fields in the expectation value. These equations are called the *Schwinger-Dyson equations* and are relations among different Green's functions. The derivation and more details can be found in Chapter 9 in Ref. [11].

In summary, one can use the path integral formalism to generalize the concept of symmetries and conserved currents to the quantum formalism, where the objects of interest are the Green's functions, and not the equations of motion. Considering spacetime dependent parameters $\alpha^a(x)$ is purely a mathematical trick at this stage, but it hints about a connection with Gauge theories [11].

2.4 Renormalization in QFT

Renormalization is one of the more confusing topics in QFT, and was subject to enormous study in the context of QED in the '30s and '40s. The theory of QED took shape after the Dirac equation was introduced in 1928 [15]. It was found that divergences appear when trying to calculate certain quantities, such as the vacuum polarization, or bare charge of the electron in perturbation theory. The divergences appear since certain loop integrals diverge, which can be both due to high momentum (UV) or low momentum (IR). To be able to match theory and finite experimental results a procedure called *renormalization* was developed. For a historical overview see e.g. Ref. [16].

The idea of renormalization is to get rid of the divergences by first *Regularizing* the integrals, i.e. making them finite, at the cost of introducing some parameter, call it d. When d is taken to some limit d_0 the original theory is restored. So called *renormalized* parameters are introduced at some energy scale, μ, and related to the original *bare* parameters through a finite relation regulated by d. By doing the same procedure for a different scale μ', the renormalized parameters of the two different scales μ and μ' can be related, and *should not* depend on d if the theory is renormalizable, and hence the $d \to d_0$ limit can be taken to restore the original theory [11].

There are several different approaches to renormalization, see Ref. [16], and a more modern approach is due to Kenneth Wilson, and is reviewed in Ref. [17]. Wilson's approach is convenient since it connects very well with effective field theories.

2.4.1 Wilson's Approach to Renormalization

Wilson's approach to renormalization is based on the path integral formulation. The idea of this approach is to isolate high- and low energy degrees of freedom and absorb high-energy loop effects in renormalized parameters. This section follows Chapter 12 in Ref. [11].

To illustrate this approach, consider a scalar field theory with Lagrangian

$$\mathcal{L}_\Lambda = \frac{1}{2}(\partial_\mu\phi)^2 - \frac{1}{2}m_\Lambda^2\phi^2 - \frac{\lambda_\Lambda}{4!}\phi^4 \tag{2.37}$$

using the same notation as in Section 2.3. The Lagrangian $\mathcal{L}_\Lambda$ that define the theory is called *bare Lagrangian* and its parameters are called bare parameters.

In Wilson's approach one considers a QFT with a momentum cutoff Λ, which is considered so big that the theory cannot be resolved to this scale. It can be taken of the order of the Planck scale for example [11]. The scalar field theory is defined by the generating functional, which can be expressed in Euclidean space time after a *Wick-rotation* ($ix^0 = x_E^0$),

$$Z[J] = \int [\mathcal{D}\phi]_\Lambda \ \exp\left[-\int d^4x_E \left(\frac{1}{2}(\partial_\mu\phi)^2 + \frac{1}{2}m_\Lambda^2\phi^2 + \frac{\lambda_\Lambda}{4!}\phi^4 - J(x)\phi(x)\right)\right], \tag{2.38}$$

$$\mathcal{L}_\Lambda^E \equiv \frac{1}{2}(\partial_\mu\phi)^2 + \frac{1}{2}m_\Lambda^2\phi^2 + \frac{\lambda_\Lambda}{4!}\phi^4, \tag{2.39}$$

where $[\mathcal{D}\phi]_\Lambda$ means that only Euclidean momenta p with $|p| \leq \Lambda$ are considered when performing the integration. Note that this theory is defined with the explicit cutoff Λ, which means that no divergences appear. However, having an explicit cutoff Λ in the definition of the theory can cause some trouble regarding symmetries [11], which is a technical issue and not considered in this thesis[7].

With an explicit cutoff already in the definition of the theory Eq. (2.38) there is no need for regularization. In all the loop integrals that Eq. (2.38) produces, the momenta are limited by $0 \leq |p| \leq \Lambda$, and therefore converge[8]. Since the bare parameters of the theory, m_Λ and λ_Λ, are not of any practical interest, they need to be related to experimental measurements on physically relevant scales $\mu < \Lambda$. Relating the bare parameters $(m_\Lambda, \lambda_\Lambda)$ to measured parameters (m_μ, λ_μ) is the *renormalization*

$$(m_\mu, \lambda_\mu) \overset{\text{ren.}}{\longleftrightarrow} (m_\Lambda, \lambda_\Lambda). \tag{2.40}$$

The next step in Wilson's approach is to separate scales. The experiments are performed at some scale μ can not excite field modes with $|p| > \mu$, the theory Eq. (2.38) can be divided into two momentum regimes

$$\begin{aligned} &0 \leq |p| \leq \mu \\ &\mu < |p| \leq \Lambda. \end{aligned} \tag{2.41}$$

The Fourier components of the field $\phi(p)$ for $\mu < |p| \leq \Lambda$ cannot be excited and can be integrated out in the generating functional in Eq. (2.38) by dividing the field into

[7] There are some more sophisticated methods of regularizing a theory taking Lorentz- and Gauge invariance into account, see eg. Ref. [18]

[8] In this analysis in ϕ^4 theory, only UV divergences appear so the limit $|p| \to 0$ is not problematic.

Fourier components

$$\begin{aligned}\tilde{\phi}(p) &= \phi(p),\ 0 \leq |p| \leq \mu \\ \hat{\phi}(p) &= \phi(p),\ \mu \leq |p| \leq \Lambda\end{aligned} \tag{2.42}$$

and dividing the integration $\int \mathcal{D}\phi = \int \mathcal{D}\tilde{\phi} \int \mathcal{D}\hat{\phi}$. Not allowing $\hat{\phi}$ to be external states means that only $\tilde{\phi}$ couple to J. The generating functional becomes

$$Z[J] = \int \mathcal{D}\tilde{\phi} \int \mathcal{D}\hat{\phi}\ \exp\left[-\int d^4x_E \left(\mathcal{L}^E_\Lambda - J\tilde{\phi}\right)\right] \tag{2.43}$$

Performing the integration over $\hat{\phi}$, dropping the tilde on the remaining ϕ, and instead using the notation $[\mathcal{D}\phi]_\mu$ gives

$$Z[J] = \int [\mathcal{D}\phi]_\mu \exp\left[-\int d^4x_E \left(\mathcal{L}^E_\mu - J\phi\right)\right]. \tag{2.44}$$

The theory is now given in terms of an *effective Lagrangian* $\mathcal{L}^E_\mu$, but since the generating functional is *the same* the theory is also unchanged, just expressed in a different form. The effective Lagrangian takes the form[9]

$$\mathcal{L}^E_\mu = \frac{1}{2}(\partial_\mu\phi)^2 + \frac{1}{2}m^2_\mu\phi^2 + \frac{\lambda_\mu}{4!}\phi^4 + \text{higher order interactions.} \tag{2.45}$$

The relation between the Lagrangians $\mathcal{L}^E_\Lambda$ and $\mathcal{L}^E_\mu$ can in principle be computed, but are in practice hard, at least exactly.

The effect of integrating out the high momentum modes and lowering the cutoff, at the expense of changing the Lagrangian parameters and getting higher order interactions is illustrated in Fig. 2.1. The relation between the bare and renormalized Lagrangian parameter λ can be expressed

$$\lambda_\mu = \lambda_\Lambda + \Delta\lambda, \tag{2.46}$$

for some $\Delta\lambda$ that is called counterterm. The counterterm can be interpreted as parameterizing the physics of higher momentum that has been integrated out.

The discussion about effective Lagrangians, like the one in Eq. (2.45), will be continued in Chapter 3. The main difficulty in constructing an effective field theory is doing the integral over $\hat{\phi}$ in Eq. (2.43). This step can be avoided using Weinbergs approach to effective field theories, which will be explained in Section 3.2, which in short gives for the form of the effective Lagrangian using symmetries.

[9] To have a canonically normalized field ϕ it needs to be renormalized. Assuming that ϕ is properly normalized after the integration of heavy modes this effect can be included in the effective couplings, see Ref. [11].

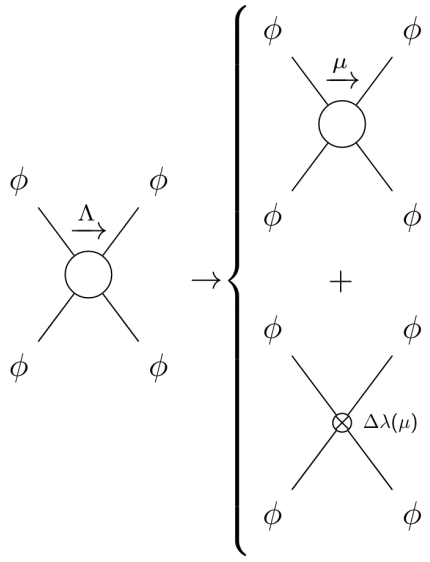

Figure 2.1: Illustration of how a $2 \to 2$ amplitude in ϕ^4-theory with cutoff Λ is transformed by renormalization to the scale μ. The quantum loop effects are divided into loop effects that are resolved in the theory defined with cutoff μ (upper blob) and the effective coupling $\lambda_\mu = \lambda_\Lambda + \Delta\lambda$, where $\Delta\lambda$ is containing the quantum loop effects of momenta that are integrated out.

2.4.2 The Renormalization Group

The discussion of renormalization will be concluded by briefly introducing the *Renormalization Group* (RG), and connect it to *relevant*, *marginal* and *irrelevant* operators. By introducing a parameter $b = \mu/\Lambda$ and rescaling the effective theory, transforming the momentum region from $0 \leq |p| \leq \mu$ back to $0 \leq |p| \leq \Lambda$, a general coupling constant, g, of an operator with mass dimension, d, in the Lagrangian will scale as

$$g_\mu = g_\Lambda b^\epsilon b^{d-4}. \tag{2.47}$$

b^ϵ is the so-called *anomalous scaling* due to quantum loop effects and is in general small, and b^{d-4} is the dominant scaling [11]. Thus, at small energies an operator with mass dimension $d > 4$ will become very small and are thus called *irrelevant*. The marginal operators have $d = 4$ and there the quantum effects determine the overall scaling. For $d < 4$ the operators will become large at small energies, and are hence called *relevant*. This re-scaling of the theory defines a *flow* in the space of couplings and is called the renormalization group flow [11]. This scaling of operators is important for assessing the relevance of operators at different scales, and making an effective field theory manageable by having some control over terms in Eq. (2.45) that are denoted "higher order interactions".

2.5 Spontaneous Symmetry Breaking and Goldstone's Theorem

The last topic in this chapter is spontaneous symmetry breaking, which is a concept of great importance in a variety of physical systems ranging from condensed matter to particle physics [11], [19]. The proof of Goldstone's theorem is given in Appendix B and is recommended to be reviewed by readers not already familiar with it. In Chapter 3 the theory of Goldstone bosons will turn out to be very useful, since pions can be identified as Goldstone bosons of the broken chiral symmetry of QCD. Hence, a brief overview of the Goldstone's theorem is provided here. For more details see Chapter 11 in Ref. [11].

The theorem will be discussed and stated in the context of a theory of n scalar fields, $\phi^i(x),\ i = 1, \ldots, n$ with Lagrangian given by

$$\mathcal{L}(\phi) = \mathcal{L}_{\text{kin}}(\phi) - V(\phi), \tag{2.48}$$

where $\mathcal{L}_{\text{kin}}(\phi)$ is the kinetic part and $V(\phi)$ is the potential. Assume that the theory is invariant under some global symmetry described by a Lie Group, G. The fields, $\phi^i(x)$, then transforms under some n-dimensional representation of G according to

$$\phi^i(x) \overset{G}{\mapsto} \exp\left(i\alpha^a T^a_{ij}\right) \phi^j(x), \tag{2.49}$$

where T^a_{ij} denote generators of the group G in the given representation. n_G denotes the dimensionality of the Lie algebra and the index $a = 1, \ldots, n_G$. The global symmetry G is said to be *spontaneously broken* to a subgroup $H \subset G$ if the ground state of the theory is only invariant under the subgroup $H \subset G$. The generators of G are then divided into $n_H < n_G$ generators of H and $n_G - n_H$ generators for G/H:

$$\begin{aligned} &T^a,\ a = 1, \ldots n_H,\ \text{generate } H \\ &T^b,\ b = n_H + 1, \ldots, n_G,\ \text{generate } G/H, \end{aligned} \tag{2.50}$$

the $n_G - n_H$ generators T^b are called *broken generators*.

Goldtone's theorem sates that for each broken generator, T^b, there exist a massless scalar particle in the spectrum. The proof of this statement is given in Appendix B.

An important note is that even when some symmetries are *spontaneously broken*, G is still the full symmetry group of the theory. Although, the full symmetry of G is partly hidden in the fact that the ground state, also called vacuum, spontaneously choose a configuration that appears to break the symmetry. Since the vacuum configuration is arbitrarily and *spontaneously* chosen, the effect of choosing a particular vacuum has no observable effect in the theory[10].

[10] The spontaneous choosing of vacuum is analogous to choosing a gauge in a gauge theory [11]. The theory and all the predictions are still gauge invariant even after choosing a particular gauge to work in.

It is important to distinguish spontaneous symmetry breaking from *explicit symmetry breaking* where the symmetry is *not* a symmetry anymore. Explicitly broken symmetries can also be of interest. For example, if the explicit symmetry breaking is small, the symmetry can often first be considered exact and the symmetry breaking effect can be treated in perturbation theory. Explicit symmetry breaking also play an important role in chiral perturbation theory (χPT) where it gives mass to pions, which will be discussed in the next chapter.

3

Chiral Effective Field Theory

In the previous chapter some important topics in Quantum Field Theory was reviewed, which will be important in this as well as coming chapters. This chapter will take QCD as a starting point, and with the help of Chiral Perturbation Theory (χPT) and Chiral Effective Field Theory (χEFT), construct an effective description of interactions between nucleons and pions. An EFT description is convenient since it automatically provides a systematic expansion of interactions in terms of some expansion parameter. This makes it possible to systematically improve the theory by including higher orders in the expansion parameter. In this chapter, and in the thesis is general, only the leading order (LO) contribution to the EFT will be studied.

Using symmetries, explicitly broken symmetries and spontaneously broken symmetries one can find an EFT for nucleons and pions, analogous to the effective field theories that were discussed briefly in the previous chapter. The effective field theory is called *chiral* Effective Field Theory since it relies on the broken chiral symmetry of low energy QCD, which will be described in more detail. The material in this chapter is largely built on, and inspired by, Ref. [20].

3.1 Chiral Perturbation Theory

Chiral perturbation theory (χPT) is a framework for studying the consequences of global flavor-symmetries of the light quarks in QCD. In this section the the dynamics of the Goldstone bosons of a spontaneously broken symmetry will be derived. For more details the interested reader can consult Chapter 4 in Ref. [20] for an excellent description.

3.1.1 Spontaneous Symmetry Breaking in QCD

The Lagrangian of QCD reads

$$\mathcal{L}_{\text{QCD}} = \sum_f \bar{\psi}_f (i\not{D} - m_f)\psi_f - \frac{1}{4} F^a_{\mu\nu} F_a^{\mu\nu}, \tag{3.1}$$

which is familiar from Chapter 2. The quark flavors, f, can be divided into three light quarks u ($m_u = 5$ MeV), d ($m_d = 9$ MeV), s ($m_s = 175$ MeV) and three heavy

quarks c, b, t with masses over 1 GeV. For the energy scales relevant to nuclear physics ($\lesssim 1$ GeV) only the u and d flavors are considered, and since $m_u, m_d \ll 1$ GeV they can to a good approximation be considered massless [20]. With these approximations the Lagrangian of low energy QCD becomes

$$\mathcal{L}^0_{\text{QCD}} = \sum_{f=u,d} \bar{\psi}_f i \not{D} \psi_f - \frac{1}{4} F^a_{\mu\nu} F^{\mu\nu}_a. \tag{3.2}$$

The limit where $m_u, m_d \to 0$ is called the *chiral limit* since the Lagrangian $\mathcal{L}^0_{\text{QCD}}$ acquires an exact *chiral symmetry* $G \equiv SU(2)_L \times SU(2)_R$, as the massless Dirac equation do not mix the chiralities of the quarks [11]. The chiral projection operators that project onto the left-handed (L) and the right-handed (R) part of the Dirac field are defined as

$$P_R = \frac{1}{2}\left(1 + \gamma^5\right), \quad P_L = \frac{1}{2}\left(1 - \gamma^5\right). \tag{3.3}$$

Defining a composite spinor ψ as,

$$\psi \equiv \begin{pmatrix} \psi_u \\ \psi_d \end{pmatrix}, \tag{3.4}$$

it can be divided into left-handed $\psi_L = P_L \psi$ and right-handed $\psi_R = P_R \psi$ components as

$$\psi = \psi_L + \psi_R = \begin{pmatrix} \psi_{L,u} \\ \psi_{L,d} \end{pmatrix} + \begin{pmatrix} \psi_{R,u} \\ \psi_{R,d} \end{pmatrix}. \tag{3.5}$$

An element $(L, R) \in G$ act as

$$\begin{pmatrix} \psi_{L,u} \\ \psi_{L,d} \end{pmatrix} \overset{G}{\mapsto} L \begin{pmatrix} \psi_{L,u} \\ \psi_{L,d} \end{pmatrix} \tag{3.6}$$

$$\begin{pmatrix} \psi_{R,u} \\ \psi_{R,d} \end{pmatrix} \overset{G}{\mapsto} R \begin{pmatrix} \psi_{R,u} \\ \psi_{R,d} \end{pmatrix} \tag{3.7}$$

where L, R are $SU(2)$ matrices. It is straightforward to check that $\mathcal{L}^0_{\text{QCD}}$ expressed in terms of ψ_L and ψ_R is invariant under G.

There are several pieces of evidence that the approximate low energy chiral symmetry of QCD is *spontaneously broken* to a subgroup $H \equiv SU(2)_V$[1], and that the Goldstone bosons produced are the three pions [20]. χPT is used to derive the Lagrangian of the pions using symmetry arguments, which will be discussed in the next sections.

3.1.2 General Transformations of Goldstone Bosons

To construct a Lagrangian for Goldstone bosons, the desired symmetry properties must be taken into account. The goal is to construct the most general Lagrangian, invariant under G, describing the Goldstone bosons. The discussion follows Ref. [20] and the foundations of this treatment of Goldstone bosons were laid out by Refs.

[1] The subscript V stands for "vector" and will be discussed more later.

[21]–[23]. The derivation in this section is done for general groups, G and H, but the case to have in mind for the purpose of this thesis is

$$G = SU(2)_L \times SU(2)_R, \quad H = SU(2)_V, \tag{3.8}$$

where n_G and n_H denote the number of generators for the respective groups.

Each Goldstone boson is described by a scalar field $\phi^i(x)$ which can be collected in a vector $\Phi(x) \equiv \Big(\phi^1(x), ..., \phi^n(x)\Big)$, where $n = n_G - n_H$ is the number of fields. The Goldstone bosons, Φ, are expected to transform in some way under G. By finding how they transform, Lagrangians invariant under G can be constructed.

Let M^4 denote Four-dimensional Minkowski space. Consider the space of fields $\phi^i : M^4 \to \mathbb{R}$ which satisfies appropriate smoothness properties, which will be implicit[2]. Define a *vector space* by

$$M_1 \equiv \{\Phi : M^4 \to \mathbb{R}^n\}. \tag{3.9}$$

The fact that Φ is a function of x will be suppressed since the analysis can be made imagining constant functions Φ and then adding the spacetime dependence where needed in the end [20].

G can act on the vector space M_1 by a *group action* $\varphi : G \times M_1 \to M_1$. By definition, the group action has to satisfy the properties

$$\varphi(\mathrm{id}, \Phi) = \Phi, \quad \forall\ \Phi \in M_1,\ \mathrm{id} \in G, \tag{3.10}$$

$$\varphi(g_1, \varphi(g_2, \Phi)) = \varphi(g_1 g_2, \Phi), \quad \forall\ g_1, g_2 \in G,\ \forall\ \Phi \in M_1. \tag{3.11}$$

where id is the identity element in G [20].

The ground state of the theory corresponds to $\Phi = \mathbf{0}$, since the theory is just contain in Goldstone bosons. The subgroup $H \subset G$ leaves the ground state invariant which imposes the constraint

$$\varphi(h, 0) = 0, \quad \forall\ h \in H, \tag{3.12}$$

on the group action. An equally important constraint comes from the assumption that G/H *does not* leave the ground state invariant. This means that φ can not be the trivial action, just leaving everything invariant, which *a priori* could be the case for a general group action.

A connection between the vector space of the Goldstone boson fields M_1 and the *coset space* $G/H \equiv \{gH \mid g \in G\}$ can be established given the constraint in Eq. (3.12). One can show that there exist an *isomorphic mapping*[3] between the coset space G/H and M_1. Ref. [20] shows that

$$\varphi(\cdot, 0) : G/H \to M_1 \tag{3.13}$$

[2]In general the fields has to be smooth enough to be able to satisfy the equations of motion.
[3]Isomorphic mapping is here referring to a injective and surjective map between the spaces.

is an isomorphic mapping, which means that all $\Phi \in M_1$ can be written as

$$\Phi = \varphi(f, 0) = \varphi(gh, 0) = \varphi(g, 0), \quad g \in G, h \in H \tag{3.14}$$

for some *representative* $f = gh \in gH$. Note that this result in some sense just is a mathematical formalization of the properties of Goldstone bosons.

It can be investigated how G act on Φ by using properties of the group action. The action of $\tilde{g} \in G$ on $\Phi \in M_1$ is

$$\varphi(\tilde{g}, \Phi) = \varphi(\tilde{g}, \varphi(gh, 0)) = \varphi(f', 0) = \Phi' \tag{3.15}$$

where $f' = \tilde{g}gh \in (\tilde{g}g)H$ is a representative of the coset.

The arguments leading to the transformation property in Eq. (3.15) are now summarized. The first assumption is that the Goldstone bosons $\Phi \in M_1$ transform in some way under the group G by the action, φ. By observing that $\Phi = \mathbf{0}$ represents the ground state, and using the assumption of spontaneous symmetry breaking (SSB) that H leaves the ground state invariant but G/H does not, give the isomorphism in Eq. (3.13) which establishes a one-to-one connection between elements of G/H and M_1. These assumptions lead to the necessary condition that the Goldstone bosons transform non-trivially under G, and can be represented with elements of the cosets. Both these properties will now be used when applying this general formalism to the case of chiral symmetry breaking in QCD to derive the dynamics if its Goldstone bosons, the pions.

3.1.3 Pions as Goldstone Bosons

The formalism derived in the previous section will be applied to the spontaneously broken chiral symmetry of QCD. The chiral symmetry $G = SU(2)_L \times SU(2)_R$ is broken to the subgroup $H = SU(2)_V \subset G$. Since $SU(N)$ has $N^2 - 1$ generators [11], the SSB $G \to H$ will give $n = n_G - n_H = 3$ Goldstone bosons, which can be identified as the pions (π^0, π^+, π^-) [20]. The superscript on the pions denotes their electric charge. The so-called vector subgroup $H \subset G$ is the subgroup of the chiral symmetry group, G, where both the right-handed and left-handed fields are rotated an equal amount:

$$G = \{(L, R) \mid L, R \in SU(2)\}, \tag{3.16}$$
$$H = \{(L, R) \mid L, R \in SU(2), V = L = R\} \subset G. \tag{3.17}$$

For a general group element $g = (L, R) \in G$ the coset gH can be represented by $U = RL^\dagger \in SU(2)$ [24] which is seen by

$$gh = (LV, RV) = (LV, RL^\dagger LV) = (\mathrm{id}, RL^\dagger)(LV, LV), \quad (LV, LV) \in H \tag{3.18}$$

and implies that

$$gH \equiv (\mathrm{id}, RL^\dagger)H$$

Hence, choosing the first element as id, the coset is represented by $U = RL^\dagger$. The general result of the previous section gives further that U is isomorphic to Φ. Physically speaking, this isomorphism means that U and Φ contain the same degrees of freedom, and U can be parameterized with Φ. The transformation of U under G is obtained by applying a group element $\tilde{g} = (\tilde{L}, \tilde{R})$ to the representative of the coset in analogy with Eq. (3.15) [20]

$$(\tilde{L}, \tilde{R})(\mathrm{id}, RL^\dagger)H = (\mathrm{id}, \tilde{R}(RL^\dagger)\tilde{L}^\dagger)H. \tag{3.19}$$

The x dependence can safely be added again, which gives the general transformation

$$U(x) \overset{G}{\mapsto} RU(x)L^\dagger, \quad (R, L) \in G. \tag{3.20}$$

Mathematically speaking Eq. (3.20) is how a representative for a coset transforms under G. This transformation property is important since the result from the previous section states that $\Phi(x)$ and $U(x)$ are isomorphic, which can be used to express $U(x)$ in terms of $\Phi(x)$, and hence obtain the transformation property of $\Phi(x)$ under G.

The isomorphism between $\Phi(x)$ and $U(x)$, or more exactly, between M_1 and $M_2 \equiv \{U : M^4 \to SU(2)\}$, can be found by observing that the Lie algebra $\mathfrak{su}(2)$ has the same dimension as M_1. Hence, Φ can be expanded in a basis of $\mathfrak{su}(2)$; the Pauli matrices, τ^i. To not confuse notation, ϕ is introduced as the expansion of Φ in this basis

$$\phi(x) = \sum_{i=1}^{3} \phi_i \tau_i = \begin{pmatrix} \phi_3 & \phi_1 - i\phi_2 \\ \phi_1 + i\phi_2 & \phi_3 \end{pmatrix} \equiv \begin{pmatrix} \pi^0 & \sqrt{2}\pi^+ \\ \sqrt{2}\pi^- & -\pi^0 \end{pmatrix}. \tag{3.21}$$

One can now define

$$U(x) \equiv \exp\left(i\frac{\phi(x)}{f_\pi}\right), \tag{3.22}$$

where f_π is a dimensionful constant with the same dimension as ϕ called the pion decay constant. A candidate for the isomorphism is thus

$$\alpha : M_1 \to M_2 \tag{3.23}$$

$$\alpha : (\phi_1, \phi_2, \phi_3) \mapsto \exp\left(i\frac{\phi(x)}{f_\pi}\right). \tag{3.24}$$

α is by definition an isomorphism if it is injective and surjective. This is the case since the map α is the *exponential map* from the Lie algebra $\mathfrak{su}(2)$ to $SU(2)$, which is injective and surjective, see Chapter 4 in [25].

A representation of the Goldstone bosons Eq. (3.22) which have a known transformation property under G Eq. (3.20) is finally known. The reason why the representation of the Goldstone bosons as the vector $\Phi \in M_1$ is less convenient than U or ϕ,

is that in the latter, the coset representation is built in. And, as we saw, to derive the transformation property of the coset representation under G straightforward.

The result of this derivation is an explicit realization of a group action (call it φ again), that act on a space M_2 isomorphic to M_1

$$\varphi : G \times M_2 \to M_2 \tag{3.25}$$
$$\varphi : [(L, R), U(x)] \mapsto RU(x)L^\dagger. \tag{3.26}$$

Even though this derivation was quite detailed, it is no proof that this representation is unique. For details regarding uniqueness, see Ref. [23].

3.1.4 Effective Pion-Pion Lagrangian

Using the results of the previous section, a leading order effective Lagrangian for pions in the low-momentum limit can derived. The condition that pions are Goldstone bosons of the spontaneously broken chiral symmetry gave the parameterization $U(x)$ with known transformation under G, summarized as [20]:

$$U(x) = \exp\left(i\frac{\phi(x)}{f_\pi}\right), \quad U(x) \overset{G}{\mapsto} RU(x)L^\dagger, \quad (L, R) \in G \tag{3.27}$$

where

$$\phi(x) = \sum_{i=1}^{3} \phi_i \tau_i = \begin{pmatrix} \phi_3 & \phi_1 - i\phi_2 \\ \phi_1 + i\phi_2 & \phi_3 \end{pmatrix} \equiv \begin{pmatrix} \pi^0 & \sqrt{2}\pi^+ \\ \sqrt{2}\pi^- & -\pi^0 \end{pmatrix}. \tag{3.28}$$

The effective Lagrangian should be invariant under G, since the theory is still invariant under the full symmetry group even in the presence of spontaneous symmetry braking, as discussed in Section 2.5. The effective theory is only expected to be valid at low energies, and hence a minimal amount of pion derivatives in the lowest order effective Lagrangian is considered, since they correspond to pion momenta in momentum space [20].

Some possible terms and their transformation properties under G are:

$$U^\dagger \overset{G}{\mapsto} LU^\dagger R^\dagger, \tag{3.29}$$
$$\partial_\mu U \overset{G}{\mapsto} R\ \partial_\mu U L^\dagger, \tag{3.30}$$
$$\partial_\mu U \partial^\mu U^\dagger \overset{G}{\mapsto} R \partial_\mu U \partial^\mu U^\dagger R^\dagger. \tag{3.31}$$

The most general G-invariant effective Lagrangian with minimal number of derivatives is given by

$$\mathcal{L}_{\text{eff}} = \frac{f_\pi^2}{4} \operatorname{Tr}(\partial_\mu U \partial^\mu U^\dagger) \tag{3.32}$$

with the property $\mathcal{L}_{\text{eff}} \mapsto \mathcal{L}_{\text{eff}}$ under G, which is easily shown, see Ref. [20]. By expanding $\mathcal{L}_{\text{eff}}$ in powers of the pion field it can be shown that the given prefactor gives a canonical kinetic term for the pion fields.

As a last step in deriving the low energy effective Lagrangian for pions one has to take into account that the chiral symmetry is also *explicitly* broken by the non-zero quark masses m_u and m_d, which gives rise to a non-zero pion mass m_π. Since these masses are small, the explicit symmetry breaking is also small which still makes the analysis in the previous sections valid to a good approximation. In Ref. [20] it is shown how the non-zero masses can be included in the effective Lagrangian in a consistent way. Adding this to the Lagrangian Eq. (3.32) and expanding to leading order (LO) in the number of pion fields give, with the notation $\boldsymbol{\pi} = (\phi^1, \phi^2, \phi^3)$,

$$\mathcal{L}_{\boldsymbol{\pi}} = \frac{1}{2}\partial_\mu \boldsymbol{\pi} \partial^\mu \boldsymbol{\pi} - \frac{1}{2} m_\pi^2 \boldsymbol{\pi}^2. \tag{3.33}$$

3.2 Chiral Effective Field Theory for Nucleons and Pions

In this section the effective theory for the pions, derived in chiral perturbation theory (χPT) will be extended to an effective theory also including nucleons, which is usually called χEFT. First, the general structure of an effective filed theory of fermions (nucleons) and scalar-particles (pions) is studied to develop an organizational scheme, called power counting, for assessing the importance of certain interactions in the EFT. When the power-counting procedure is established the leading order Lagrangian for nucleons and pions will be derived in the non-relativistic limit. Finally a leading order nucleon-nucleon potential is obtained, and is the most essential product of this chapter to understand, since it will be the piece of information that summarize the analysis in theses first two chapters.

3.2.1 Weinberg Power Counting

Stephen Weinberg investigated and laid the foundations of using EFT in nuclear physics in a series of important papers, see Refs. [6]–[8]. For the development of EFT in nuclear physics, the so-called separation of scales in the meson mass spectrum is crucial. There is a large mass gap between the the pion mass (~ 140 MeV) and the heavier mesons ρ (~ 770 MeV) and ω (~ 782 MeV). This suggests an expansion in the *soft scale* $Q \sim m_\pi$ over the *hard scale*, also called *chiral symmetry breaking scale*, $\Lambda_\chi \sim 1$ GeV [26]. External nucleon momenta are considered to be of order Q.

In the previous sections the effective pion Lagrangian was derived. The fact that the effective Lagrangian in principle contained *all* terms consistent with the symmetries was not actually explained properly, but relied on a theorem by Weinberg called the folk theorem [6]. In short, the theorem states that the effective Lagrangian will contain *all* possible terms consistent with the symmetries of the underlying

theory[4]. The power counting procedure developed by Weinberg is crucial, since it systematically orders these (possibly infinite) number of terms in the effective Lagrangian as powers $\left(Q/\Lambda_\chi\right)^\nu$, where ν is called the *chiral order* and $Q/\Lambda_\chi \sim 0.1$ [26]. This scheme is called Weinberg power counting (WPC).

The power-counting scheme will in some ways rely on that the general structure of the pion-nucleon Lagrangian is known, and the construction of the pion-nucleon Lagrangian will depend on the power counting. Having this in mind, some things introduced can not really be well motivated until the end of this chapter. This is unfortunately an inevitable consequence of trying to explaining an iterative process in a non-iterative way. The following analysis will be done assuming an interacting theory of pions and nucleons. Pions are scalar particles and are depicted by dashed lines in Feynman diagrams, whereas nucleons are fermions and are depicted by solid lines.

3.2.1.1 Chiral Dimension of Feynman Diagrams

The chiral dimension, ν, was first analyzed in Ref. [7]. For diagrams only involving pions, with two external pions, the chiral dimension is given by

$$\nu = 2 + 2L + \sum_i (d_i - 2)V_i, \tag{3.34}$$

where L is number of loops in the diagram, d_i is the number of derivatives/pion masses for vertex type i, and V_i is the number of vertices of type i, see Ref. [26]. Two examples are shown in Fig. 3.1.

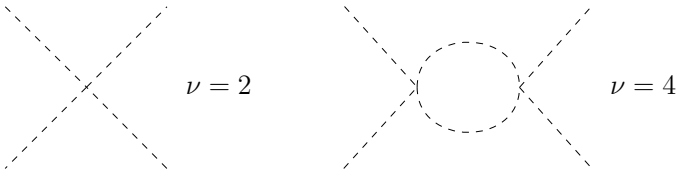

Figure 3.1: Chiral dimension of pion diagrams with four external legs.

In the two nucleon (NN) sector with pions included, the chiral dimension of a given diagram is given by [26]

$$\nu = 4L - 2I_\pi - I_N + \sum_i d_i V_i, \tag{3.35}$$

where L, d_i and V_i denote the same quantities as in the pion sector, and I_π (I_N) are the number of pion (nucleon) propagators. In Fig. 3.2 and Fig. 3.3 some examples of nucleon-pion diagrams are shown.

[4]To connect back to Chapter 2, this is the statement that gives you a way of constructing the EFT without explicitly performing an integral of the type Eq. (2.43) which was pointed out as difficult.

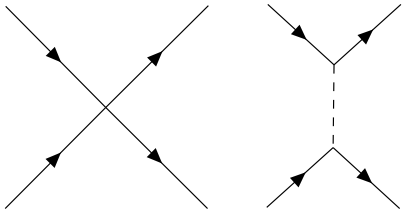

(a) Pion-nucleon diagrams with the lowest chiral order $\nu = 0$. These diagrams are two-particle irreducible.

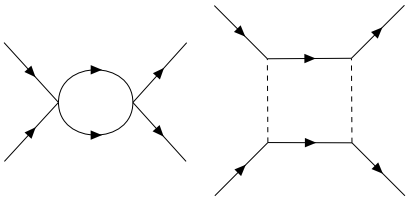

(b) Example of two-particle reducible pion-nucleon diagrams of chiral order $\nu = 2$.

Figure 3.2

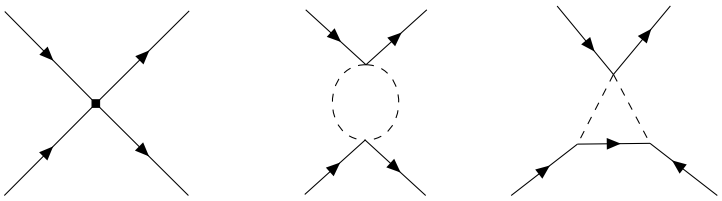

Figure 3.3: Example of two-particle irreducible pion-nucleon diagrams of chiral order $\nu = 2$. The square in the leftmost diagram indicated that is has higher chiral order than the four-point interaction in Fig. 3.2a.

It turns out that due to an effect called *infrared enhancement*, reducible diagrams with purely nucleonic intermediate states (e.g. diagrams in Fig. 3.2b) are enhanced and do *not* scale as their chiral order indicates [27]. This calls for a non-perturbative treatment of such diagrams, meaning that *all* diagrams need to be taken into account.

3.2.1.2 Potential from Irreducible Diagrams

The non-perturbative summation of reducible diagrams can be captured as follows. The full scattering amplitude for NN scattering is denoted by $\mathcal{M}$, and is depicted by a round blob in Feynman diagrams. The amplitude can be expanded in terms of the sum of all irreducible diagrams, denoted $\mathcal{V}$. For an illustration see Fig. 3.4. If $\mathcal{G}$ denotes the two nucleon propagator, then the amplitude satisfies

$$\mathcal{M} = \mathcal{V} + \mathcal{V}\mathcal{G}\mathcal{M} \tag{3.36}$$

which is equivalent to the infinite sum in Fig. 3.4 [3].

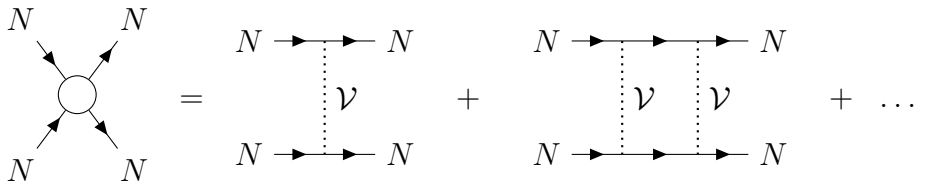

Figure 3.4: The total scattering amplitude $\mathcal{M}$ can be written as a sum of two-particle irreducible diagrams $\mathcal{V}$ that are summed with two-nucleon intermediate states which have the propagator $\mathcal{G}$.

Skipping some details that are explained in Refs. [26], [27], the non-relativistic effective potential can be identified as the irreducible diagrams, $\mathcal{V}$. The LO ($\nu = 0$) potentials that will be used in this thesis consists of the following diagrams,

$$V_{\text{WPC}}^{[\text{LO}]} = \quad + \qquad (3.37)$$

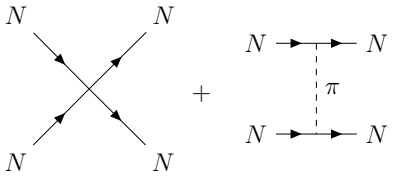

and

$$V_{\text{MWPC}}^{[\text{LO}]} = \quad + \quad + \quad + \quad . \qquad (3.38)$$

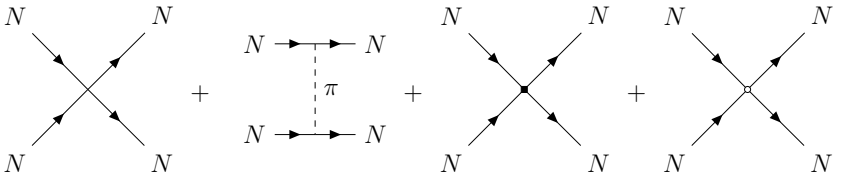

The last two contact interactions in $V_{\text{MWPC}}^{[\text{LO}]}$ symbolizes higher order counterterms that are promoted to leading order in *modified Weinberg power counting* (MWPC). The LECs corresponding to the promoted counterterms are the ones in NN scattering channels with LS-terms: ${}^3P_0$, ${}^3P_2$ and ${}^3D_2$ [26]. The potentials can be computed from the pion-nucleon and nucleon-nucleon effective Lagrangians, which will be done in coming sections.

3.2.1.3 EFT Expansion and Expected Errors

When computing observable quantities in χEFT, e.g. cross sections σ, they are expected to have expansions

$$\sigma = \sigma_{\text{ref}} \sum_{\nu=0}^{\infty} c_\nu \left(\frac{Q}{\Lambda_\chi}\right)^\nu$$

where σ_{ref} are some reference scale and c_ν are observable coefficients of order one. Since $c_1 = 0$ the induced model error from just keeping the LO ($\nu = 0$) in the above sum is expected to be

$$\sigma_{\text{err}} = \sigma - \sigma_{\text{ref}} c_0 = \sum_{\nu=2}^{\infty} c_\nu \left(\frac{Q}{\Lambda_\chi}\right)^\nu .$$

Knowing the model error is a great advantage, since it can be taken into account when doing inference, see Ref. [26].

3.2.2 Pion-Nucleon Effective Lagrangian

The next step is to include the lightest baryons in the picture, i.e. the nucleons. If the mass difference of the up- and down quark is assumed to be zero, the *isospin symmetry* is exact and the proton (p) and neutron (n) can be described as the $+\frac{1}{2}$ and $-\frac{1}{2}$ projections of an isospin $\frac{1}{2}$ particle, Ψ, called the *nucleon*

$$\Psi = \begin{pmatrix} \psi_p \\ \psi_n \end{pmatrix}. \tag{3.39}$$

ψ_p and ψ_n are the four component Dirac spinors describing the proton and neutron respectively. As before, let

$$U(x) = \exp\left(i\frac{\phi(x)}{f_\pi}\right) \tag{3.40}$$

be the $SU(2)$ matrix containing the pion fields $\phi(x)$ (see Eq. (3.28)). In the same spirit as in the pure pionic case, the goal is to infer a transformation property of the physical degrees of freedom under the chiral symmetry group G.

Following Ref. [20] one can construct a group action, φ, on the set

$$M \equiv \{(U(x), \Psi(x))\}$$

by

$$\varphi : G \times M \to M \tag{3.41}$$

$$\varphi(g) : \begin{pmatrix} U(x) \\ \Psi(x) \end{pmatrix} \mapsto \begin{pmatrix} RU(x)L^\dagger \\ K(L,R,U(x))\Psi(x) \end{pmatrix} \tag{3.42}$$

where

$$K(L,R,U(x)) = \sqrt{RU(x)L^\dagger}^{-1} R \sqrt{U(x)}. \tag{3.43}$$

Ref. [20] shows that φ defines a group action and that Ψ *transforms linearly*[5] under the subgroup $H = SU(2)_V$ of this group action. Why this particular K is chosen is not obvious. K naturally arises as a *compensator field*[6] for $u \equiv \sqrt{U}$, which is analogous to the compensator field introduced in a gauge theory. More details are found in Ref. [28].

If one sets aside the somewhat mysterious appearance of K and accepts the transformation properties of (U, Ψ) under G, the nucleon-pion interaction Lagrangian, $\mathcal{L}_{\pi N}$, can be derived. The interactions are introduced in the same way as in a gauge

[5]Transform linearly refers to that under this subgroup the group action $\varphi(h)$, $h \in H$ is also a linear function, and hence a *representation*.

[6]The name is inspired by the same type of compensator field that is needed in gauge theories to be able to construct gauge invariant Lagrangians [11, Chapter 15].

theory—promoting the global symmetry G to a local symmetry where the group elements $g = (L, R) \in G$ are allowed to depend on the spacetime coordinate as $g(x) = (L(x), R(x)) \in G$. The local G symmetry will lead to necessary interactions via covariant derivatives in analogy with how it works in gauge theories, discussed in Section 2.2. There are some good field theoretic arguments involving the generating functional and Ward identities for promoting the symmetry to a local symmetry, see Ref. [29] for a detailed discussion.

The starting point is the field content and the transformation property under $G = SU(2)_L \times SU(2)_R$ which is promoted to a local transformation

$$\varphi(g(x)) : \begin{pmatrix} U(x) \\ \Psi(x) \end{pmatrix} \mapsto \begin{pmatrix} R(x)UL^\dagger(x) \\ K(L(x), R(x), U(x))\Psi(x) \end{pmatrix}. \tag{3.44}$$

In the same way as in a gauge theory case one needs to introduce a covariant derivative D_μ with the property that $D_\mu\Psi$ transforms in the same way as Ψ to be able to have G-invariant derivative terms.

The most general Lagrangian, to leading order in the number of derivatives, is given in Ref. [30] and looks like

$$\mathcal{L}_{\pi N} = \bar{\Psi}\left(i\not{D} - M_N + \frac{g_A}{2}\gamma^\mu\gamma^5 u_\mu\right)\Psi, \tag{3.45}$$

where $M_N = 938.9$ MeV is the nucleon mass[7] and g_A is the *axial coupling*. The covariant derivative is given by

$$D_\mu = \partial_\mu + \Gamma_\mu, \tag{3.46}$$

$$\Gamma_\mu = \frac{1}{2}\left(u^\dagger\partial_\mu u + u\partial_\mu u^\dagger\right), \tag{3.47}$$

where u_μ is called the *vielbein* which is defined as

$$u_\mu \equiv i\left(u^\dagger\partial_\mu u - u\partial_\mu u^\dagger\right). \tag{3.48}$$

More details regarding the construction of the effective Lagrangian is found in Ref. [20].

As pointed out in Ref. [31] the relativistic form of the above effective Lagrangian in Eq. (3.45) is somewhat problematic, due to the fact that ∂_0 acting on Ψ does not give a small quantity in the chiral limit. To this end, a non-relativistic reduction of $\mathcal{L}_{\pi N}$ is needed to have a consistent power counting.

Before doing the non-relativistic reduction some simplifications can be made to Eq. (3.45), since only the leading order interactions are of interest. It will turn out to be sufficient to expand the vielbein as

$$u_\mu = i(u^\dagger\partial_\mu u - u\partial_\mu u^\dagger) = -\frac{1}{f_\pi}\boldsymbol{\tau}\cdot\partial_\mu\boldsymbol{\pi} + \mathcal{O}(\boldsymbol{\pi}^3) \tag{3.49}$$

[7]The nucleon mass $M_N \equiv 2m_N$, where $m_N = (m_p m_n)/(m_n + m_p)$ is the reduced mass of the neutron-proton system [26].

and the connection in the covariant derivative as

$$\Gamma_\mu = \frac{1}{2}(u^\dagger \partial_\mu u + u \partial_\mu u^\dagger) = \frac{i}{4f_\pi^2} \boldsymbol{\tau} \cdot \boldsymbol{\pi} \times \partial_\mu \boldsymbol{\pi} + \mathcal{O}(\boldsymbol{\pi}^4) = \mathcal{O}(\boldsymbol{\pi}^2). \tag{3.50}$$

Here $\boldsymbol{\tau} = (\tau^1, \tau^2, \tau^3)$ denotes the Pauli matrices and $\boldsymbol{\pi} = (\phi^1, \phi^2, \phi^3)$ the pion fields. Inserting this into Eq. (3.45) gives

$$\mathcal{L}_{\pi N} = \bar{\Psi} \left(i \not{\partial} - M_N - \frac{g_A}{2} \gamma^\mu \gamma^5 \frac{1}{f_\pi} \boldsymbol{\tau} \cdot \partial_\mu \boldsymbol{\pi} + \mathcal{O}(\boldsymbol{\pi}^2) \right) \Psi. \tag{3.51}$$

Keeping only the leading order interaction one obtains

$$\mathcal{L}_{\pi N}^{[LO]} \equiv \bar{\Psi} \left(i \not{\partial} - M_N - \frac{g_A}{2} \gamma^\mu \gamma^5 \frac{1}{f_\pi} \boldsymbol{\tau} \cdot \partial_\mu \boldsymbol{\pi} \right) \Psi. \tag{3.52}$$

This Lagrangian will be the starting point for the non-relativistic reduction in the next section.

3.2.3 Non-Relativistic Reduction and the Non-Relativistic Nucleon Field

The non-relativistic reduction of the nucleon field can be done in the so called *heavy baryon formalism*, as described in [31]. Starting with the LO Lagrangian in Eq. (3.52), the four momentum of the nucleon can be decomposed as

$$p_\mu = M_N v_\mu + q_\mu, \tag{3.53}$$

with $v_\mu v^\mu = 1$ and $v^\mu q_\mu / M_N \ll 1$. A new field, $\psi(x)$, satisfying

$$\Psi(x) \equiv e^{-iM_N v^\mu x_\mu} \psi(x),$$

is defined to separate out the kinematical dependence of Ψ on the nucleon mass. Substituting $\psi(x)$ into Eq. (3.52) the leading order Lagrangian will take the form

$$\mathcal{L}_{\pi N}^{[LO]} = \bar{\psi} \left(i \not{\partial} + (\not{v} - 1) M_N - \frac{g_A}{2} \gamma^5 \frac{1}{f_\pi} \boldsymbol{\tau} \cdot \not{\partial} \boldsymbol{\pi} \right) \psi. \tag{3.54}$$

The expression can be simplified by introducing projection operators

$$P_\pm^v = \frac{1 \pm \not{v}}{2} \tag{3.55}$$

that are defined for a general four vector, v^μ, satisfying $v^2 = 1$ and $v^0 \geq 1$. Ref. [20] shows that these operators satisfy the necessary properties for projection operators, namely:

$$P_+^v + P_+^v = 1, \quad \left(P_\pm^v\right)^2 = P_\pm^v, \quad P_\pm^v P_\mp^v = 0. \tag{3.56}$$

These operators are used to decompose the four-component spinor, $\psi(x)$, to $N(x)$ and $h(x)$ as follows

$$\psi(x) = N(x) + h(x), \quad N(x) = P_+^v \psi(x), \quad h(x) = P_-^v \psi(x). \tag{3.57}$$

N and h is called the *light* and *heavy* component of ψ respectively. Following Ref. [20], this decomposition can be motivated by considering positive energy plane wave solutions to the Dirac equation

$$\psi_{\boldsymbol{p}}(x) = u_s(\boldsymbol{p})e^{-ipx} \tag{3.58}$$

$$u_s(\boldsymbol{p}) = \sqrt{E(\boldsymbol{p}) + M_N}\begin{pmatrix} \chi_s \\ \frac{\boldsymbol{\sigma}\cdot\boldsymbol{p}}{E(\boldsymbol{p})+M_N}\chi_s \end{pmatrix} \tag{3.59}$$

where $\boldsymbol{p}$ is the three momentum, $E(\boldsymbol{p}) = \sqrt{\boldsymbol{p}^2 + M_N^2}$ is the energy, χ_s is a two component Pauli spinor and $\boldsymbol{\sigma}$ is a vector of the Pauli matrices $\boldsymbol{\sigma} = (\sigma^1, \sigma^2, \sigma^3)$. For the special case of choosing $v^\mu = (1, \mathbf{0})$ the projectors $P^v_\pm$ are, in 2×2 component form, given by

$$P^v_+ = \begin{pmatrix} 1 & 0 \\ 0 & 0 \end{pmatrix}, \quad P^v_- = \begin{pmatrix} 0 & 0 \\ 0 & 1 \end{pmatrix}. \tag{3.60}$$

This gives that $N(x)$ and $h(x)$ correspond to the upper- and lower components of the four spinor ψ,

$$N(x) = \sqrt{E(\boldsymbol{p}) + M_N}\begin{pmatrix} \chi_s \\ \mathbf{0} \end{pmatrix} e^{-i(E(\boldsymbol{p})-M_N)x^0}e^{-i\boldsymbol{p}\boldsymbol{x}}, \tag{3.61}$$

$$h(x) = \sqrt{E(\boldsymbol{p}) + M_N}\begin{pmatrix} \mathbf{0} \\ \frac{\boldsymbol{\sigma}\cdot\boldsymbol{p}}{E(\boldsymbol{p})+M_N}\chi_s \end{pmatrix} e^{-i(E(\boldsymbol{p})-M_N)x^0}e^{-i\boldsymbol{p}\boldsymbol{x}}. \tag{3.62}$$

In the non-relativistic limit, $(E(\boldsymbol{p}) - M_N)/M_N \ll 1$, $h(x)$ is suppressed by a factor of M_N^{-1} compared to N. By redefining N and h as two-component spinors,

$$N(x) \equiv \sqrt{E(\boldsymbol{p}) + M_N}\chi^{(\alpha)}e^{iM_Nx^0}e^{-i\boldsymbol{p}\boldsymbol{x}}, \tag{3.63}$$

$$h(x) \equiv \sqrt{E(\boldsymbol{p}) + M_N}\frac{\boldsymbol{\sigma}\cdot\boldsymbol{p}}{E(\boldsymbol{p}) + M_N}\chi^{(\alpha)}e^{iM_Nx^0}e^{-i\boldsymbol{p}\boldsymbol{x}}, \tag{3.64}$$

the notation can be simplified since the four component spinor ψ can be written as

$$\psi(x) = \begin{pmatrix} N(x) \\ h(x) \end{pmatrix}. \tag{3.65}$$

Now, in our case we do not have the free Dirac equation, but motivated by this discussion we do the same decomposition of $\psi(x)$ to a light general field N, and a heavy field h that is suppressed by M_N^{-1} compared to N [20].

In the non-relativistic limit the Lagrangian in Eq. (3.54) can be simplified to

$$\mathcal{L}_{\pi N} = N^\dagger\left(i\partial_0 - \frac{1}{2}g_A(\boldsymbol{\sigma}\cdot\boldsymbol{\nabla})\frac{\boldsymbol{\tau}\cdot\boldsymbol{\pi}}{f_\pi}\right)N, \tag{3.66}$$

where all positive powers of M_N^{-1} are not included anymore [31] and hence the $h(x)$ field is not included. Relativistic corrections to Eq. (3.66) are also of order M_N^{-1} [20], hence the Lagrangian is valid in frames that are "close to" the rest frame of the nucleon, $v^\mu = (1, \mathbf{0})$. In Eq. (3.66) the leading order pion-nucleon interaction term can be identified as

$$\mathcal{L}_{\text{int}} = -\frac{g_A}{2f_\pi}N^\dagger(\boldsymbol{\sigma}\cdot\boldsymbol{\nabla})(\boldsymbol{\tau}\cdot\boldsymbol{\pi})N. \tag{3.67}$$

3.2.4 Nucleon-Nucleon Effective Lagrangian

So far the pion Lagrangian $\mathcal{L}_{\boldsymbol{\pi}}$ and the nucleon-pion Lagrangian $\mathcal{L}_{\boldsymbol{\pi}N}$ has been constructed and the last piece is the nucleon-nucleon Lagrangian $\mathcal{L}_{NN}$.

Ref. [32] states that the most general Lagrangian involving only two nucleons, described by the non-relativistic nucleon field, N, is:

$$\mathcal{L} = N^\dagger \left(i\partial_0 + \frac{\boldsymbol{\nabla}^2}{2M_N} + ... \right) N - C_{0t}(N^\dagger P_t N)^2 - C_{0s}(N^\dagger P_s N)^2 + ... \tag{3.68}$$

where

$$P_t^i = \frac{1}{\sqrt{8}}\sigma_2\sigma^i\tau_2, \qquad P_s^a = \frac{1}{\sqrt{8}}\tau_2\tau^a\sigma_2, \quad i,a = 1,2,3. \tag{3.69}$$

The dots stands for terms with more derivatives, which will be sub-leading considering small momenta. The projectors P_t^i and P_s^i are the projectors into spin triplet and spin singlet respectively, which is the two total spin states that the the two nucleon system can occupy. The convention used is that σ^i act in spin space and τ^i act in isospin space. C_{0t} and C_{0s} are LECs in spin triplet, and spin singlet respectively. Hence, the LO Lagrangian reads

$$\mathcal{L}_{NN}^{[LO]} = N^\dagger \left(i\partial_0 + \frac{\boldsymbol{\nabla}^2}{2M_N} \right) N - C_{0t}(N^\dagger P_t N)^2 - C_{0s}(N^\dagger P_s N)^2 \tag{3.70}$$

Contrary to the one-nucleon sector, the kinetic piece $N^\dagger \left(\boldsymbol{\nabla}^2/(2M_N)\right) N$ is included at LO. This term is responsible for *infrared enhancement* of nucleon diagrams which contain purely nucleonic intermediate states, meaning that the importance of diagrams with many loops will not decrease, as discussed earlier.

3.3 NN potential in Weinberg- and Modified Weinberg Power Counting

This last section will summarize the LO Lagrangian, and state the potentials that can be obtained by calculating the Feynman-diagram expressions of the potentials given in Eq. (3.37) and Eq. (3.38).

The full leading order non-relativistic Lagrangian in WPC describing the dynamics of pions, $\boldsymbol{\pi}$, and nucleons, N, read

$$\begin{aligned}\mathcal{L}_{\text{WPC}}^{[\text{LO}]} &= \frac{1}{2}\partial_\mu\boldsymbol{\pi}\partial^\mu\boldsymbol{\pi} - \frac{1}{2}m_\pi^2\boldsymbol{\pi}^2 + N^\dagger\left(i\partial_0 + \frac{\nabla^2}{2M_N}\right)N \\ &- \frac{g_A}{2f_\pi}N^\dagger(\boldsymbol{\sigma}\cdot\boldsymbol{\nabla})(\boldsymbol{\tau}\cdot\boldsymbol{\pi})N - C_{0t}(N^\dagger P_t N)^2 - C_{0s}(N^\dagger P_s N)^2.\end{aligned} \tag{3.71}$$

As a reminder, g_A is the axial coupling, f_π is the pion decay constant, M_N is the nucleon mass and m_π is the pions mass. $\boldsymbol{\sigma}$ and $\boldsymbol{\tau}$ are the spin and isospin operators.

In MWPC, more counterterms are promoted to LO, which will be shown in the computed potentials.

Having the LO Lagrangian 3.71 it is only a matter of calculations to obtain the NN potentials defined in Eq. (3.37) and Eq. (3.38). In MWPC, the only difference is extra LECs in higher partial waves, so this Lagrangian is not explicitly written out. Using the notation $\boldsymbol{p}$ ($\boldsymbol{p}'$) for the ingoing (outgoing) nucleon momenta, $\boldsymbol{q} = \boldsymbol{p}' - \boldsymbol{p}$ for the momentum transfer, and $p = |\boldsymbol{p}|$, $p' = |\boldsymbol{p}'|$, the potentials read [26]

$$V_{\text{WPC}}^{[\text{LO}]}(\boldsymbol{p}', \boldsymbol{p}) = -\frac{g_A^2}{4f_\pi^2}\frac{(\boldsymbol{\sigma}_1 \cdot \boldsymbol{q})(\boldsymbol{\sigma}_2 \cdot \boldsymbol{q})}{\boldsymbol{q}^2 + m_\pi^2}(\boldsymbol{\tau}_1 \cdot \boldsymbol{\tau}_2) + C_{^1S_0} + C_{^3S_1}, \tag{3.72}$$

$$\begin{aligned} V_{\text{MWPC}}^{[\text{LO}]}(\boldsymbol{p}', \boldsymbol{p}) = &-\frac{g_A^2}{4f_\pi^2}\frac{(\boldsymbol{\sigma}_1 \cdot \boldsymbol{q})(\boldsymbol{\sigma}_2 \cdot \boldsymbol{q})}{\boldsymbol{q}^2 + m_\pi^2}(\boldsymbol{\tau}_1 \cdot \boldsymbol{\tau}_2) + \\ &+ C_{^1S_0} + C_{^3S_1} + (C_{^3P_0} + C_{^3P_2})pp' + C_{^3D_2}(p^2 + p'^2). \end{aligned} \tag{3.73}$$

$\boldsymbol{\sigma}_1$ and $\boldsymbol{\sigma}_2$ are the spins of the respective nucleons in the interaction, and $\boldsymbol{\tau}_1$ and $\boldsymbol{\tau}_2$ are their respective isospin. The LECs, C_X, are indicated by which partial wave[8] they act in, e.g. $^1S_0$ or $^3S_1$. These potentials are the most important thing to remember and understand from this chapter going forward in the thesis.

[8]The quantum numbers of NN states will be described in detail in Chapter 4.

4

Scattering Theory

Scattering theory is roughly the theory about how a well-defined initial (quantum) state is transformed to a well-defined final state through the action of some interaction process. A scattering process can in general involve any number of particles in the initial and final state. However, the focus of this thesis is to describe the process of two nucleons scattering of each other, which is a process with two particles in the initial and final state. The description of two particle scattering can be reduced to the simpler problem of one particle scattering of a fixed potential.

First, one particle scattering of a fixed potential is considered to develop some intuition for the basic ingredients of scattering theory such as the S- and T- operators, the *scattering amplitude*, and the observable *cross section*. Furthermore, the relation between scattering operators and the system Hamiltonian is obtained from the Lippmann-Schwinger (LS) equation. It is shown that the two-particle scattering problem can be reduced to one particle scattering of a fixed potential by considering relative coordinates. Finally, the developed theory is applied to neutron-proton (np) scattering in χEFT. The content of this chapter is largely inspired by the book by J. R. Taylor, Ref. [33] as well as Chapter 6 in Ref. [34].

4.1 Cross Sections and the S-operator

An important observable in particle scattering experiments is the *differential cross section*, $d\sigma$. A scattering experiment typically has two important measurable quantities; the incoming flux of particles, j_{in} [$\text{s}^{-1}\text{m}^{-2}$], and the number of particles per unit time that end up in a region of solid angle $d\Omega$, N_{out} [s^{-1}]. From these quantities the differential cross section is defined as

$$d\sigma \equiv \frac{N_{\text{out}} d\Omega}{j_{\text{in}}}, \implies \frac{d\sigma}{d\Omega} = \frac{N_{\text{out}}}{j_{\text{in}}}. \tag{4.1}$$

The *total cross section*, σ [m^2][1], is defined as the integral of the differential cross section over all solid angles,

$$\sigma \equiv \int d\Omega \, \frac{d\sigma}{d\Omega}. \tag{4.2}$$

[1] A common unit to use for the cross section is *barn*, which is defined as 1 barn = 10^{-28} m^2.

The goal of non-relativistic scattering theory is to compute observables, e.g. differential cross sections Eq. (4.1), using quantum mechanics.

A quantum mechanical system consisting of one particle with mass m with canonical coordinates $(\boldsymbol{r}, \boldsymbol{p})$ that is subject to some interaction potential, $V(\boldsymbol{r})$, is described by the Hamiltonian

$$H = H_0 + V(\boldsymbol{r}), \quad H_0 = \frac{\boldsymbol{p}^2}{2m}. \tag{4.3}$$

The Hilbert space of states for this system is denoted $\mathscr{H}$. To be able to treat this as a scattering problem a necessary assumption is that the potential is strong in a fairly small region in space compared to the length-scale of the experiment, and that the potential goes to zero sufficiently fast[2] as $|\boldsymbol{r}| \to \infty$. Assume from now on that these assumptions hold. The general solution to the time-dependent Schrödinger equation can be written as

$$|\psi(t)\rangle = U(t)\,|\psi\rangle \equiv e^{-iHt}\,|\psi\rangle\,, \tag{4.4}$$

where $U(t)$ is the time evolution operator, $|\psi(t)\rangle \in \mathscr{H}$ is the state of the system at time t and $|\psi\rangle \in \mathscr{H}$ is the state of the system at time $t = 0$. The time parameter is chosen such that the particle is in the vicinity of the region of non-zero potential around time $t = 0$. This choice of time parameter implies that at times $t_i \approx -\infty$ and $t_f \approx \infty$ the time evolution operator $U(t)$ will approximately be the time evolution operator for the free particle $U_0(t) \equiv e^{-iH_0 t}$, since $V \approx 0$ at these times.

The evolution $U(t)\,|\psi\rangle$ can be thought of as a trajectory in $\mathscr{H}$, much like a classical trajectory of a particle in three-dimensional space. The fact that the evolution resembles free evolution for early and late times can be quantified by $U(t)\,|\psi\rangle$ is approaching a *free particle asymptote* as $t \to \pm\infty$:

$$\lim_{t\to-\infty} \|U(t)\,|\psi\rangle - U_0(t)\,|\psi_{\text{in}}\rangle\| = 0, \tag{4.5}$$

$$\lim_{t\to+\infty} \|U(t)\,|\psi\rangle - U_0(t)\,|\psi_{\text{out}}\rangle\| = 0. \tag{4.6}$$

$|\psi_{\text{in}}\rangle$, $|\psi_{\text{out}}\rangle \in \mathscr{H}$ are some states defined at time $t = 0$. The norm $\|\cdot\|$ is defined for any $|\phi\rangle \in \mathscr{H}$ as $\||\phi\rangle\| \equiv \sqrt{\langle\phi|\phi\rangle}$. For an illustration see Fig. 4.1. One can prove that these asymptotes exist for relevant potentials, see Ref. [33]. Using that result, operators $\Omega_\pm$ can be defined as follows:

$$|\psi\rangle = \lim_{t\to-\infty} U^\dagger(t)U_0(t)\,|\psi_{\text{in}}\rangle \equiv \Omega_+\,|\psi_{\text{in}}\rangle\,, \tag{4.7}$$

$$|\psi\rangle = \lim_{t\to\infty} U^\dagger(t)U_0(t)\,|\psi_{\text{out}}\rangle \equiv \Omega_-\,|\psi_{\text{out}}\rangle\,. \tag{4.8}$$

These operators are called *Møller operators*, and relate the actual state of the scattered particle at time $t = 0$ to the in- and outgoing asymptotic states of the system.

[2]We will not bother to go into the mathematical details, the interested reader can consult Ref. [33].

Using the definitions in Eq. (4.8) one can show that the operators $\Omega_\pm$ are *isometric*, and hence satisfy $\Omega_\pm^\dagger \Omega_\pm = \mathrm{id}$ which gives the relation

$$|\psi_{\mathrm{out}}\rangle = \Omega_-^\dagger \Omega_+ |\psi_{\mathrm{in}}\rangle \,. \tag{4.9}$$

The *scattering operator, S,* is defined as

$$S \equiv \Omega_-^\dagger \Omega_+, \tag{4.10}$$

and contains all the observable information of the scattering process, since only the asymptotic states are observable. The S-operator is directly related to the probability of observing a particular out asymptote $|\phi\rangle$ given an in asymptote $|\chi\rangle$ which is denoted $\mathrm{pr}(\chi \to \phi)$. The probability is, as usual, given by the Born rule but for the *actual states* of the system at $t = 0$ corresponding to the given asymptotes. The relation reads

$$\mathrm{pr}(\chi \to \phi) = \left| \langle \phi | \, \Omega_-^\dagger \Omega_+ \, |\chi\rangle \right|^2 = |\langle \phi | S | \chi \rangle|^2 \,. \tag{4.11}$$

The *probability amplitude* for the scattering process, $\langle \phi | S | \chi \rangle$, is called an *$S$-matrix element*[3].

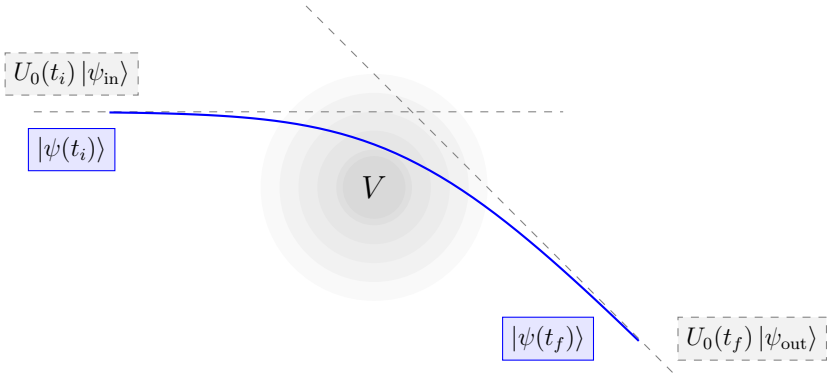

Figure 4.1: An illustration of how the quantum state $|\psi(t)\rangle$ (blue solid line) of the system approaches asymptotic quantum states, $U_0(t_i)\,|\psi_{\mathrm{in}}\rangle$ and $U_0(t_f)\,|\psi_{\mathrm{out}}\rangle$ (grey dashed lines) for early- and late times t_i, t_f. For times where $|\psi(t)\rangle$ are far away from the range of the potential V the evolution will resemble the evolution of the free Hamiltonian.

4.2 The Lippmann-Schwinger Equation

In this section, the on-shell T-operator will be defined and related to the S-operator. From the definition of the Møller operators the following relation can be derived [33],

$$\Omega_\pm^\dagger H \Omega_\pm = H_0. \tag{4.12}$$

[3]The term S-operator is synonymous with S-matrix in the literature and these terms are often used interchangeably.

Using this one can show that $[S, H_0] = 0$, which means that the energy is conserved in the scattering process. To exploit this symmetry, the scattering operator is evaluated for eigenstates $|\boldsymbol{p}\rangle$ of H_0, which satisfy

$$H_0 |\boldsymbol{p}\rangle = \frac{\boldsymbol{p}^2}{2m} |\boldsymbol{p}\rangle , \quad E_{\boldsymbol{p}} \equiv \frac{\boldsymbol{p}^2}{2m}, \tag{4.13}$$

where $\boldsymbol{p}$ is the momentum, and the states are normalized as

$$\langle \boldsymbol{p}' | \boldsymbol{p} \rangle = \delta^{(3)}(\boldsymbol{p}' - \boldsymbol{p}). \tag{4.14}$$

Conservation of energy gives the following constraint on the S-matrix elements

$$0 = \langle \boldsymbol{p}' | [S, H_0] | \boldsymbol{p} \rangle = (E_{\boldsymbol{p}} - E_{\boldsymbol{p}'}) \langle \boldsymbol{p}' | S | \boldsymbol{p} \rangle . \tag{4.15}$$

The T-operator is defined in terms of the following decomposition of the S-operator,

$$\langle \boldsymbol{p}' | S | \boldsymbol{p} \rangle \equiv \delta^{(3)}(\boldsymbol{p}' - \boldsymbol{p}) - 2\pi i \delta(E_{\boldsymbol{p}'} - E_{\boldsymbol{p}}) T(\boldsymbol{p}', \boldsymbol{p}). \tag{4.16}$$

The notation $T(\boldsymbol{p}', \boldsymbol{p}) \equiv \langle \boldsymbol{p}' | T | \boldsymbol{p} \rangle$ is introduced for convenience, and will be used for more operators than just T. The decomposition in Eq. (4.16) is convenient since it separates the parts of the S-matrix that correspond to trivial and non-trivial interactions, where the latter is governed by the T-operator. The T-operator is directly linked to the differential cross section as [33]

$$\frac{d\sigma}{d\Omega}(\boldsymbol{p} \to \boldsymbol{p}') = \left(\frac{m}{2\pi} \right)^2 \left| T(\boldsymbol{p}', \boldsymbol{p}) \right|^2 . \tag{4.17}$$

This equation encodes the important link between the quantum description and the experimentally observable differential cross section. For a given potential it is possible to compute the T-operator, since it can be shown that the T-operator satisfies the *Lippmann-Schwinger equation*

$$T(\boldsymbol{p}', \boldsymbol{p}) = V(\boldsymbol{p}', \boldsymbol{p}) + \int d^3\boldsymbol{k} \; V(\boldsymbol{p}', \boldsymbol{k}) \frac{2m}{\boldsymbol{p}^2 - \boldsymbol{k}^2 + i\epsilon} T(\boldsymbol{k}, \boldsymbol{p}), \tag{4.18}$$

where $\lim_{\epsilon \to 0}$ is implicit, as usual, and will amount to evaluate the *Cauchy principal value* of the integral [33].

In the case where the particle of interest has other degrees of freedom (e.g. in the case of nucleons; spin and isospin) the only thing that will change is that $T(\boldsymbol{p}', \boldsymbol{p})$ and $V(\boldsymbol{p}', \boldsymbol{p})$ will be operators on the Hilbert space of those degrees of freedom as well. By using symmetries, the T-, S- and V- operators can be further decomposed for these additional degrees of freedom completely analogous to Eq. (4.15). Such an analysis is described in further detail in Section 4.4.

4.3 Two-Particle Scattering

The theory introduced in the previous section will be applied to the case where two massive particles are scattered of each other through a mutual interaction potential.

A two-particle system with masses and canonical coordinates given by $(m_i, \boldsymbol{r}_i, \boldsymbol{p}_i)$, $i = 1, 2$, are described by the Hamiltonian

$$H = \frac{\boldsymbol{p}_1^2}{2m_1} + \frac{\boldsymbol{p}_2^2}{2m_2} + V_{12}(\boldsymbol{r}_1 - \boldsymbol{r}_2), \tag{4.19}$$

where the interaction potential V_{12} is assumed to be local and transitionally invariant, just depending on the relative position of the particles; $\boldsymbol{r}_{\text{rel}} \equiv \boldsymbol{r}_1 - \boldsymbol{r}_2$. The state space for the composite system will be the the tensor product of the individual Hilbert spaces for the two particles $\mathscr{H}_1$ and $\mathscr{H}_2$;

$$\mathscr{H}_{12} \equiv \mathscr{H}_1 \otimes \mathscr{H}_2. \tag{4.20}$$

By introducing new momentum coordinates $(\bar{\boldsymbol{p}}, \boldsymbol{p}_{\text{rel}})$ defined by

$$\bar{\boldsymbol{p}} \equiv \boldsymbol{p}_1 + \boldsymbol{p}_2, \quad \boldsymbol{p}_{\text{rel}} \equiv \frac{m_2\boldsymbol{p}_1 - m_1\boldsymbol{p}_2}{m_1 + m_2}, \tag{4.21}$$

and defining the total- and reduced mass of the two-particle system as

$$M = m_1 + m_2, \quad m = \frac{m_1 m_2}{m_1 + m_2}, \tag{4.22}$$

the Hamiltonian in Eq. (4.19) can be written

$$H = \frac{\bar{\boldsymbol{p}}^2}{2M} + \left[\frac{\boldsymbol{p}_{\text{rel}}^2}{2m} + V_{12}(\boldsymbol{r}_1 - \boldsymbol{r}_2)\right] \equiv H_{\text{cm}} + H_{\text{rel}}. \tag{4.23}$$

$\boldsymbol{p}_{\text{rel}}$ can be shown to be the canonical conjugate to $\boldsymbol{r}_{\text{rel}} \equiv \boldsymbol{r}_1 - \boldsymbol{r}_2$, which means that the Hilbert space can be factored as [33]

$$\mathscr{H}_{12} = \mathscr{H}_{\text{cm}} \otimes \mathscr{H}_{\text{rel}}. \tag{4.24}$$

Since the Hamiltonian decomposes onto a part just acting on $\mathscr{H}_{\text{cm}}$ and one acting on $\mathscr{H}_{\text{rel}}$, the corresponding time-evolution operator will decompose as [33]

$$U(t) = e^{-iH_{\text{cm}}t} \otimes e^{-iH_{\text{rel}}t}. \tag{4.25}$$

Due to conservation of momentum[4], the corresponding scattering operator reads

$$S = \text{id}_{\text{cm}} \otimes S_{\text{rel}}, \tag{4.26}$$

where S_{rel} is the one-particle scattering operator computed from H_{rel} [33].

Finally, one finds that the S-matrix elements of the two-particle Hamiltonian in Eq. (4.19) can be decomposed as

$$\langle \boldsymbol{p}_1', \boldsymbol{p}_2' | S | \boldsymbol{p}_1, \boldsymbol{p}_2 \rangle = \delta^3(\bar{\boldsymbol{p}}' - \bar{\boldsymbol{p}}) \, \langle \boldsymbol{p}_{\text{rel}}' | S_{\text{rel}} | \boldsymbol{p}_{\text{rel}} \rangle \,, \tag{4.27}$$

[4] $[\bar{\boldsymbol{p}}, H] = 0$ since H does not depend on the canonical conjugate to $\bar{\boldsymbol{p}}$.

where $(\boldsymbol{p}_1, \boldsymbol{p}_2)$ and $(\boldsymbol{p}'_1, \boldsymbol{p}'_2)$ denotes the ingoing and outgoing momenta respectively. $\boldsymbol{p}_{\text{rel}}$ and $\boldsymbol{p}'_{\text{rel}}$ are the relative momenta (see Eq. (4.21)) for the primed and unprimed coordinates.

The conclusion is that the two-particle scattering problem is reduced to the one-particle scattering problem of relative momenta with Hamiltonian H_{rel}. As a last note, when $\boldsymbol{p}_1$ and $\boldsymbol{p}_2$ are expressed in the laboratory frame, $\boldsymbol{p}_{\text{rel}}$ will also be in the laboratory frame. Since the Hamiltonian H_{rel} is *Galilean invariant* one can choose to describe the system in the center-of-mass frame where the expressions simplifies since $\boldsymbol{p}_1 = -\boldsymbol{p}_2$.

4.4 Nucleon-Nucleon Scattering

The last part of this chapter will be devoted to nucleon-nucleon (NN) scattering utilizing the theory developed previously in this chapter. Specifically neutron-proton (np) scattering will be the focus, see Fig. 4.2 for an illustration.

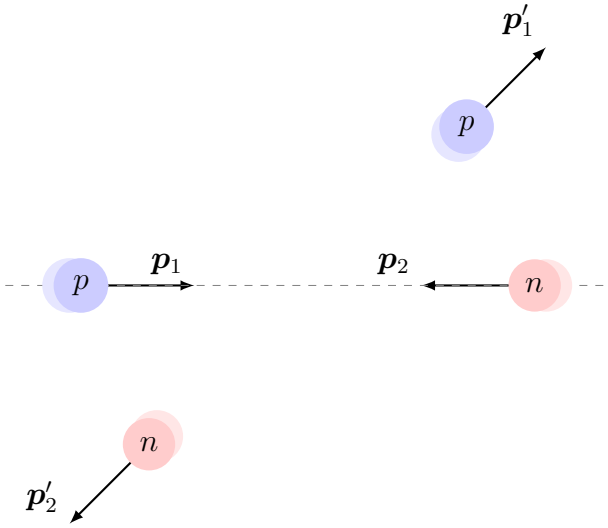

Figure 4.2: Kinematics of np scattering in the center-of-mass frame. $(\boldsymbol{p}_1, \boldsymbol{p}_2)$ and $(\boldsymbol{p}'_1, \boldsymbol{p}'_2)$ denotes the ingoing and outgoing momenta, respectively, for the proton (p) and neutron (n) in the center-of-mass frame.

4.4.1 Nucleon-Nucleon System

The Hilbert space of a single nucleon, denoted by $\mathscr{H}$, consists of three parts;

$$\mathscr{H} \equiv \mathscr{H}^{\text{space}} \otimes \mathscr{H}^{\text{spin}} \otimes \mathscr{H}^{\text{isospin}}, \tag{4.28}$$

where the nucleon has spin and isospin $\frac{1}{2}$. The Hilbert space of two nucleons, denoted $\mathscr{H}_{12}$, is the tensor product of the Hilbert spaces of the two individual nucleons, $\mathscr{H}_{12} = \mathscr{H}_1 \otimes \mathscr{H}_2$. In the previous section it was shown that only the relative motion is relevant for scattering, since the S-operator decomposes as Eq. (4.27). Thus, the

NN-scattering problem can conveniently be described in the center-of-mass frame. The two-nucleon Hilbert space reads

$$\mathscr{H}_{12} = \mathscr{H}^{\text{cm. space}} \otimes \mathscr{H}^{\text{rel. space}} \otimes \mathscr{H}_1^{\text{spin}} \otimes \mathscr{H}_2^{\text{spin}} \otimes \mathscr{H}_1^{\text{isospin}} \otimes \mathscr{H}_2^{\text{isospin}} \tag{4.29}$$

$$\equiv \mathscr{H}^{\text{cm. space}} \otimes \mathscr{H}_{\text{NN}}, \tag{4.30}$$

with the space part decomposed in center-of-mass and relative part. The scattering problem is reduced to the scattering problem where a NN two-particle state[5] $|\psi_{\text{NN}}\rangle \in \mathscr{H}_{\text{NN}}$ is scattered through the Hamiltonian

$$H = \frac{\boldsymbol{p}_{\text{rel}}^2}{2m_N} + V_{\text{NN}} \equiv H_0 + V_{\text{NN}}, \tag{4.31}$$

where m_N is the reduced mass of the two nucleons, $\boldsymbol{p}_{\text{rel}}$ is the relative momentum of the two nucleons (see Eq. (4.21)) and V_{NN} is a NN potential. Since all coordinates from now on will be relative, the subscript *rel* will be dropped. The potentials that will be considered are $V_{\text{NN}} \in \{V_{\text{WPC}}^{[\text{LO}]}, V_{\text{MWPC}}^{[\text{LO}]}\}$; see Chapter 3.

Since the nucleons have both spin and isospin degrees of freedom the Hilbert space $\mathscr{H}_{\text{NN}}$ is a bit more complicated than the relative Hilbert space in the previous section, see Eq. (4.24). Basis states for $\mathscr{H}_{\text{NN}}$ can be formed by tensor products of basis states for the individual Hilbert spaces as

$$|\boldsymbol{p}, s_1, m_{s_1}, s_2, m_{s_2}, t_1, t_{z1}, t_2, t_{z2}\rangle \equiv \tag{4.32}$$

$$|\boldsymbol{p}\rangle \otimes |s_1, m_{s_1}\rangle \otimes |s_2, m_{s_2}\rangle \otimes |t_1, t_{z1}\rangle \otimes |t_2, t_{z2}\rangle \tag{4.33}$$

where $|s_i, m_{s_i}\rangle$ are basis states for $\mathscr{H}_i^{\text{spin}}$ and $|t_i, t_{zi}\rangle$ are basis states for $\mathscr{H}_i^{\text{isospin}}$, $i = 1, 2$. Consequently, $s_1 = s_2 = t_1 = t_2 = \frac{1}{2}$, and the projections m_{s_i} and t_{zi} take values $\pm\frac{1}{2}$. The spin- and isospin operators for the two nucleons are denoted[6]

$$\boldsymbol{S}_1, \boldsymbol{S}_2, \boldsymbol{T}_1, \boldsymbol{T}_2, \tag{4.34}$$

respectively. The total spin- and isospin operators are defined as

$$\boldsymbol{S} \equiv \boldsymbol{S}_1 + \boldsymbol{S}_2, \quad \boldsymbol{T} \equiv \boldsymbol{T}_1 + \boldsymbol{T}_2. \tag{4.35}$$

Using the theory of spin addition, see e.g. Ref. [34], the spin states of the two nucleons $|s_1, m_{s_1}\rangle \otimes |s_2, m_{s_2}\rangle$ are related to the total spin, s, and total spin projection, m_s, through the Clebsch-Gordan coefficients[7], $C^{s,m_s}_{s_1,s_2;m_{s_1}m_{s_2}}$,

$$|s, m_s\rangle = \sum_{m_{s_1}, m_{s_2}} C^{s,m_s}_{s_1,s_2;m_{s_1}m_{s_2}} |s_1, m_{s_1}\rangle \otimes |s_2, m_{s_2}\rangle . \tag{4.36}$$

[5] In the same way as in the previous section the state $|\psi_{\text{NN}}\rangle$ can be thought of as a one-particle state described by the relative one-particle Hamiltonian Eq. (4.31).

[6] Spin, isospin and angular momentum operators, e.g. $\boldsymbol{S}, \boldsymbol{T}, \boldsymbol{J}, \boldsymbol{L}$ are denoted by bold-face uppercase letters to not confuse with other operators. The corresponding quantum numbers to an operator is denote with the same lowercase letter.

[7] For general angular momentum states $|j_1, m_1\rangle , |j_2, m_2\rangle$ and $|j, m\rangle$ the Clebsch-Gordan coefficients are defined as follows. The matrix denotes the so called Wigner $3j$-symbol, which will also be used later [34].

$$C^{j,m}_{j_1,j_2;m_1m_2} \equiv \langle j_1, j_2; m_1m_2 | j_1j_2; jm\rangle = (-1)^{j_1-j_2+m}\sqrt{2j+1}\begin{pmatrix} j_1 & j_2 & j \\ m_1 & m_2 & -m \end{pmatrix}.$$

The total spin, s, can take the values $s \in \{0, 1\}$ and the spin-projection $m_s \in \{-1, 0, 1\}$. The situation is completely analogous for isospin, where the total isospin is denoted t, with total isospin projection t_z. Hence, an equivalent and more convenient set of basis states than the ones in Eq. (4.33) are of the form

$$|\boldsymbol{p}, s, m_s, t, t_z\rangle \,. \tag{4.37}$$

The orbital angular momentum operator is denoted $\boldsymbol{L}$ and the total angular momentum operator, $\boldsymbol{J}$, is defined as

$$\boldsymbol{J} \equiv \boldsymbol{L} + \boldsymbol{S}. \tag{4.38}$$

Simultaneous energy- and angular-momentum eigenstates, $|p, l, m_l\rangle$, are defined to satisfy the relations

$$H_0 \,|p, l, m_l,\rangle = \frac{p^2}{2m_N} \,|p, l, m_l\rangle \,, \quad E_p \equiv \frac{p^2}{2m_N}, \tag{4.39}$$

$$\boldsymbol{L}^2 \,|p, l, m_l\rangle = l(l+1) \,|p, l, m_l\rangle \,, \tag{4.40}$$

$$\boldsymbol{L}_z \,|p, l, m_l\rangle = m_l \,|p, l, m_l\rangle \,. \tag{4.41}$$

Momentum eigenstates $|\boldsymbol{p}\rangle$ are related to $|p, l, m_l\rangle$ as

$$|\boldsymbol{p}\rangle = \sum_{l=0}^{\infty} \sum_{m_l=-l}^{l} \frac{1}{\sqrt{m_N p}} Y_l^{m_l^*}(\hat{\boldsymbol{p}}) \,|p, l, m_l\rangle \,, \tag{4.42}$$

where $p \equiv |\boldsymbol{p}|$ and $\hat{\boldsymbol{p}} \equiv \boldsymbol{p}/|\boldsymbol{p}|$ [34]. Coupling $\boldsymbol{L}$ and $\boldsymbol{S}$ analogous to coupling $\boldsymbol{S}_1$ and $\boldsymbol{S}_2$ in Eq. (4.36) gives basis states of the from

$$|p, j, s, l, m_j, t, t_z\rangle \,. \tag{4.43}$$

Such a basis is referred to as a *partial wave* basis. For the special case of np scattering, the states satisfy $t_z = 0$. Since these states will be the ones considered from now on, t_z will be omitted.

The LS equation for obtaining T-matrix elements reads

$$T(\boldsymbol{p}', \boldsymbol{p}) = V_{\mathrm{NN}}(\boldsymbol{p}', \boldsymbol{p}) + \int d^3\boldsymbol{k} \; V_{\mathrm{NN}}(\boldsymbol{p}', \boldsymbol{k}) \frac{2m_N}{\boldsymbol{p}^2 - \boldsymbol{k}^2 + i\epsilon} T(\boldsymbol{k}, \boldsymbol{p}), \tag{4.44}$$

where the same notation as in Eq. (4.18) for operators T and V sandwiched between momentum states are used; $T(\boldsymbol{p}', \boldsymbol{p}) \equiv \langle \boldsymbol{p}'|T|\boldsymbol{p}\rangle$. The crucial difference now, compared to the spinless case, is that both $V(\boldsymbol{p}', \boldsymbol{p})$ and $T(\boldsymbol{p}', \boldsymbol{p})$ are operators in the remaining parts of the NN Hilbert space—namely the total spin and total isospin parts. By doing a *partial wave decomposition* Eq. (4.44) will be converted from the basis states in Eq. (4.33) to the basis states in Eq. (4.43). An important reservation is that Eq. (4.44) will change slightly when including regulators and relativistic corrections in later sections.

4.4.2 Symmetries

As seen in the previous section, basis states for a general NN state $|\psi_{\text{NN}}\rangle \in \mathscr{H}_{\text{NN}}$ can be taken to be

$$|p, j, l, s, m_j, t, t_z\rangle\,, \tag{4.45}$$

where $t_z = 0$ from now on is omitted, since a neutron-proton state is of interest. Since nucleons are fermions, the total two-particle state should be anti-symmetric under particle exchange. This amounts to the constraint

$$(-1)^{l+s+t} = -1. \tag{4.46}$$

The dynamical symmetries of the NN scattering problem comes from the operators that commute with the Hamiltonian in Eq. (4.31) [33]. For the nucleon-nucleon potentials used in this thesis (see. Eq. (3.72) and Eq. (3.73)), one can show that the Hamiltonian commutes with the total isospin operator, $\boldsymbol{T}$, total angular momentum operator, $\boldsymbol{J}$, and parity operator, $\hat{\mathcal{P}}$:

$$[\boldsymbol{J}, H] = 0 \implies j \text{ and } m_j \text{ are conserved}, \tag{4.47}$$
$$[\boldsymbol{T}, H] = 0 \implies t \text{ and } t_z \text{ are conserved}, \tag{4.48}$$
$$[\hat{\mathcal{P}}, H] = 0 \implies \text{ parity is conserved}. \tag{4.49}$$

These conservation laws set constraints on S-matrix elements;

$$\langle p', j', l', s', m_j', t'|S|p, j, l, s, m_j, t\rangle\,, \tag{4.50}$$

in analogy with the example in Eq. (4.15). By combining Eq. (4.46) with isospin and parity conservation one gets the constraint

$$\Delta s \equiv s' - s = \text{ even}. \tag{4.51}$$

Since $s, s' \in \{0, 1\}$, it implies that $\Delta s = 0$ and total spin is also conserved. For the non-zero S-matrix elements the notation $S_{l'l}^{j,s,t}(p', p)$ is used which is defined by

$$\begin{aligned}&\langle p', j', l', s', m_j', t'|S|p, j, l, s, m_j, t\rangle \equiv \\ &\equiv \delta_{j'j}\delta_{s's}\delta_{t't}\delta_{m_j'm_j}\,\langle p', l'|S^{j,s,t}|p, l\rangle \equiv \delta_{j'j}\delta_{s's}\delta_{t't}\delta_{m_j'm_j}S_{l'l}^{j,s,t}(p', p).\end{aligned} \tag{4.52}$$

The convention is that conserved quantum numbers, $\{j, s, t\}$, are superscripts while non-conserved ones are subscripts. The same notation will be used later for the T-operator and the potential. There is no m_j index on S, since the matrix element cannot depend on the projection quantum number by the Wigner-Eckart Theorem [34] (the same is true for t_z). By the constraint in Eq. (4.46), isospin can be omitted in the notation, since it becomes fixed by the other quantum numbers. However, even if t is not explicitly written out, S-matrix elements in general still depends on t.

4.4.3 Regularization and Relativistic Corrections

The LS-equation, Eq. (4.44), is an integral equation over the momentum $\boldsymbol{k}$. Depending on the form of the potential, the integral might diverge, which is a problem that requires some kind of regularization and renormalization. However, even if the integral equation does not diverge, when solving the equation numerically one needs to truncate the integral at some maximum momentum, due to computational reasons. This means that regularization and renormalization is important in either case.

The momentum cutoff is usually implemented by modifying the potential with an exponential factor of the form [26]

$$V_{\mathrm{NN}}(\boldsymbol{p}', \boldsymbol{p}) \mapsto V_{\mathrm{NN}}(\boldsymbol{p}', \boldsymbol{p}) \exp\left[-\left(\frac{p'}{\Lambda}\right)^6 - \left(\frac{p}{\Lambda}\right)^6\right], \tag{4.53}$$

where $p' = |\boldsymbol{p}'|$ and $p = |\boldsymbol{p}|$ denotes the modulus of the momenta[8]. Λ is a constant called the *cutoff* (see the discussion in Section 2.4), which in principle could be chosen arbitrarily above the pion mass, but there are of course also constraints due to computational reasons. There are discussions in the literature on how this cutoff should best be treated; see e.g. [9], [35], [36]. The reason not to impose a so-called *hard* momentum cutoff in the form of a step function is that the exponential factor smooths out the cutoff, which is more numerically stable [37].

So far in this chapter the treatment of the scattering problem has been completely non-relativistic. Let us therefore briefly discuss relativistic corrections. In short, the approach taken in this thesis can be summarized by the following steps:

1. Construct an effective leading-order Lagrangian for nucleons and pions by considering non-relativistic limit using the heavy-baryon formalism.

2. Use an appropriate power counting (WPC or MWPC) to construct a nucleon-nucleon potential by considering the lowest order Feynman diagrams in the QFT scattering process.

3. Disregard the QFT origin and use the nucleon-nucleon potential in the non-relativistic description of two-particle scattering.

4. Obtain the scattering amplitude for nucleon-nucleon scattering by solving the LS equation, and use scattering theory to relate the T-matrix to relevant observables.

This approach is convenient since the different steps have a well-defined input and output. For example, all you need to know from steps 1-2 to continue in step 3 is the potential, and you can forget about the details that went into the derivation. The downside is of course that it is hard to track the impact of certain assumptions on the end result.

[8] In general the exponent is chosen as $2n$, for some $n = 1, 2, \ldots$. Here, $n = 3$ is chosen.

To see how relativistic corrections can be incorporated in the description used in this thesis, one can take a look at another approach. This approach is described in Ref. [26], and in more detail in Refs. [2], [3]. One starts with the Bethe-Salpeter equation [38] describing the two nucleon scattering process in QFT,

$$\mathcal{M} = \mathcal{V} + \mathcal{V}\mathcal{G}\mathcal{M}, \tag{4.54}$$

just as in chapter Chapter 3. The non-relativistic reduction of the Lagrangian used for calculating these diagrams is not needed up until this point. Since this equation is expressed in four-dimensional Minkowski space it is very hard to solve without making some approximations. Blankenbeckler and Sugar proposed an approach which is widely used, making reasonable approximations to both the potential and the two-nucleon propagator [39]. Under these approximations, matrix elements between positive energy nucleons yield the following equation in momentum space

$$\bar{T}(\boldsymbol{p}', \boldsymbol{p}) = \bar{V}(\boldsymbol{p}', \boldsymbol{p}) + \int \frac{d^3\boldsymbol{k}}{(2\pi)^3} \bar{V}(\boldsymbol{p}', \boldsymbol{k}) \frac{4m_N^2}{E_k} \frac{1}{\boldsymbol{p}^2 - \boldsymbol{k}^2 + i\epsilon} \bar{T}(\boldsymbol{k}, \boldsymbol{p}). \tag{4.55}$$

Here, the spin and isospin indices are suppressed. By doing the so-called minimal relativity transformations

$$\bar{V}(\boldsymbol{p}', \boldsymbol{p}) \mapsto V(\boldsymbol{p}', \boldsymbol{p}) = \frac{1}{(2\pi)^3} \sqrt{\frac{2m_N}{E_{p'}}} \bar{V}(\boldsymbol{p}', \boldsymbol{p}) \sqrt{\frac{2m_N}{E_p}}, \tag{4.56}$$

$$\bar{T}(\boldsymbol{p}', \boldsymbol{p}) \mapsto T(\boldsymbol{p}', \boldsymbol{p}) = \frac{1}{(2\pi)^3} \sqrt{\frac{2m_N}{E_{p'}}} \bar{T}(\boldsymbol{p}', \boldsymbol{p}) \sqrt{\frac{2m_N}{E_p}}, \tag{4.57}$$

Eq. (4.55) reduces to the standard LS equation:

$$T(\boldsymbol{p}', \boldsymbol{p}) = V(\boldsymbol{p}', \boldsymbol{p}) + \int d^3\boldsymbol{k}\; V(\boldsymbol{p}', \boldsymbol{k}) \frac{2m_N}{\boldsymbol{p}^2 - \boldsymbol{k}^2 + i\epsilon} T(\boldsymbol{k}, \boldsymbol{p}), \tag{4.58}$$

Here, T is the usual non-relativistic T-matrix and V is the the NN potential with the additional factors from Eq. (4.56), see Ref. [26].

The takeaway from this procedure is that relativistic corrections can be included in the non-relativistic LS-equation by doing the minimal relativity transformations. This effectively transforms the non-relativistic description of the scattering problem, in terms of the LS equation, to an equation satisfying the relativistic equation Eq. (4.55).

Using these results, Eq. (4.44) will take the form

$$T(\boldsymbol{p}', \boldsymbol{p}) = V(\boldsymbol{p}', \boldsymbol{p}) + \int d^3\boldsymbol{k}\; V(\boldsymbol{p}', \boldsymbol{k}) \frac{2m_N}{\boldsymbol{p}^2 - \boldsymbol{k}^2 + i\epsilon} T(\boldsymbol{k}, \boldsymbol{p}), \tag{4.59}$$

$$V(\boldsymbol{p}', \boldsymbol{p}) = \frac{1}{(2\pi)^3} \sqrt{\frac{2m_N}{E_{p'}}} V_{\mathrm{NN}}(\boldsymbol{p}', \boldsymbol{p}) \sqrt{\frac{2m_N}{E_p}} \exp\left[-\left(\frac{p'}{\Lambda}\right)^6 - \left(\frac{p}{\Lambda}\right)^6 \right], \tag{4.60}$$

where both relativistic corrections and regulator function are included.

4.4.4 Partial Wave Decomposition

Expressing the LS equation (4.59), in the basis (4.45) is known as a partial wave decomposition. The S- and T-operators can be decomposed as in Eq. (4.52)

$$\langle p', j', l', s', m_j', t'|S|p, j, l, s, m_j, t\rangle \equiv \delta_{j'j}\delta_{s's}\delta_{t't}\delta_{m_j'm_j} S_{l'l}^{j,s}(p', p), \tag{4.61}$$

$$\langle p', j', l', s', m_j', t'|T|p, j, l, s, m_j, t\rangle \equiv \delta_{j'j}\delta_{s's}\delta_{t't}\delta_{m_j'm_j} T_{l'l}^{j,s}(p', p), \tag{4.62}$$

where the conserved quantum numbers are indicated by superscripts, and the total isospin is constrained by Eq. (4.46) and therefore omitted. Sometimes, the Kronecker deltas are not explicitly written out due to notational convenience. Only neutron-proton scattering is considered here, therefore t_z is always zero and hence omitted.

The relevant potentials V_{NN} that are considered in Eq. (4.60) are $V_{\text{WPC}}^{[\text{LO}]}$ and $V_{\text{MWPC}}^{[\text{LO}]}$, see Chapter 3. Since the relativistic corrections and regulator part of Eq. (4.60) only depend on the magnitude of the momenta, p and p', they are already in the correct basis and do not need to be considered. The counterterms with LECs that appear in both $V_{\text{WPC}}^{[\text{LO}]}$ and $V_{\text{MWPC}}^{[\text{LO}]}$ are also in in the correct basis, acting in well-defined partial waves. The part of the potentials that need to be considered in the basis change is the one-pion-exchange (OPE) potential

$$V_{\text{OPE}}(\boldsymbol{p}', \boldsymbol{p}) = -\frac{g_A^2}{4f_\pi^2}\frac{(\boldsymbol{\sigma}_1 \cdot \boldsymbol{q})(\boldsymbol{\sigma}_2 \cdot \boldsymbol{q})}{\boldsymbol{q}^2 + m_\pi^2}\left(\boldsymbol{\tau}_1 \cdot \boldsymbol{\tau}_2\right), \quad \boldsymbol{q} = \boldsymbol{p}' - \boldsymbol{p}, \tag{4.63}$$

see Eq. (3.72). By the same symmetry arguments used for the decomposition of S and T, the potential can be decomposed as

$$\langle p', j', l', s', m_j', t'|V|p, j, l, s, m_j, t\rangle \equiv \delta_{j'j}\delta_{s's}\delta_{t't}\delta_{m_j'm_j}(V_{\text{OPE}})_{l'l}^{j,s}(p', p). \tag{4.64}$$

Knowing how V_{OPE} acts in the naive basis (Eq. (4.33)), the partial wave potential matrix elements can be obtained by a basis transformation. For $|\Psi\rangle$ denoting a basis state in the naive basis this transformation can schematically be written by inserting the resolution of identity as

$$\begin{aligned}
&(V_{\text{OPE}})_{l'l}^{j,s}(p', p)\delta_{j'j}\delta_{s's}\delta_{t't}\delta_{m_j'm_j} = \langle p', j', l', s', m_j', t'|V|p, j, l, s, m_j, t\rangle = \\
&= \langle p', j', l', s', m_j', t'|\int d\Psi' \ |\Psi'\rangle\langle\Psi'|\, V_{\text{OPE}} \int d\Psi \ |\Psi\rangle\langle\Psi|\, |p, j, l, s, m_j, t\rangle = \\
&= \int d\Psi' \int d\Psi \ \langle p', j', l', s', m_j', t'|\Psi'\rangle\langle\Psi'|\, V_{\text{OPE}}\, |\Psi\rangle\langle\Psi|p, j, l, s, m_j, t\rangle\,.
\end{aligned} \tag{4.65}$$

The final expressions for the matrix elements $(V_{\text{OPE}})_{l'l}^{j,s}(p', p)$ are given in Ref. [40], and they are used in this thesis.

After all this work, the final version of the LS equation can be written down in the partial wave basis and reads [41]

$$T_{l'l}^{j,s}(p', p) = V_{l'l}^{j,s}(p', p) + \frac{2}{\pi}\sum_{l''}\int_0^\infty dk \ k^2 V_{l'l''}^{j,s}(p', k)\frac{2m_N}{p^2 - k^2 + i\epsilon}T_{l''l}^{j,s}(k, p), \tag{4.66}$$

where $V_{l'l}^{j,s}(p', p)$ is the potential V in Eq. (4.60) in which V_{NN} is decomposed into partial waves.

4.4.5 Phase Shifts from T-operator in Partial Wave Basis

In this section the form of the T-matrix will be discussed and related to the *phase shifts* parameterizing the S-matrix. Since $\boldsymbol{J}, \boldsymbol{L}$ and $\boldsymbol{S}$ satisfy the operator relation $\boldsymbol{J} = \boldsymbol{L} + \boldsymbol{S}$, the corresponding quantum numbers obey [34]

$$|j - s| \leq l \leq j + s. \tag{4.67}$$

It is convenient to think of $T^{j,s}_{l'l}$ as a matrix in $l'l$-space for a given set of (j, s). A few important cases will be identified.

Spin-singlet ($s = 0$) channels imply $l = j$ due to Eq. (4.67). Therefore, since j is conserved, so is l. In matrix form this can be expressed as

$$T^{j,s=0} = \begin{matrix} l = j \\ \begin{pmatrix} \star \end{pmatrix} \end{matrix} \begin{matrix} \\ l' = j \end{matrix} \tag{4.68}$$

where $\star$ denotes a non-zero *uncoupled* matrix element.

For spin-triplet ($s = 1$) channels there are two cases, where $\diamond$ denotes a non-zero *coupled* matrix element:

$$j > 0: \quad T^{j,s=1} = \begin{matrix} l = j-1 & l = j & l = j+1 \\ \begin{pmatrix} \diamond & 0 & \diamond \\ 0 & \star & 0 \\ \diamond & 0 & \diamond \end{pmatrix} \end{matrix} \begin{matrix} l' = j-1 \\ l' = j \\ l' = j+1 \end{matrix} \tag{4.69}$$

$$j = 0: \quad T^{j=0,s=1} = \begin{matrix} l = 0 & l = 1 \\ \begin{pmatrix} \star & 0 \\ 0 & \star \end{pmatrix} \end{matrix} \begin{matrix} l' = 0 \\ l' = 1 \end{matrix} \tag{4.70}$$

The non-zero elements are deduced from the constraint $\Delta l = l' - l = 0, 2$, which comes from parity conservation.

For an uncoupled channel, i.e. where $j = 0$ or $j > 0$ and $j = l = l'$, the phase shifts $\delta^{j,s}_l$ are easily computed from the relation[9] [41]

$$S = 1 - 4im_N pT \tag{4.71}$$

and read

$$S^{j,s}_l = e^{i2\delta^{j,s}_l} \implies \delta^{j,s}_l = \frac{1}{2i} \ln\left(1 - 4im_N pT^{j,s}_{ll}\right). \tag{4.72}$$

For a coupled channel the phase shifts can be parameterized by a 2×2 matrix, describing the $\diamond$-elements in Eq. (4.69). The Blatt-Biedenharn (BB) parametrization of the phase shifts $(\delta_-, \delta_+, \epsilon_j)$ are

$$S^{j,s=1} = U^{-1} \begin{pmatrix} e^{2i\delta^{j,s=1}_-} & 0 \\ 0 & e^{2i\delta^{j,s=1}_+} \end{pmatrix} U, \tag{4.73}$$

[9] The exact relation between S and T is heavily convention dependent. See e.g. Ref. [3].

where

$$U = \begin{pmatrix} \cos(\epsilon_j) & \sin(\epsilon_j) \\ -\sin(\epsilon_j) & \cos(\epsilon_j) \end{pmatrix}. \tag{4.74}$$

There is also the Stapp convention, $\left(\bar{\delta}_-^{j,s}, \bar{\delta}_+^{j,s}, \bar{\epsilon}_j\right)$, which are related to the BB phases by [42]

$$\bar{\delta}_-^{j,s} + \bar{\delta}_+^{j,s} = \delta_-^{j,s} + \delta_+^{j,s} \tag{4.75}$$

$$\sin\left(\bar{\delta}_-^{j,s} - \bar{\delta}_+^{j,s}\right) = \frac{\tan 2\bar{\epsilon}_j}{\tan 2\epsilon_j} \tag{4.76}$$

$$\sin\left(\delta_-^{j,s} - \delta_+^{j,s}\right) = \frac{\sin 2\bar{\epsilon}_j}{\sin 2\epsilon_j}. \tag{4.77}$$

In the coming chapter, the Stapp convention will be used, and the phase shifts will be referred to by spectroscopic notation: ${}^{(2s+1)}l_j$.

4.4.6 Cross Sections from Phase Shifts

After quite a detour, this final section will take us back to the beginning of the chapter by relating the phase shifts to cross sections. There are several different conventions and definitions of scattering operators that capture various important aspects. So far the S- and T- operators have been discussed.

So-called spin-observables are important in scattering experiments and are often written in terms of the M-operator,

$$M \equiv \frac{2\pi}{ip}\left(S - \mathrm{id}\right), \tag{4.78}$$

where p denotes the magnitude of the on-shell relative momentum, and S is the S-operator. Spin observables are expressed as the following matrix elements of M,

$$M^{s's}_{m'_s m_s}(\theta, \phi) \equiv \langle \boldsymbol{p}', s', m'_s | M | \boldsymbol{p}, s, m_s \rangle, \tag{4.79}$$

where M only depends on the angle, θ, between the incident ($\boldsymbol{p}$) and outgoing ($\boldsymbol{p}'$) relative momentum since S, and hence M, conserve energy. The azimuthal angle ϕ can be taken to be zero by considering the rotational symmetry of the problem along the incident momentum $\boldsymbol{p}$. For an illustration of the kinematics, see Fig. 4.3. In the potentials, V_{NN}, used in this thesis spin is also conserved ($s' = s$) which implies that $M^s_{m'_s m_s}(\theta, \phi) \equiv M^{s'=s,s}_{m'_s m_s}(\theta, \phi)$ are the relevant matrix elements.

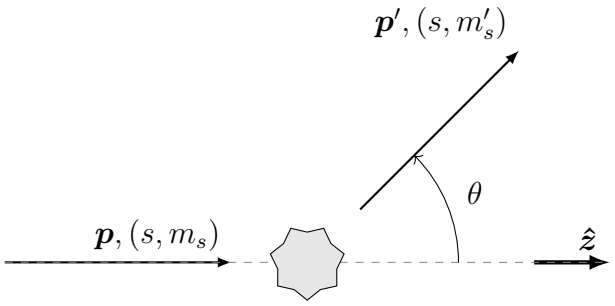

Figure 4.3: Kinematics of NN scattering in relative coordinates. The incoming state with relative momentum $\boldsymbol{p}$ and spin (s, m_s) is transformed, via the scattering interaction, to the outgoing state with relative momentum $\boldsymbol{p}'$ and spin (s, m_s'). θ is the angle between the ingoing and outgoing momenta and the azimuthal polar angle is conventionally taken to be zero, $\phi = 0$.

Following Ref. [42] the M-matrix elements can be related to the S-matrix elements, and hence the phase shifts, via the relation

$$M^s_{m_s' m_s}(\theta, \phi) = \frac{\sqrt{4\pi}}{2ip} \sum_{j,l,l'} i^{l-l'} (2j+1) \sqrt{2l+1}\; Y^{l'}_{m_s - m_s'}(\theta, \phi) \tag{4.80}$$

$$\cdot \begin{pmatrix} l' & s' & j \\ m_s - m_s' & m_s' & -m_s \end{pmatrix} \cdot \begin{pmatrix} l & s & j \\ 0 & m_s & -m_s \end{pmatrix} \tag{4.81}$$

$$\cdot \langle l' | S^{j,s} - 1 | l \rangle \,. \tag{4.82}$$

$Y^l_m(\theta, \phi)$ is the usual spherical harmonics and the matrices denotes the Wigner $3j$-symbols, see e.g. [34]. The sum over j, l, l' includes $j = 0, 1, ...$ and for each j the allowed l's are summed over. In practice, this sum is truncated at some maximum j denoted $j_{\max}$.

To compute the total np-scattering cross section, σ^{tot}_{np}, from the M-matrix elements the so-called Scalay-amplitudes can be used [41]. If only the total cross section is sought after, the *optical theorem* can offer a helping hand giving [41]

$$\sigma^{\text{tot}}_{np} = \frac{2\pi}{p} \,\text{Im}\left[a(\theta = 0, \phi = 0) + b(\theta = 0, \phi = 0)\right], \tag{4.83}$$

where

$$a(\theta, \phi) = \frac{1}{2}\left(M^1_{1,1}(\theta, \phi) + M^1_{0,0}(\theta, \phi) + M^1_{1,-1}(\theta, \phi)\right), \tag{4.84}$$

$$b(\theta, \phi) = \frac{1}{2}\left(M^1_{1,1}(\theta, \phi) + M^0_{0,0}(\theta, \phi) + M^1_{1,-1}(\theta, \phi)\right). \tag{4.85}$$

The magnitude of the relative momentum, p, of the ingoing state for np-scattering can be related to the lab-energy of the incoming particle, E_{lab}, with relativistic kinematics as

$$p^2 = \frac{E_{\text{lab}} m_p^2 (E_{\text{lab}} + 2m_p)}{(m_p + m_n)^2 + 2m_p E_{\text{lab}}}, \tag{4.86}$$

where m_p is the proton mass and m_n is the neutron mass, see Ref. [43].

This chapter has introduced the necessary scattering concepts to finally be able to compute the total np scattering cross section, σ_{np}^{tot}. Given an interaction potential V_{NN}, which is a function of (yet to be determined) LECs, the total scattering cross section can be computed for a given lab energy.

Part II

Implementation and Results

5

Neutron-Proton Phase Shifts in MWPC

The main studies and results will be described in this Part II of the thesis. The material that was developed and presented in Part I will be used in this chapter to numerically solve the *np* scattering problem and obtain phase shifts in various channels. A specific goal is to reproduce various results from Ref. [9], demonstrating that the MWPC potential provides RG invariant predictions of phase shifts, in contrast to the WPC potential.

The chapter starts by briefly describing the methods used to solve the LS equation and continues with a numerical study of how the RG-dependence of phase shifts changes in MWPC compared to WPC.

5.1 Numerical Solution of LS Equation

The LS equation in the partial wave basis (4.66) needs to be solved numerically for the potentials considered in this thesis. A common approach is to use a matrix inversion method, first proposed in Ref. [37]. The method utilizes that the integral equation can be discretized using *Gaussian quadrature*, which is a method for approximating an integral by a finite sum. A `python` code implementing the solution of the LS equation was kindly provided by A. Ekström and S. Miller [44].

With weights $\{w_i\}_{i=1}^{N_p}$ and momenta $\{k_i\}_{i=1}^{N_p}$, specified by the Gaussian quadrature algorithm, the integral equation (4.66) can be approximated by

$$T^{j,s}_{l'l}(p',p) = V^{j,s}_{l'l}(p',p) + \frac{2}{\pi}\sum_{l''}\sum_{i=1}^{N_p} w_i k_i^2 \; V^{j,s}_{l'l''}(p',k_i)\frac{2m_N}{p^2-k_i^2+i\epsilon}T^{j,s}_{l''l}(k_i,p). \qquad (5.1)$$

The on-shell T-matrix is given by $T^{j,s}_{l'l}(p,p)$, since the energy is conserved in the scattering process. These matrix elements are obtained by solving Eq. (5.1) for $T^{j,s}_{l'l}(p,p)$, see Ref. [41]. The phase shifts are then obtained as described in Section 4.4.5. Physical constants used in the computation are listed in Table 5.1.

The construction of the potential, $V^{j,s}_{l'l}(p',p)$, in the partial wave basis is the biggest

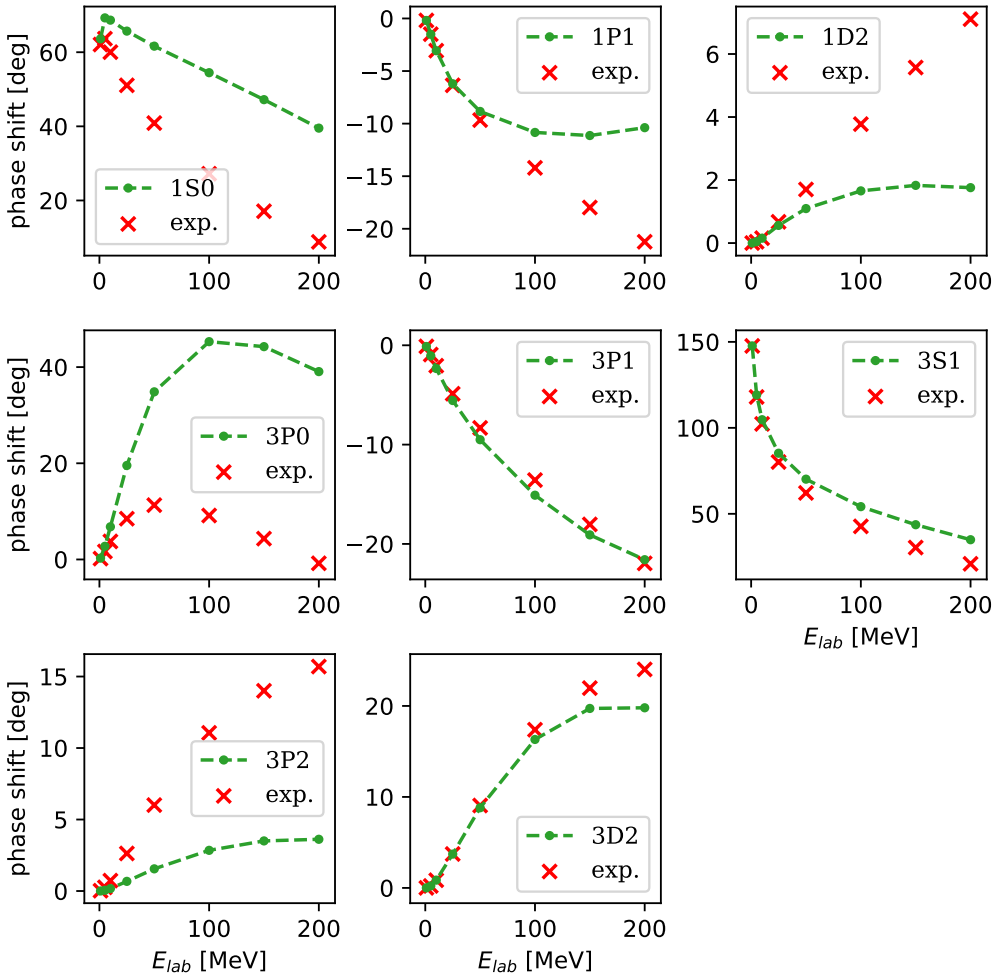

Figure 5.1: Phase shifts in various channels produced with $\Lambda = 450$ MeV, $N_p = 40$ and $\boldsymbol{\alpha} = (-0.11, -0.087, 0, 0, 0)$. The red crosses indicate experimental phase shifts from Refs. [46], [47].

computational bottle-neck. Since the same code later will be used for purposes requiring speed, this part was first re-written in `C` and imported to `python` with the help of the python-package `cython` [45].

Table 5.1: Constants used in the calculation of phase shifts.

Constant	symbol	value	unit
axial coupling	g_A	1.29	1
pion decay constant	f_π	92.2	MeV
pion mass	m_π	138.04	MeV
proton mass	m_p	938.27	MeV
neutron mass	m_n	939.56	MeV
np reduced mass	m_N	469.46	MeV

5.2 Determining LECs from Phase Shifts

In this section the algorithm for determining LECs from *np* scattering phase shift will be described. The experiential[1] phase shifts used are from the Granada database, [46], [47].

The basis for the proposal by Ref. [9] to promote the LECs: ${}^3P_0$, ${}^3P_2$, and ${}^3D_2$ to LO is that the so-called "implicit assumption" made when doing the non-perturbative treatment of the scattering problem may not hold. It is assumed that the LECs included at LO are sufficient to also renormalize the non-perturbative amplitude. This assumption does not hold in general, and is indeed found to be false for specific partial waves. Ref. [9] finds that promotion of additional LECs to LO is necessary to obtain RG invariant phase shifts in *attractive* partial waves.

The inclusion of counterterms in the ${}^3D_2$ and ${}^3P_2$ channels at LO may in fact not be necessary, since Ref. [48] finds that a perturbative treatment of NN scattering is applicable in these partial waves, meaning that the effect of resummation of the amplitude in the LS equation is small. However, in the power-counting scheme analyzed in this thesis these counterterms are still included at LO.

5.2.1 Phase shifts in MWPC and WPC

Computed phase shifts in selected partial waves for *np* scattering in WPC are shown in Fig. 5.1. For notational simplicity the LECs are collected in a vector, $\boldsymbol{\alpha}$, according to

$$\boldsymbol{\alpha} \equiv \left(C_{^1S_0}, C_{^3S_1}, C_{^3P_0}, C_{^3P_2}, C_{^3D_2}\right), \tag{5.2}$$

where the units for each LEC follow the convention in Ref. [26] and are

$$\left(10^4\ \text{GeV}^{-2}, 10^4\ \text{GeV}^{-2}, 10^4\ \text{GeV}^{-4}, 10^4\ \text{GeV}^{-4}, 10^4\ \text{GeV}^{-6}\right). \tag{5.3}$$

These units will be used for LECs throughout this thesis unless otherwise stated. As pointed out by various papers, e.g. Ref. [9], it is the phase shifts in *attractive*[2] channels that are problematic in WPC. Figs. 5.2 and 5.3 show phase shifts in channels ${}^1S_0$, ${}^3S_1$, ${}^3P_0$, ${}^3P_2$ and ${}^3D_2$ computed in WPC and MWPC for various values of the cutoff, Λ. The LECs are fitted to reproduce the experimental phase shifts at a certain lab energy as stated in the figure captions.

The procedure used to determine the LECs for a fixed value of Λ and generate the results shown in Figs. 5.2 and 5.3 is the following. An error function is defined as

$$f_e(C_X) \equiv \delta_X^{\text{exp}}(E) - \delta_X^{\text{th}}(E, \Lambda, C_X), \tag{5.4}$$

where C_X is the LEC in the given partial wave, X, and δ_X^{exp} and δ_X^{th} are the experimental and theoretical phase shifts, respectively. The LEC is determined by

[1] These phase shifts are not purely experimental, since they are in fact model-dependent and extracted from observed cross sections through a partial wave analysis.

[2] Attractive channels are characterized by positive phase shifts.

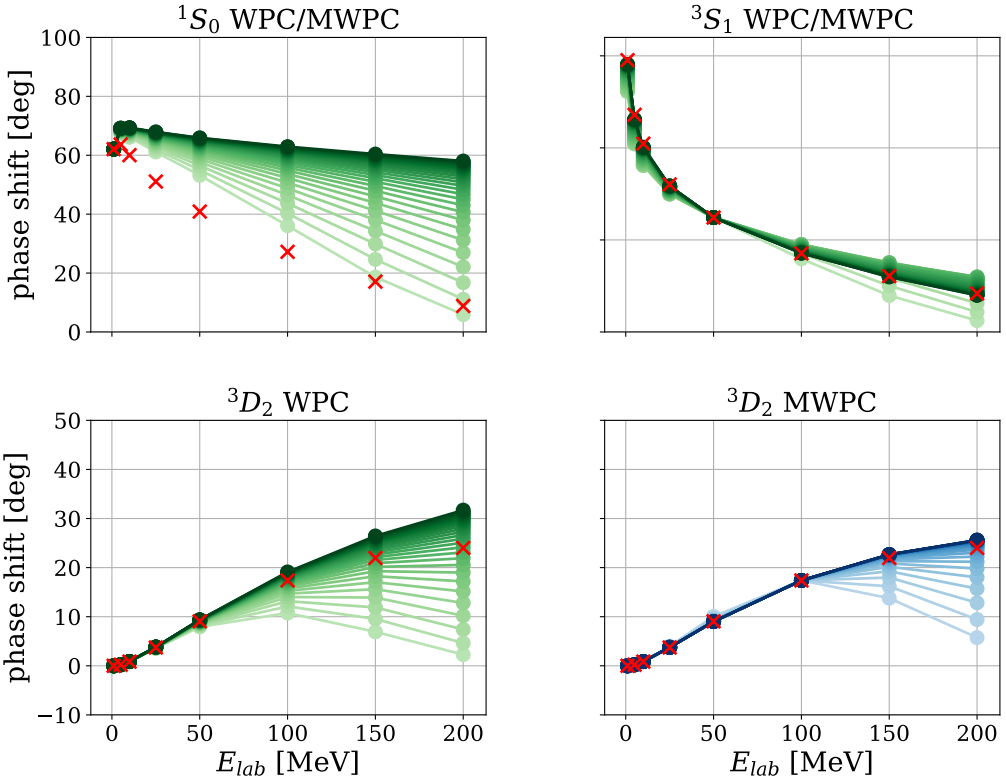

Figure 5.2: Phase shifts computed with various cutoffs in the range $300 \leq \Lambda \leq 800$ MeV, with steps of 20 MeV. Lighter (darker) color indicates lower (higher) Λ. The red crosses show experimental phase shifts, taken from Refs. [46], [47]. The result illustrates how the Λ-dependence of the phase shifts becomes smaller in MWPC, i.e. when extra LECs are included and fitted to experimental data. $C_{^1S_0}$ ($C_{^3S_1}$) is fitted to reproduce the phase shift at 1 (50) MeV, and $C_{^3D_2}$ in MWPC is fitted to reproduce the phase shift at 100 MeV. $N_p = 40$ is used in the computations.

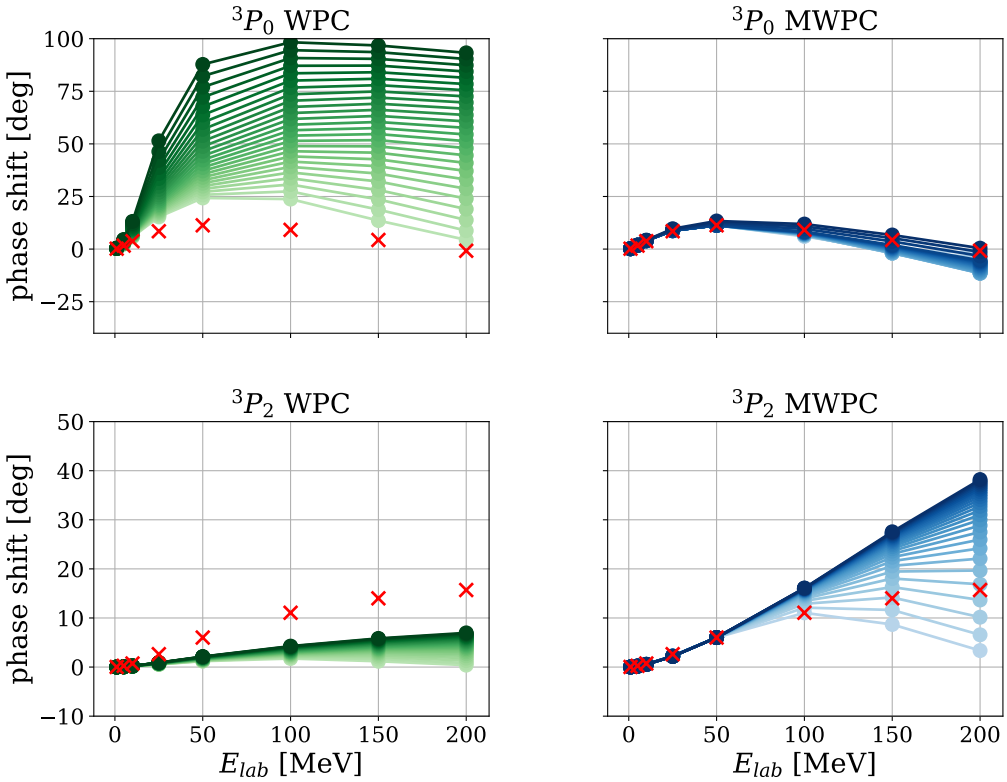

Figure 5.3: Phase shifts computed with various cutoffs in the range $300 \leq \Lambda \leq 800$ MeV, with steps of 20 MeV. The red crosses show experimental phase shifts, taken from Refs. [46], [47]. Lighter (darker) color indicates lower (higher) Λ. The result illustrates how the Λ-dependence of the phase shifts becomes smaller in MWPC, i.e. when extra LECa are included and fitted to experimental data. Both $C_{^3P_0}$ and $C_{^3P_2}$ are fitted to reproduce the phase shift at $E_{\text{lab}} = 50$ MeV. $N_p = 40$ is used in the computation.

Table 5.2: LECs fitted to reproduce phase shifts at various cutoffs, Λ. The units are as in Eq. (5.3).

LEC	$\Lambda = 350$ MeV	$\Lambda = 450$ MeV	$\Lambda = 550$ MeV	$\Lambda = 650$ MeV
$C_{^1S_0}$	-0.126	-0.113	-0.105	-0.0990
$C_{^3S_1}$	-0.113	-0.0746	-0.0411	-0.00297
$C_{^3P_0}$	0.756	0.800	0.934	1.49
$C_{^3P_2}$	-0.309	-0.247	-0.197	-0.157
$C_{^3D_2}$	-1.80	-0.307	0.0389	0.139

solving

$$f_e(C_X(\Lambda)) = 0 \tag{5.5}$$

numerically, where the tolerance 10^{-5} is used to determine convergence. Since the theoretical phase shifts depend on Λ, the inferred LECs, $C_X(\Lambda)$, will also depend on Λ. This dependence is sometimes referred to as the LECs are "running". The dependence on Λ for the various LECs is shown in Fig. 5.4, and in Fig. C.1 in Appendix C for a wider range of cutoff values.

To quantify the RG dependence of predictions, the phase shifts at other energies energies $E' \neq E$ are computed for the various cutoffs using the infered LECs by evaluating the function

$$\delta_X^{\text{th}}(E', \Lambda, C_X(\Lambda)). \tag{5.6}$$

The Λ dependence of predicted $^3P_0$ phase shifts for various lab energies is shown in Fig. 5.5. This figure basically illustrates the same information as Figs. 5.2 and 5.3, but as a function of Λ instead of lab energy. The RG invariance is significantly improved in MWPC compared to WPC. However, some known features arise when the cutoff is varied, as studied in detail in Ref. [9]. At certain values of the cutoff some LECs seem to diverge. One example is the $C_{^3P_0}$ LEC at the cutoff $\Lambda \sim 700$ MeV, which is seen in Fig. 5.4. This behavior makes it numerically difficult to find the optimal LEC, and is known as a limit cycle [9].

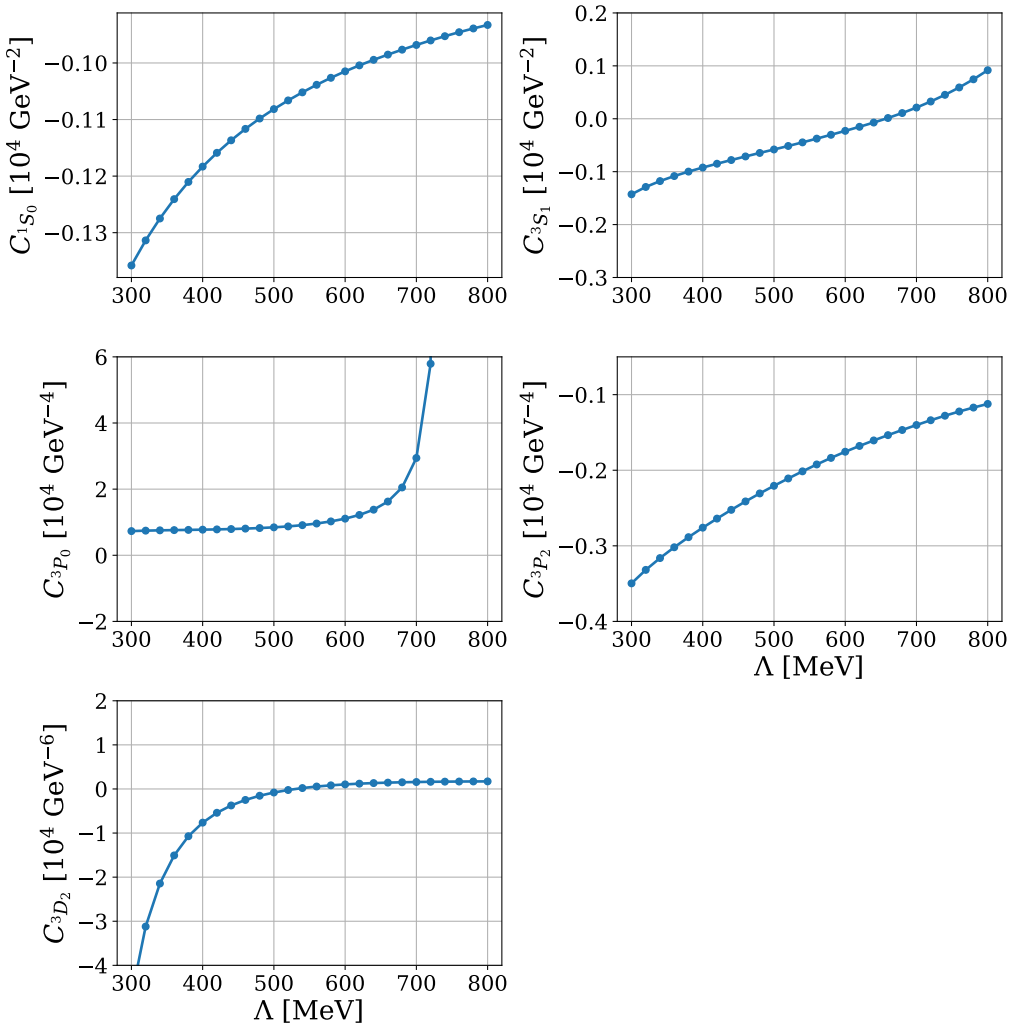

Figure 5.4: Cutoff dependence of fitted LECs. The units used are as in Eq. (5.3).

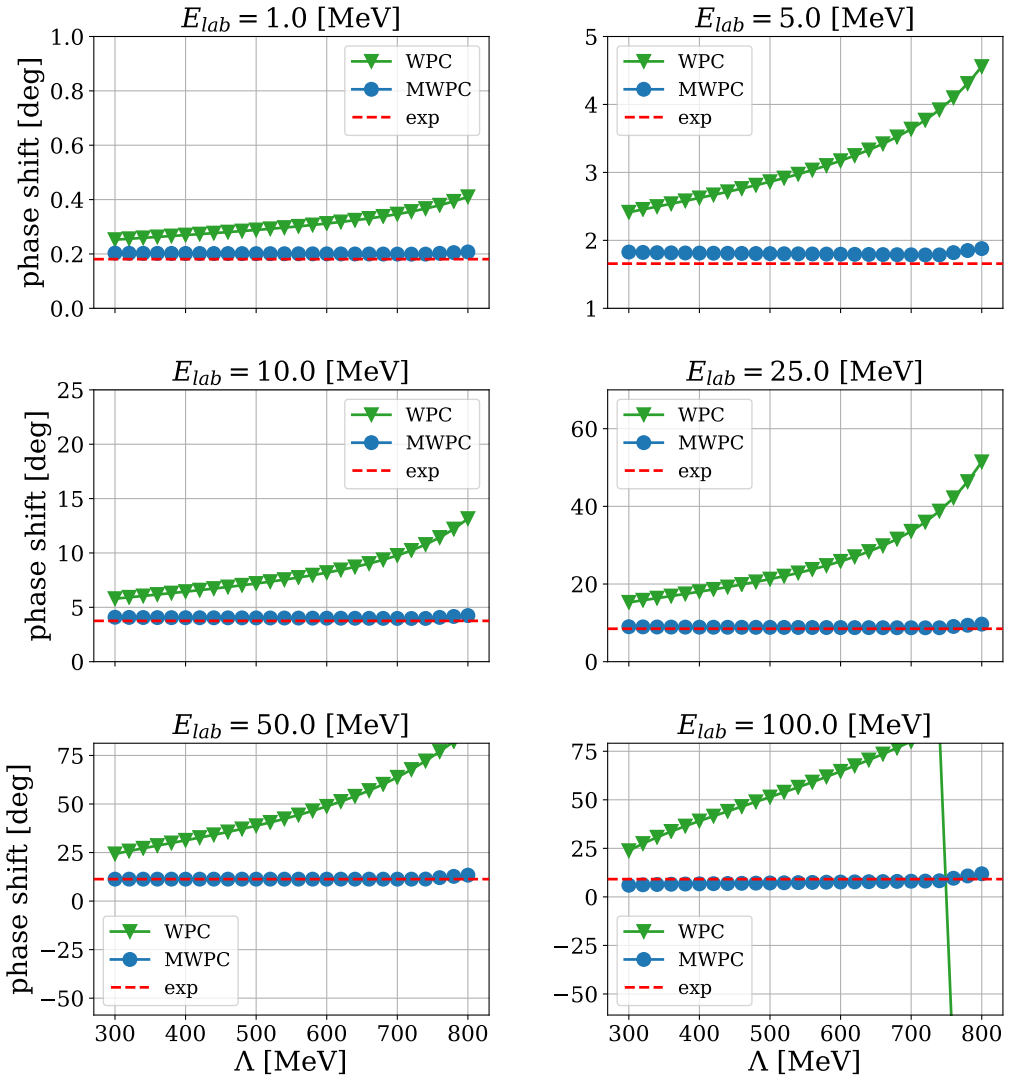

Figure 5.5: Cutoff dependence of predicted ${}^3P_0$ phase shifts for various lab-energies, E_{lab}. In MWPC, which includes a counterterm in this channel, $C_{{}^3P_0}$ is fitted to reproduce the phase shift at 50 MeV. Predictions of phase shifts at other lab energies are then made using the theoretical model, Eq. (5.6). The dashed red line shows the experimental phase shift, taken from Refs. [46], [47]. It is seen that the Λ dependence almost disappears in MWPC.

6

Bayesian Inference of LECs

The behavior of phase shifts in WPC and MWPC were analyzed in the previous chapter by performing single-energy fits. Phase shifts are not experimental quantities, but are extracted in a *partial wave analysis*, see Refs. [46], [47], which makes it harder to do an adequate error analysis. In this chapter Bayesian inference of LECs will be done from experimental total np scattering cross sections. In this analysis both theoretical and experimental errors will be taken into account, by constructing a Bayesian statistical model.

First, the computation of cross sections will be reviewed and some numerical approximations in this computation will be justified. Then, a small introduction to Bayesian data analysis is provided, and the statistical model used to connect experimental and theoretical data will be constructed. The LECs, $\boldsymbol{\alpha}$, (see Eq. (5.2)) will be inferred in the Bayesian framework by using Markov Chain Monte Carlo (MCMC) sampling, and results in form of posterior pdfs for LECs, and posterior predictives for the theoretical cross sections will be presented. Finally, the RG invariance of predictions will be investigated by varying the cutoff, Λ.

6.1 Computing np Cross Sections

Computing cross sections is relatively easy given their relation with phase shifts (Section 4.4.6), where the latter can be obtained numerically using the method described in Section 5.1.

There are two important hyperparameters that need to be specified when doing the numerical cross section computations: N_p, the number of momentum-grid points when solving the LS equation (5.1) and $j_{\max}$, the maximum j included in the sum (4.82). To achieve fast computation speeds, both $j_{\max}$ and N_p are chosen as small as possible, while still obtaining sufficiently accurate results. The convergence in these parameters is studied by computing the relative error between the truncated and the fully converged calculation. It is found that a fully converged result is obtained by using $j_{\max} = 15$ and $N_p = 100$. The outcome of this analysis is shown in Fig. 6.1. Based on these results, the hyperparameters chosen in the computations of cross sections are shown in Table 6.1.

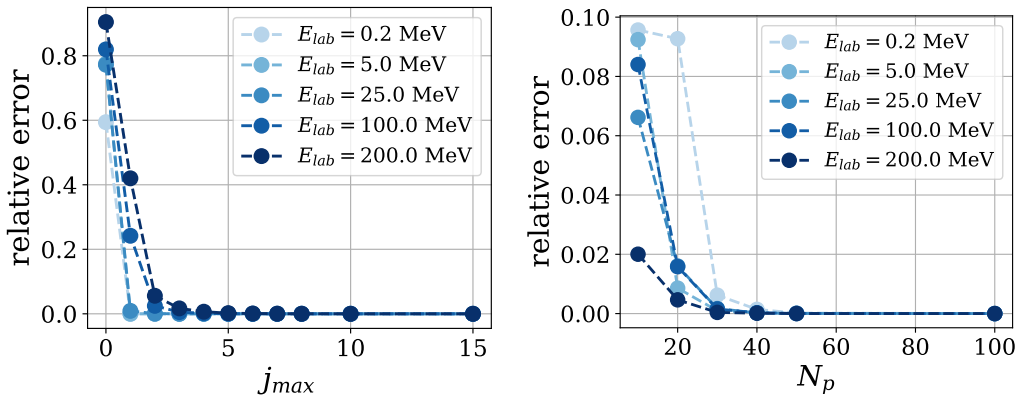

(a) **(b)**

Figure 6.1: These figures show the relative error in the computation of cross sections at various lab energies, E_{lab}, when the hyperparameters are varied. The cutoff $\Lambda = 450$ MeV is used.

Table 6.1: Hyperparameters used in computations of total cross sections. With this choice of hyperparameters, the relative error is smaller than 10^{-2}.

Parameter	Value
j_{max}	4
N_p	40

6.2 Bayesian Data Analysis

The inference of LECs in Chapter 5 was done without taking neither experimental- nor model errors into account. This was intentional, since the purpose was to demonstrate how the phase shifts are affected by the inclusion of extra LECs in MWPC. However, if one wants to infer the LECs to eventually be able to make predictions with proper error bars, one needs to more carefully consider various sources of uncertainty. Since both the EFT model and experimental data come with uncertainties, so do the inferred LECs. To analyze this, and also be able to take additional information into account, the Bayesian framework of statistics is very useful. The coming sections are a short interlude explaining the basics of Bayesian statistics.

6.2.1 Basics of Bayesian Statistics

Frequentist and Bayesian are two common approaches to statistics. In the frequentist approach to statistics, probabilities are bases on frequencies of outcomes whereas in the Bayesian approach a certain degree-of-belief (DoB) is assigned given the information at hand. One important and fundamental difference in these approaches is the view of model parameters. In the Bayesian framework, parameters are considered random variables, which have some probability density function (pdf) reflecting the knowledge about them, whereas in the frequentist approach the parameters are thought of as numbers with a fixed true value.

Bayes' theorem relates various pdfs involving the parameters[1], $\boldsymbol{\theta}$, observed data, D, and prior information, I, and reads

$$\mathrm{pr}(\boldsymbol{\theta}|D,I) = \frac{\mathrm{pr}(D|\boldsymbol{\theta},I)\cdot\mathrm{pr}(\boldsymbol{\theta}|I)}{\mathrm{pr}(D|I)}. \tag{6.1}$$

$\mathrm{pr}(\boldsymbol{\theta}|D,I)$ is called the *posterior* pdf, $\mathrm{pr}(\boldsymbol{\theta}|I)$ the *prior*, $\mathrm{pr}(D|\boldsymbol{\theta},I)$ the *likelihood* and $\mathrm{pr}(D|I)$ the model evidence [49]. Since the integral of a pdf over the whole parameter range is one, the parameter-independent model evidence does not need to be computed when doing parameter estimation. Hence, Bayes' theorem is often used in the form

$$\mathrm{pr}(\boldsymbol{\theta}|D,I) \propto \mathrm{pr}(D|\boldsymbol{\theta},I)\cdot\mathrm{pr}(\boldsymbol{\theta}|I), \tag{6.2}$$

where the likelihood and prior just needs to be determined up to a multiplicative normalization constant.

The prior, $\mathrm{pr}(\boldsymbol{\theta}|I)$, reflects the knowledge of the parameters, $\boldsymbol{\theta}$, given the information I—before taking any data into account. For example, in χEFT, the prior will incorporate information about the expected size of the LECs, given by dimensional analysis [26]. There is however an element of subjectivity in choosing the prior, even though there are several general methods that can be applied [50]. The role of the prior is usually one of the arguments used against the Bayesian approach, but the

[1]Note that in this section (Section 6.2) the notation $\boldsymbol{\theta}$ is used for a general set of parameters in a model. In later sections where the specific parameters are LECs the notation, $\boldsymbol{\alpha}$, will be used.

argument can also be turned around. For example, a maximum likelihood estimation is from the Bayesian point of view implicitly assuming a uniform prior, and the Bayesian framework can actually modify this assumption to make the inference more informative. To put it more concretely; just as it is important to take into account information you *do have*, it is important to not implicitly take into account information that you *do not* have, and this is more naturally handled in the Bayesian framework[2] [49].

6.2.2 Posterior Predictive and Error Propagation

In the Bayesian framework, predictions can be made by marginalization over the model parameters when the posterior pdf is known. The posterior predictive pdf for y, given some experimental data, $D = \{y^i_{\text{exp}}\}_i$, and prior information, I, can be expressed as

$$\text{pr}(y|D,I) = \int d\boldsymbol{\theta}\ \text{pr}(y|\boldsymbol{\theta},D,I)\cdot\text{pr}(\boldsymbol{\theta}|D,I), \tag{6.3}$$

where $\text{pr}(y|\boldsymbol{\theta},D,I)$ represents a statistical model that relates the theoretical model with reality and $\text{pr}(\boldsymbol{\theta}|D,I)$ is the posterior pdf for $\boldsymbol{\theta}$. For a simple theoretical model $y = y_{\text{th}}(\boldsymbol{\theta}) + \Delta y_{\text{th}}$, where Δy_{th} is a random variable with some known pdf, $\text{pr}(y|\boldsymbol{\theta},D,I)$ can be computed. The posterior predictive $\text{pr}(y|D,I)$ describes the DoB for the true value of y, given the experimental data, prior information, and theoretical model. Making predictions using marginalization over the model parameters properly propagates the errors in model parameters to an induced error in the model prediction, y [49].

The integral over $\boldsymbol{\theta}$ in Eq. (6.3) can be approximated with samples from the posterior as

$$\int d\boldsymbol{\theta}\ \text{pr}(y|\boldsymbol{\theta},D,I)\cdot\text{pr}(\boldsymbol{\theta}|D,I) \approx \frac{1}{N}\sum_{i=1}^{N}\text{pr}(y|\boldsymbol{\theta}_i,D,I), \tag{6.4}$$

where $\{\boldsymbol{\theta}_i\}_{i=1}^N$ are usually obtained using Markov Chain Monte Carlo methods [49].

6.3 Likelihood and Prior in EFT

The Bayesian framework will now be applied to infer LECs, $\boldsymbol{\alpha}$, in the MWPC potential, V_{NN}, (3.73). The experimental data, $\boldsymbol{y}_{\text{exp}}$, with corresponding errors, $\boldsymbol{\sigma}_{\text{exp}}$, consists of total np cross sections, at 10 lab energies $\boldsymbol{E}_{\text{lab}}$. This data is shown in Table 6.2. The output from the theoretical model[3], $\boldsymbol{y}_{\text{th}}(\boldsymbol{\alpha})$, is a vector of length 10, containing cross sections computed with the LO MWPC χEFT model with LECs $\boldsymbol{\alpha}$. Using this model and data, Bayes' theorem can be used to give an expression for the posterior pdf for the sought-after LECs. The likelihood and prior are obtained by constructing a statistical model using the prior knowledge and appropriate assumptions.

[2] The use of a so-called *symmetric prior* in straight line fitting illustrates this point very well, see Ref [50].

[3] This will be the only model considered in this chapter, and it will often be referred to as "the model".

Let us start with linking the EFT description of an observable with reality. As described in Chapter 3, observables expressed in an EFT model are expected to converge according to the expansion

$$\boldsymbol{y}_i = (\boldsymbol{y}_{\text{ref}})_i \sum_{\nu=0}^{\infty} c_{\nu,i} \left(\frac{Q_i}{\Lambda_\chi}\right)^\nu, \tag{6.5}$$

where ν is the chiral order, $c_{\nu,i}$ are observable coefficients of order one, Λ_χ is the breakdown scale for the EFT and

$$Q_i = \max\{m_\pi, p_i\} \tag{6.6}$$

is the maximum of the pion mass and the magnitude of the incoming relative momentum corresponding to the lab energy $(\boldsymbol{E}_{\text{lab}})_i$ [51]. $\boldsymbol{y}$ is the vector of true model values for the total cross section, and $\boldsymbol{y}_{\text{ref}}$ is a reference scale which is assumed to be equal to $\boldsymbol{y}_{\text{exp}}$ in this analysis. Since a LO ($\nu = 0$) theoretical model is considered, the true model value separates into

$$\boldsymbol{y}_i = (\boldsymbol{y}_{\text{th}}(\boldsymbol{\alpha}))_i + (\boldsymbol{y}_{\text{ref}})_i \sum_{\nu=2}^{\infty} c_{\nu,i} \left(\frac{Q_i}{\Lambda_\chi}\right)^\nu \equiv (\boldsymbol{y}_{\text{th}}(\boldsymbol{\alpha}))_i + (\Delta\boldsymbol{y}_{\text{th}})_i \tag{6.7}$$

where the theoretical/model error is defined as the second term. For convenience, define $\hat{Q}_i \equiv Q_i/\Lambda_\chi$.

Following Ref. [51], the observable coefficients $c_{\nu,i}$ are assumed to be normally distributed random variables, $c_{\nu,i} \sim \mathcal{N}(0, \bar{c}^2)$[4], where $\bar{c} = 1$ in this analysis. The distribution for the theoretical error can be computed to be

$$(\Delta\boldsymbol{y}_{\text{th}})_i \sim \mathcal{N}\left(0, \frac{((\boldsymbol{y}_{\text{ref}})_i)^2\ \bar{c}^2\hat{Q}_i^4}{1-\hat{Q}_i^2}\right), \tag{6.8}$$

since it is a geometric series of i.i.d. normally distributed random variables. The theoretical covariance matrix, Σ_{th}, is modeled to be diagonal, i.e the errors are assumed to be uncorrelated

$$(\Sigma_{\text{th}})_{ij} = \frac{((\boldsymbol{y}_{\text{ref}})_i)^2\ \bar{c}^2\hat{Q}_i^4}{1-\hat{Q}_i^2}\ \delta_{ij} \equiv \left((\boldsymbol{\sigma}_{\text{th}})_i\right)^2\ \delta_{ij}. \tag{6.9}$$

Taking both experimental and theoretical errors into account, the statistical model that connects the experimental data $\boldsymbol{y}_{\text{exp}}$ and theoretical model, $\boldsymbol{y}_{\text{th}}$, is

$$\boldsymbol{y}_{\text{exp}} = \boldsymbol{y}_{\text{th}} + \Delta\boldsymbol{y}_{\text{th}} + \Delta\boldsymbol{y}_{\text{exp}}. \tag{6.10}$$

The experimental errors are assumed to be *uncorrelated* and normally distributed,

$$\Delta\boldsymbol{y}_{\text{exp}} \sim \mathcal{N}(0, \Sigma_{\text{exp}}), \tag{6.11}$$

[4]A random variable, Y, which is normally distributed with mean μ and variance σ^2 is denoted by $Y \sim \mathcal{N}(\mu, \sigma^2)$. The corresponding multivariable expression is $\boldsymbol{Y} \sim \mathcal{N}(\boldsymbol{\mu}, \Sigma)$.

Table 6.2: Experimental data used in the inference. The data consists of total np cross sections, $\boldsymbol{y}_{\text{exp}}$, at various lab energies, $\boldsymbol{E}_{\text{lab}}$, with corresponding standard deviations, $\boldsymbol{\sigma}_{\text{exp}}$. All these quantities are vectors of length 10.

$\boldsymbol{E}_{\text{lab}}$ [MeV]	$\boldsymbol{y}_{\text{exp}}$ [mb]	$\boldsymbol{\sigma}_{\text{exp}}$ [mb]	Reference
0.20	9580.00	140.00	[52]
0.60	5725.00	85.00	[52]
1.00	4259.02	7.73	[53]
5.00	1621.25	13.42	[53]
10.00	949.16	21.22	[53]
24.62	358.58	49.54	[53]
51.00	163.10	1.35	[54]
99.00	75.25	0.37	[54]
150.00	51.02	0.30	[54]
200.00	42.50	0.90	[46]

which means that the covaraiance matrix, Σ_{exp}, is also assumed to be diagonal,

$$\left(\Sigma_{\text{exp}}\right)_{ij} = \left((\boldsymbol{\sigma}_{\text{exp}})_i\right)^2 \ \delta_{ij}. \tag{6.12}$$

Errors due to the choice of method, numerical implementation and other possible errors are considered to be small and will not be taken into account in this analysis.

With the statistical model connecting experimental data and theoretical predictions in place, the *likelihood* can be constructed and reads [51]

$$\text{pr}(\boldsymbol{y}_{\text{exp}}|\boldsymbol{\alpha}, \Sigma_{\text{exp}}, \Sigma_{\text{th}}) \propto \exp\left(-\frac{1}{2}\boldsymbol{r}^{\text{T}} \cdot \left(\Sigma_{\text{exp}} + \Sigma_{\text{th}}\right)^{-1} \cdot \boldsymbol{r}\right), \tag{6.13}$$

where the so-called residuals are

$$\boldsymbol{r} \equiv \boldsymbol{y}_{\text{exp}} - \boldsymbol{y}_{\text{th}}(\boldsymbol{\alpha}). \tag{6.14}$$

The prior for the LECs, $\text{pr}(\boldsymbol{\alpha}|I)$, will incorporate the information that LECs are expected to be of a natural size, ~ 1, with respect to some reference scale found by dimensional analysis [26]. This condition is often referred to as *naturalness*. The natural scales for the various LECs are given by

$$C_{^1S_0}, C_{^3S_1} \sim 10^3 \text{ GeV}^{-2}, \tag{6.15}$$

$$C_{^3P_0}, C_{^3P_2} \sim \ 6 \cdot 10^3 \ \left(\frac{500}{\Lambda}\right)^2 \ \text{GeV}^{-4}, \tag{6.16}$$

$$C_{^3D_2} \sim 2.5 \cdot 10^4 \left(\frac{500}{\Lambda}\right)^4 \ \text{GeV}^{-6}, \tag{6.17}$$

Table 6.3: Summary of notation used in the Bayesian model.

$\boldsymbol{y}_{\text{exp}}$	experimental cross sections at various lab energies
$\boldsymbol{\sigma}_{\text{exp}}$	experimental errors at various lab energies
$\boldsymbol{\sigma}_{\text{th}}$	theoretical errors at various lab energies
$\boldsymbol{y}_{\text{th}}$	theoretical cross sections at various lab energies
$\bar{c}$	standard deviation of $c_{\nu,i}$'s in EFT expansion of observables
$\bar{a}$	standard deviation in Gaussian priors for LECs
$\boldsymbol{\alpha}$	vector of LECs as in Eq. (5.2)
$\boldsymbol{\beta}$	vector of natural scales see Eq. (6.18)
$\hat{Q}_i$	EFT expansion parameter

with Λ given in MeV [26]. Let $\boldsymbol{\beta}$ denote the vector of natural scales in Eq. (6.17) in the units in Eq. (5.3) i.e.

$$\boldsymbol{\beta} = \left(0.1,\ 0.1,\ 0.6 \cdot \left(\frac{500}{\Lambda}\right)^2,\ 0.6 \cdot \left(\frac{500}{\Lambda}\right)^2,\ 2.5 \cdot \left(\frac{500}{\Lambda}\right)^4\right). \tag{6.18}$$

The prior is chosen as a normal distribution with standard deviation $\bar{a} = 4$ with respect to the natural scale for each LEC, which explicitly reads

$$\text{pr}(\boldsymbol{\alpha}|I) \propto \exp\left(-\frac{\boldsymbol{\alpha}^2}{2(\bar{a}\boldsymbol{\beta})^2}\right). \tag{6.19}$$

Finally, using Bayes' theorem, the posterior pdf for $\boldsymbol{\alpha}$ reads

$$\text{pr}(\boldsymbol{\alpha}|\boldsymbol{y}_{\text{exp}}, \Sigma_{\text{exp}}, \Sigma_{\text{th}}, I) \propto \text{pr}(\boldsymbol{y}_{\text{exp}}|\boldsymbol{\alpha}, \Sigma_{\text{exp}}, \Sigma_{\text{th}}) \cdot \text{pr}(\boldsymbol{\alpha}|I). \tag{6.20}$$

When new data and/or information is available, one can take the posterior as a new prior, and use Bayes' theorem with a new likelihood and obtain an updated posterior. This is sometimes called a Bayesian update. Table 6.3 summarizes the notation introduced in this section.

6.4 Sampling the Posterior with Markov Chain Monte Carlo

Due to the number of LECs and the relatively large computational time that is needed to evaluate the model, $\boldsymbol{y}_{\text{th}}(\boldsymbol{\alpha})$, it is unfeasible to compute the posterior on a sufficiently dense grid of LEC values. Instead, Markov Chain Monte Carlo (MCMC) is a numerical approach that can be used to sample pdfs without the need for a closed form expression, or brute-force evaluation on a grid [55]. MCMC sampling algorithms will not be described in detail here, for details the reader is referred to e.g. [55].

Table 6.4: Parameters used in the emcee sampling of the posterior pdf for the LECs $\boldsymbol{\alpha}$.

Parameter	Value
number of walkers	50
burn-in steps	2000
number of samples, N	18000
$\bar{c}$	1
$\bar{a}$	4
breakdown scale Λ_χ	600 MeV

The sampling of the posterior given in Eq. (6.20) is done in python with the help of the package `emcee` [55], which is an open-source implementation of an affine-invariant ensemble sampler for MCMC. The sampler consists of several *walkers* that "walk around" in parameter space, i.e. update their positions and try to find regions of high probability density in the posterior. The walkers are randomly initialized at some start positions in parameter space. Here, the starting positions for the walkers are chosen from a normal distribution with standard deviation $0.5\boldsymbol{\beta}$, where $\boldsymbol{\beta}$ denotes the natural scales of the LECs, see Eq. (6.17). It takes quite a few steps before the walkers have stabilized after the initialization, why some of the first samples are thrown away. This is sometimes called a burn-in period.

The emcee sampling is parallelized using `multiprocessing.Pool` in the python standard library, which offers almost an order of magnitude speedup. The parameters used in the emcee sampling is shown in Table 6.4 as well as Table 6.1. The result is a list of samples $\{\boldsymbol{\alpha}_i\}_{i=1}^N$, that represents samples taken from the pdf.

6.5 Posterior Sampling and Predictions

The posterior pdf for $\boldsymbol{\alpha}$, shown in Eq. (6.20), is sampled for some different values the cutoff, $\Lambda \in \{350, 450, 550, 650, 750\}$ MeV. These cutoffs are chosen with consideration of the qualitative behavior of the LECs shown in Fig. 5.4, to avoid regions where the LECs magnitude are not natural, or even diverge.

6.5.1 Posterior pdf for LECs

This section will focus on results for $\Lambda = 450$ MeV, and results for other cutoffs are provided in Appendix C. The posterior pdf for $\boldsymbol{\alpha}$ from the MCMC sampling is visualized in Fig. 6.2. The results obtained here are consistent with the results in Refs. [9], [56]. Fig. 6.3 shows histograms oven the marginal pdf for each LEC with some more clarity than the so-called corner plot in Fig. 6.2.

The posterior clearly indicates that the data does not constrain the values of the LECs that much, and allows multiple modes of alternative fits. This behavior can

depend on a number of reasons that will be discussed further in the coming sections.

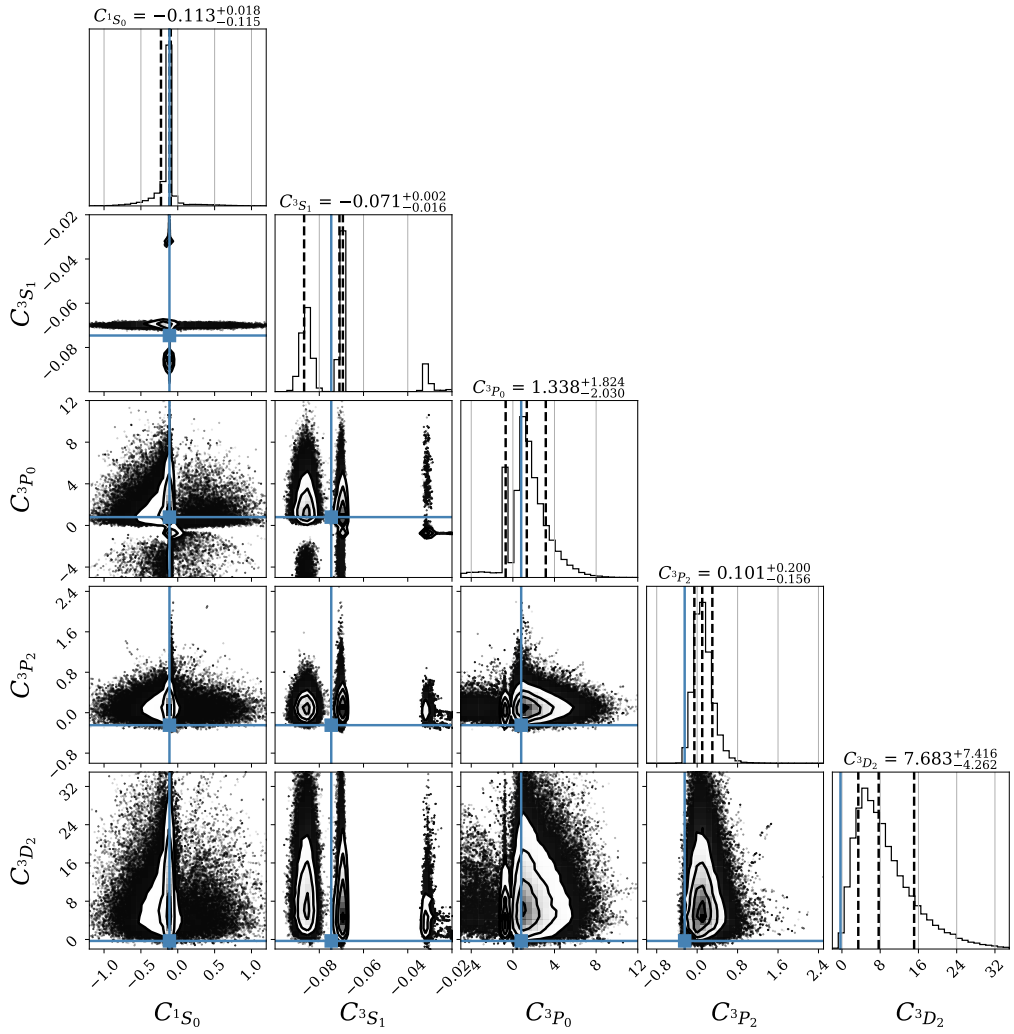

Figure 6.2: Corner plot [57] of the joint posterior pdf for the LECs. The units are as in Eq. (5.3) and $\Lambda = 450$ MeV. The blue square indicates the LEC values fitted to the phase shifts in Chapter 5, as also shown in Table 5.2. The dashed black lines indicate the median and 68 % DoB regions for each individual LEC, even though they are not that informative due to a high degree of multi-modality.

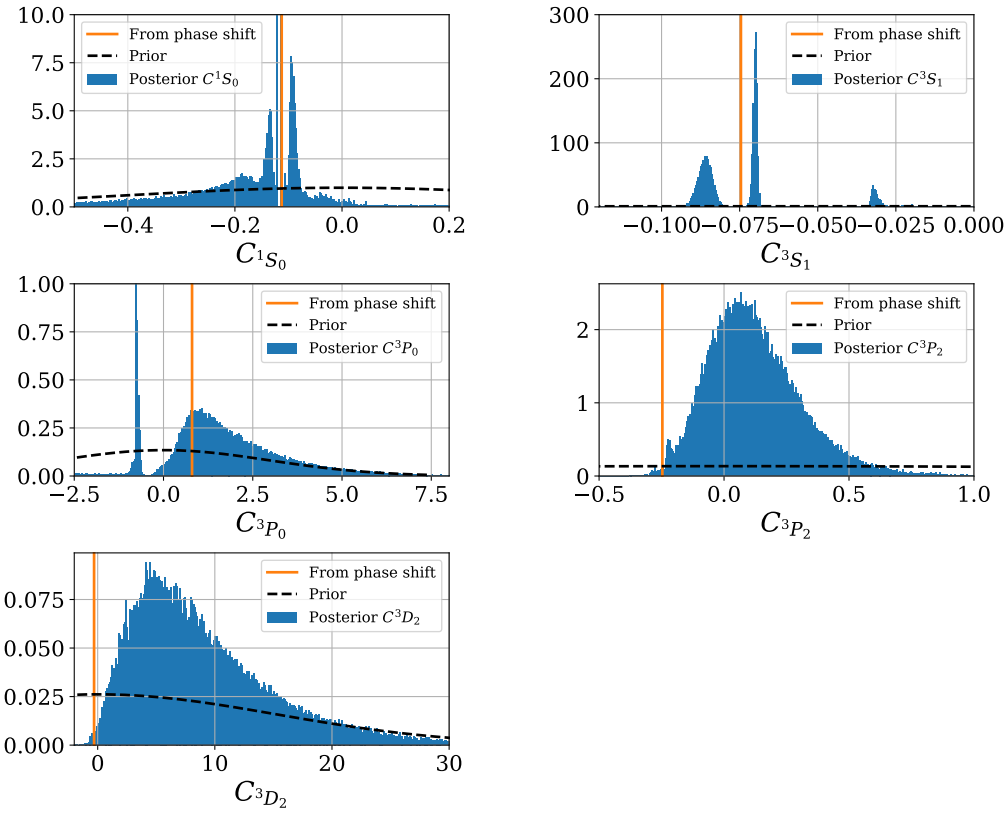

Figure 6.3: The marginal posterior pdfs for each LEC is shown together with the prior and the point estimate from the phase shifts done in Chapter 5, shown in Table 5.2. The units are as in Eq. (5.3) and the cutoff is $\Lambda = 450$ MeV.

6.5.2 Predicted Cross Sections

Using the obtained posterior pdf, $\mathrm{pr}(\boldsymbol{\alpha}|\boldsymbol{y}_{\mathrm{exp}}, \Sigma_{\mathrm{exp}}, \Sigma_{\mathrm{th}}, I)$, in the from of N samples $\{\boldsymbol{\alpha}_i\}_{i=1}^{N}$, shown in the previous section, a posterior predictive is constructed for the cross section using Eq. (6.4). Fig. 6.4 shows the pdf

$$\mathrm{pr}(\boldsymbol{y}|\boldsymbol{y}_{\mathrm{exp}}, \Sigma_{\mathrm{exp}}, \Sigma_{\mathrm{th}}, I) \approx \frac{1}{N}\sum_{i=1}^{N} \mathrm{pr}(\boldsymbol{y}|\boldsymbol{\alpha}_i, I), \tag{6.21}$$

where N is the number of samples and

$$\mathrm{pr}(\boldsymbol{y}|\boldsymbol{\alpha}, I) \propto \exp\left(-\frac{1}{2}\left(\boldsymbol{y} - \boldsymbol{y}_{\mathrm{th}}(\boldsymbol{\alpha})\right)^{\mathrm{T}} \cdot \Sigma_{\mathrm{th}}^{-1} \cdot \left(\boldsymbol{y} - \boldsymbol{y}_{\mathrm{th}}(\boldsymbol{\alpha})\right)\right). \tag{6.22}$$

The Λ dependence of the posterior predictive cross sections is shown in Fig. 6.5, for a set of lab energies not included in the inference.

Even though there are a lot of different values of the LECs that are consistent with the data, as shown in Fig. 6.2, the validity of the inference is indicated by the fact that the posterior predictive agrees quite well with the experimental data. The posterior predictive serves as sanity check that the method used has produced results that are consistent with the data.

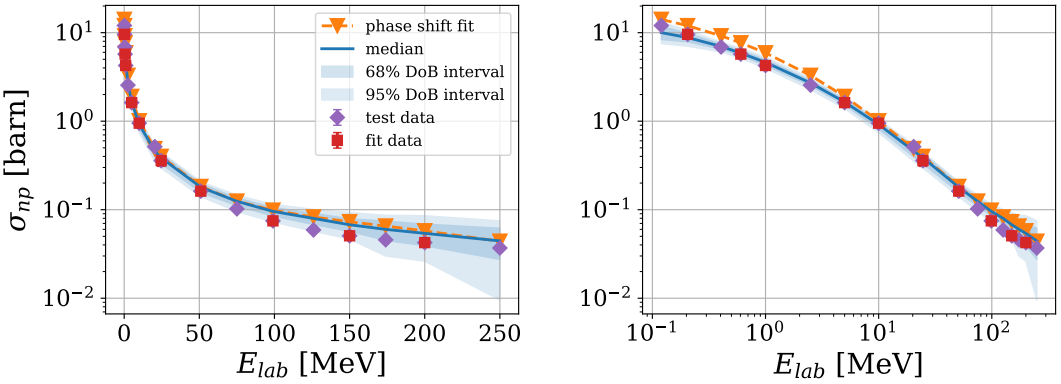

Figure 6.4: Posterior predictive for cross sections with $\Lambda = 450$ MeV. The data is the same in both panels but the left (right) panel has a linear (logarithmic) energy scale. *Fit data* are experimental cross sections that were used in the inference, and *test data* are additional experimental values, not included in the inference. The experimental errors are shown with error bars, but are in almost all cases smaller than the size of the square indicating the value. The LECs from phase shift fits are shown in Table 5.2.

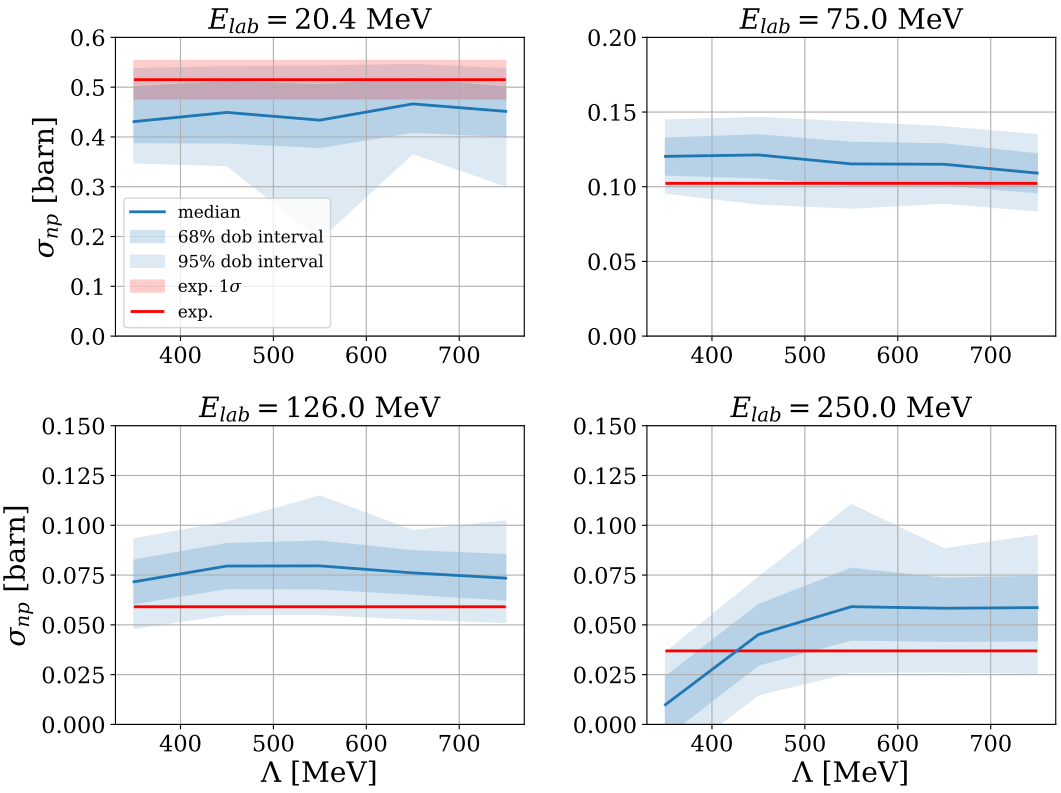

Figure 6.5: The posterior predictive for cross sections at various lab energies. For each lab energy the posterior predictive is evaluated for the different $\Lambda \in \{350, 450, 550, 650, 750\}$ MeV. The experimental value of the cross section is shown for each lab energy, with accompanying standard deviation. For some lab energies the standard deviation of the experimental value is so small that it is not visible.

6.6 Discussion

The posterior pdf in Figs. 6.2 and 6.3 clearly show that the LECs are not strongly constrained by the data used. We note, however, that the point estimates for the LECs obtained from the phase-shifts fits coincide rather well with regions that have large probability density. Furthermore, the posterior predictive for the total cross section shown in Fig. 6.4 agrees quite well with both the experimental data used in the inference as well as additional experimental data points. This result gives some validation to the hypothesis that the total cross section data is consistent with a large variety of LECs. When taking the model uncertainty into account we note that the uncertainty is rather large for a LO prediction and that it increases with increasing lab energy. Comparing the posterior predictive for the cross section to preliminary results in Ref. [58] shows that LO MWPC performs better than LO WPC.

The posterior pdf in Figs. 6.2 and 6.3 do not only cover a large range of LEC values, but also reveals distinct features such as multiple distinguished peaks. Fig. 6.6 displays the same pdf as Fig. 6.2 but four peaks are marked with colored ellipses. The red and yellow ellipses mark the peaks which show the correlation between $C_{^1S_0}$ and $C_{^3S_1}$. It is clear that the two peaks in $C_{^3S_1}$ correspond to distinct features in $C_{^1S_0}$, namely the yellow peak is narrow, while the red peak is wider.

In general more/less attraction in one channel can cancel less/more attraction in another one, and a correlation between LECs are therefore expected. In Fig. 6.2 we see that $C_{^3P_0}$, $C_{^3P_2}$ and $C_{^3D_2}$ are all poorly constrained—indicating that the data does not contain much information about them.

Studying the correlation between $C_{^3S_1}$ and $C_{^3P_0}$ in figure Fig. 6.6, the green and magenta ellipses mark two regions of interest. Analogously with the correlation between $C_{^1S_0}$ and $C_{^3S_1}$, the green and magenta peaks have distinct features. The magenta peak goes sharply to zero when $C_{^3P_0}$ goes to zero, while the green peak has a bimodal behavior, and has a peak around $C_{^3P_0} \approx -1$. This peak can more clearly be seen in Fig. 6.3. It is clear that the red- and green peaks have a strong correlation and that the yellow- and magenta peaks also have a strong correlation. The correlations are revealed by the correlations with $C_{^3S_1}$.

Even though the data used in the inference can not distinguish enough between which of these peaks correspond to the correct value (if any), there are some ways this can be analyzed further without costly scattering calculations. One important piece of information one can include is which channels contain physical bound states, i.e. have some negative eigenvalue of the Hamiltonian. It is known that the only bound nucleon-nucleon system is the deuteron in the ${}^3S_1 - {}^3D_1$ channel, see Ref. [59]. Some of the peaks appearing in the posterior might arise due to unphysical bound states are appearing for certain too attractive values of the LECs—that however are consistent with the data used in the inference.

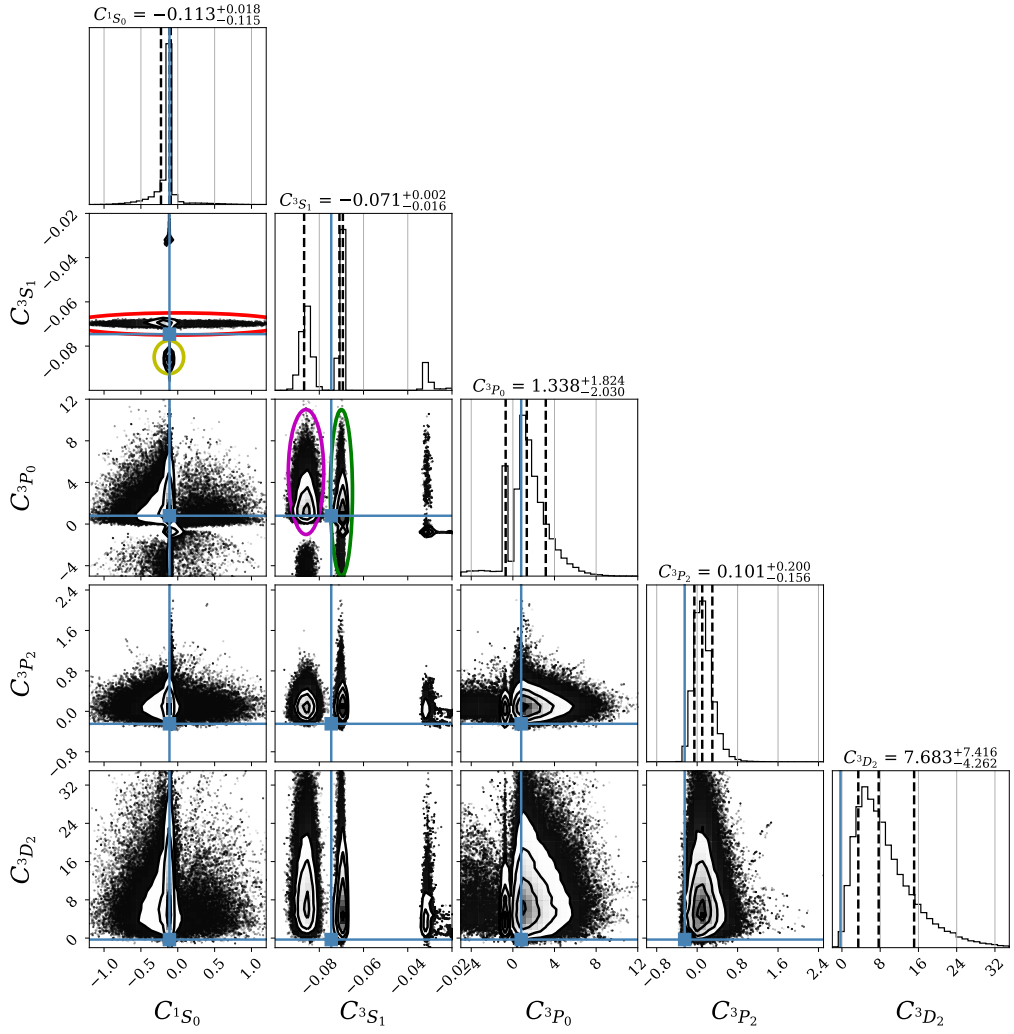

Figure 6.6: Same pdf as Fig. 6.2 with some ellipses marking certain peaks.

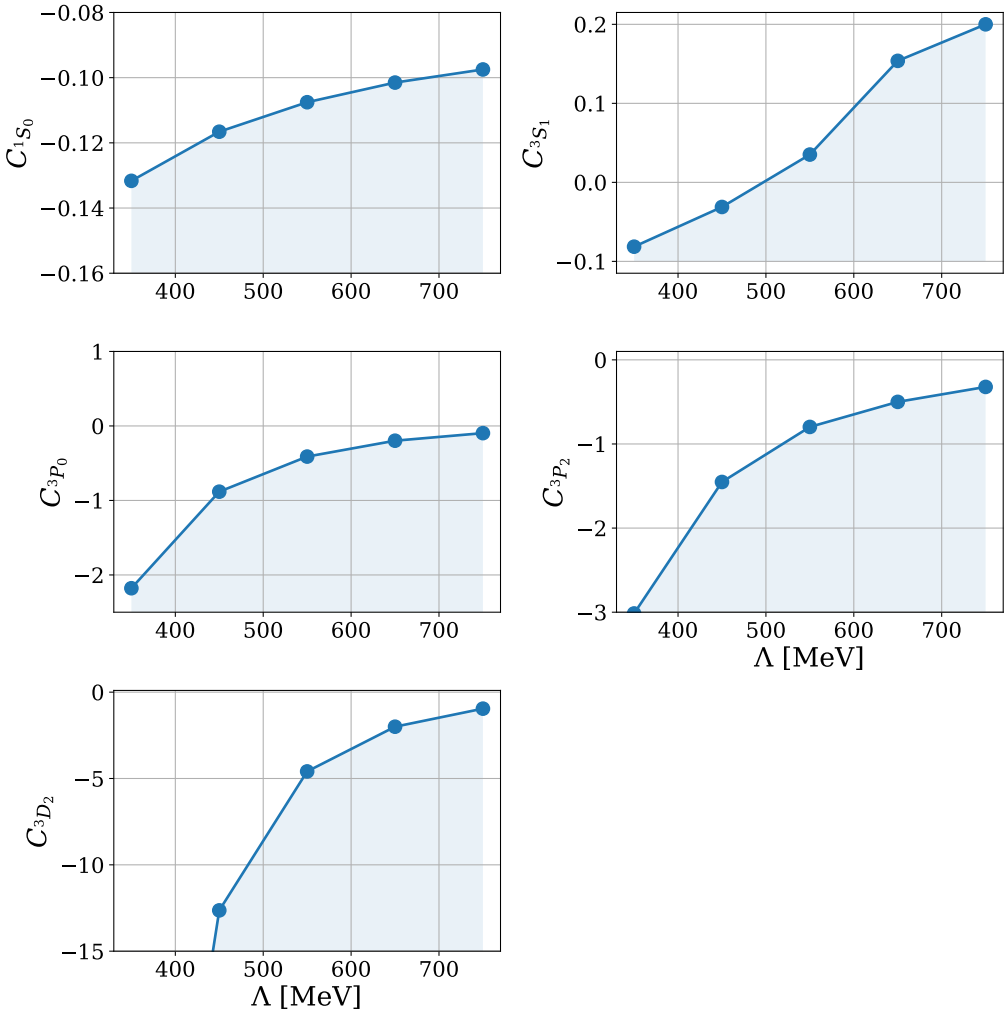

Figure 6.7: This figure shows the values of LECs that produce a bound state in its respective channel, for varying cutoff Λ. In the blue shaded area the channel contains at least one bound state, and in the region above the blue line no bound states exists. The units of the LECs are as in Eq. (5.3).

The existence of bound states in different channels can be checked by setting up the Hamiltonian in the given channel and computing its eigenvalues for varying LECs. Doing this for the channels containing LECs gives two regions, one in which bound states exists, and one in which no bound states exist. The result of this small analysis is shown in figure Fig. 6.7, where regions where there exist bound states are shown.

By doing a Bayesian update, including the information which channels contain bound states, a step-function likelihood is multiplied to the posterior in Fig. 6.2, effectively discarding regions of samples. The posterior pdf after this update is shown in figure Fig. 6.8. It is seen that this has an effect on the posterior, mainly taking away samples in the red- and green ellipse that corresponds to unphysical bound states. There is however not that big of an improvement since the high

degree of bimodality is still present. Although, it is interesting that it is the red- and green region in which samples are unphysical, since they correlate strongly with each other. This could possibly indicate that those whole regions are unphysical which are not accurately discarded by the data used in the inference. It can also be seen that the peak in $C_{^3P_0}$ around -1, discussed earlier, is correlated with the green region, and is just above the limit for producing a bound state in $C_{^3P_0}$.

Although one should not make to strong conclusions of the facts emphasized above, it is at least promising that the problematic regions are tightly linked, which indicates that the physically relevant regions are the yellow and magenta peaks. Preliminary results from Ref. [58] regarding LO WPC do not quite support this hypothesis though. However, it is not entirely clear that it is an adequate comparison given that the power counting is different, hence it is actually hard to draw any conclusions from the comparison. The easiest way to straighten out these question marks is including more data in the inference. Additional data that would be of interest to include is differential cross sections, which might contain more data to constrain the LECs with $l > 0$.

The cutoff dependence of posterior predictive for cross sections for various lab energies, shown in Fig. 6.5, is looking promising. Since only a LO model is used here, the error bands are quite wide, which is expected. They are anyhow completely consistent with the experimental data. It is seen that the Λ dependence seems to be larger for $E_{\text{lab}} = 250$ MeV, which is also expected, see Ref. [26].

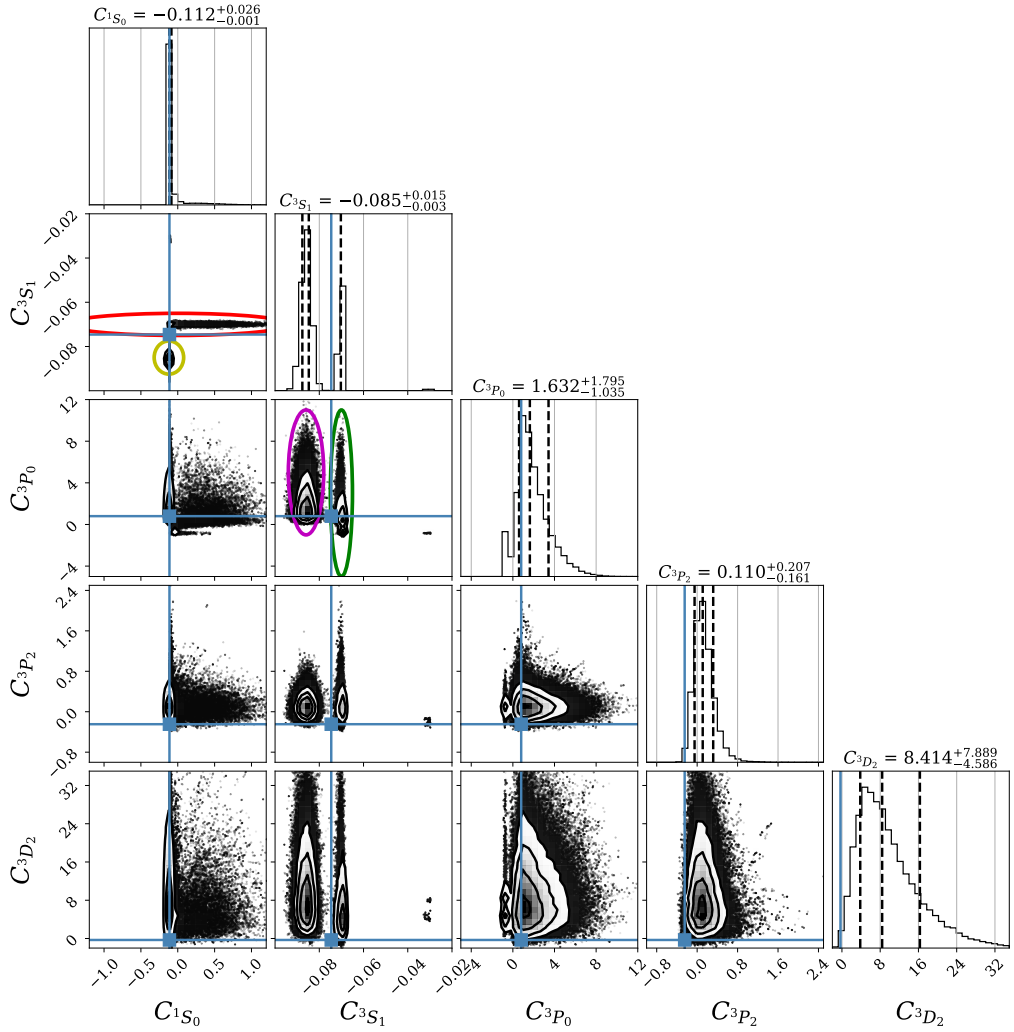

Figure 6.8: The same pdf as in Fig. 6.6 is shown after the Bayesian update. The main difference compared to Fig. 6.6 is that samples in the red- and green ellipse for negative values have disappeared.

7

Conclusions and Outlook

This chapter contains a brief summary of this work and provides some conclusions connected to the questions raised in the introduction. Finally, a number of suggested improvements and further directions of research are outlined.

7.1 Summary and Conclusions

The thesis has gone from discussing QFT, QCD, and gauge theories in Chapter 2 to a quantitative study of model predictions of observables in Chapter 6. This journey has covered most parts of the process in going from a theory, to experiments, and back again.

The theory in Chapters 2 and 3 gave quite a detailed introduction to various relevant concepts, important to understanding how one can construct a leading order χEFT Lagrangian. It was discussed how various approximations were made to finally give expressions for non-relativistic quantum mechanical NN potentials. The end result was the LO NN potentials shown in Eq. (3.72) and Eq. (3.73). Chapter 4 gave a brief introduction to non-relativistic scattering theory in quantum mechanics, important for solving the NN scattering problem.

In Chapter 5, *np* scattering phase shifts produced with the two potentials from Chapter 3 were studied. The LS equation was solved numerically for different cutoffs, Λ, and it was concluded that the Λ dependence is almost completely removed in the partial waves where counterterms are promoted to LO in MWPC. This showed that MWPC performs better than WPC at predicting RG-invariant *np* scattering phase shifts in the energy- and cutoff range studied.

In Chapter 6 Bayesian inference of LECs in the LO MWPC potential in Eq. (3.73) was performed. The data used was 10 total *np* scattering cross sections at lab energies from 0.2 to 200 MeV. Naturalness of LECs was encoded in the prior and EFT truncation errors were considered in the data likelihood. The resulting posterior pdf for the LECs was sampled using MCMC methods and it was found that these model parameters are note particularly well constrained using the considered calibration data. However, the posterior predictive pdf for the cross sections was found to

agree quite well with experimental data—in fact much better than with a LO WPC potential. Furthermore, the Λ dependence of the posterior predictive pdf was found to be small in the cutoff range studied. The predictions are essentially RG invariant if one takes into account the allowed uncertainty due to the model just being a LO approximation.

7.2 Suggested Improvements and Outlook

Here we list possible improvements and directions of further studies.

- The most obvious improvement, discussed a few times already, would be the inclusion of additional data in the inference. In this study the data consisted of ten total *np* cross sections at lab energies ranging from 0.2 – 200 MeV, as shown in Table 6.2. The inclusion of additional observables, such as differential cross sections, might help to better constrain the LECs in partial waves with $l > 0$. Other data such as the binding energy of the deuteron and spin-polarized scattering observables could also be of interest to include.

- The statistical error model, $\boldsymbol{y}_{\text{exp}} = \boldsymbol{y}_{\text{th}} + \Delta\boldsymbol{y}_{\text{th}} + \Delta\boldsymbol{y}_{\text{exp}}$, used in the Bayesian inference relies on some strong assumptions and simplifications. Method errors due to truncation of the model space as well as numerical errors were not considered, but could be included in a future analysis. The theoretical errors were assumed to be uncorrelated, which certainly is an assumption that should be relaxed in further studies. The model also makes other assumptions, e.g. $\boldsymbol{y}_{\text{ref}} = \boldsymbol{y}_{\text{exp}}$ and $\bar{c} = 1$ which should be investigated further. Better error models for χEFT are found in several existing works, e.g. [51], [58], [60], [61].

- The optimization algorithm used in the determination of LECs from *np* scattering phase shift in Chapter 5 could be improved to be able to study a wider range of cutoffs with higher accuracy. The optimization of LECs was done by fitting the theoretical phase shift to reproduce the "experimental" phase shift at one specific (rather arbitrary) lab energy, usually 50 MeV. This procedure could be improved to a more sophisticated method that includes less arbitrariness. One can for example use phase shifts at a wide range of energies with some proper EFT weight that incorporates the expected model error [62].

- It would be interesting to use Bayesian inference to compare WPC and MPWC at various orders in the χEFT expansion. By doing this, the discrepancies between WPC and MWPC at different orders in the EFT could be quantified and the validity of the EFT expansion could be investigated.

- Apart from the assumptions already mentioned here, there are a lot of assumptions made on the way. Many of these assumptions and approximations are standard in the literature, and empirically produce quite small errors. It would anyway be valuable to try to quantify the errors and approximations, e.g. from relativistic corrections and the approximations in the Bethe-Salpeter

equation, more thoroughly.

References

[1] H. Yukawa, "On the interaction of elementary particles," *Proceedings of the Physico-Mathematical Society of Japan*, vol. 17, p. 48, 1935. DOI: https://doi.org/10.1143/PTPS.1.1.

[2] C. J. Batty, E. Friedman, H. Gils, R. Machleidt, and H. Rebel, *Advances in nuclear physics*, J. Negele and E. Vogt, Eds., 1989. DOI: 10.1007/978-1-4613-9907-0.

[3] R. Machleidt, "High-precision, charge-dependent bonn nucleon-nucleon potential," *Physical Review C*, vol. 63, no. 2, 2001-01. DOI: 10.1103/physrevc.63.024001.

[4] D. J. Gross, "The discovery of asymptotic freedom and the emergence of qcd," *Proceedings of the National Academy of Sciences*, vol. 102, no. 26, pp. 9099–9108, 2005. DOI: 10.1073/pnas.0503831102.

[5] R. Gupta, "Introduction to lattice QCD: Course," in *Les Houches Summer School in Theoretical Physics, Session 68: Probing the Standard Model of Particle Interactions*, 1997-07. arXiv: hep-lat/9807028.

[6] S. Weinberg, "Phenomenological lagrangians," *Physica A*, vol. 96, pp. 327–240, 1979. DOI: https://doi.org/10.1016/0378-4371(79)90223-1.

[7] S. Weinberg, "Nuclear forces from chiral lagrangians," *Physics Letters B*, vol. 251, pp. 288–292, 1990. DOI: https://doi.org/10.1016/0370-2693(90)90938-3.

[8] S. Weinberg, "Effective chiral lagrangians for nucleon - pion interactions and nuclear forces," *Nuclear Physics B*, vol. 363, pp. 3–18, 1991. DOI: https://doi.org/10.1016/0550-3213(91)90231-L.

[9] A. Nogga, R. G. E. Timmermans, and U. van Kolck, "Renormalization of one-pion exchange and power counting," *Physical Review C*, vol. 72, p. 054 006, 2005. arXiv: nucl-th/0506005.

[10] C. .-J. Yang, A. Ekström, C. Forssén, and G. Hagen. (2020). "Power counting in chiral effective field theory and nuclear binding." arXiv: 2011.11584 [nucl-th].

[11] M. E. Peskin and D. V. Schroeder, *An Introduction to quantum field theory*. Reading, USA: Addison-Wesley, 1995, ISBN: 978-0-201-50397-5.

[12] S. Weinberg, "The making of the standard model," *The European Physical Journal C*, vol. 34, no. 1, pp. 5–13, 2004.

[13] R. P. Feynman, "Space-time approach to non-relativistic quantum mechanics," *Reviews of Modern Physics*, vol. 20, pp. 367–387, 2 1948.

[14] G. Isidori, *Quantum field theory II, lectures notes - part I: The path integral formulation of QFT*, v 2.0, 2020-03. [Online]. Available: https://www.physik.uzh.ch/dam/jcr:89238699-422c-476e-b67b-f7cf72ed98f6/QFT_2020_I.pdf.

[15] P. A. M. Dirac and R. H. Fowler, "The quantum theory of the electron," *Proceedings of the Royal Society of London. Series A, Containing Papers of a Mathematical and Physical Character*, vol. 117, no. 778, pp. 610–624, 1928. DOI: 10.1098/rspa.1928.0023.

[16] K. Huang. (2013). "A critical history of renormalization." arXiv: 1310.5533 [hep-ph].

[17] K. G. Wilson and J. Kogut, "The renormalization group and the expansion," *Physics Reports*, vol. 12, no. 2, pp. 75–199, 1974. DOI: https://doi.org/10.1016/0370-1573(74)90023-4.

[18] G. Cynolter and E. Lendvai. (2015). "Cutoff regularization method in gauge theories." arXiv: 1509.07407 [hep-ph].

[19] K. G. Wilson, "The renormalization group and critical phenomena," *Reviews of Modern Physics*, vol. 55, pp. 583–600, 3 1983.

[20] S. Scherer, *Introduction to chiral perturbation theory*, arXiv:0210398 [hep-ph], 2002.

[21] S. Weinberg, "Nonlinear realizations of chiral symmetry," *Physical Review*, vol. 166, pp. 1568–1577, 5 1968. DOI: 10.1103/PhysRev.166.1568.

[22] S. Coleman, J. Wess, and B. Zumino, "Structure of phenomenological lagrangians. i," *Physical Review*, vol. 177, pp. 2239–2247, 5 1969. DOI: 10.1103/PhysRev.177.2239.

[23] C. G. Callan, S. Coleman, J. Wess, and B. Zumino, "Structure of phenomenological lagrangians. ii," *Physical Review*, vol. 177, pp. 2247–2250, 5 1969. DOI: 10.1103/PhysRev.177.2247.

[24] A. P. Balachandran, G. Marmo, B. S. Skagerstam, and A. Stern, *Classical Topology and Quantum States*, 1st ed. World Scientific, 1991.

[25] J. Stillwell, *Naive Lie Theory*, 1st ed. Springer-Verlag, 2008.

[26] R. Machleidt and D. Entem, "Chiral effective field theory and nuclear forces," *Physics Reports*, vol. 503, no. 1, pp. 1–75, 2011-06. DOI: 10.1016/j.physrep.2011.02.001.

[27] E. Epelbaum. (2010). "Nuclear forces from chiral effective field theory: A primer." arXiv: 1001.3229 [nucl-th].

[28] G. Ecker, "Chiral perturbation theory," *Progress in Particle and Nuclear Physics*, vol. 35, pp. 1–80, 1995, ISSN: 0146-6410. DOI: https://doi.org/10.1016/0146-6410(95)00041-G.

[29] H. Leutwyler, "On the foundations of chiral perturbation theory," *Annals of Physics*, vol. 235, no. 1, pp. 165–203, 1994. DOI: 10.1006/aphy.1994.1094.

[30] J. Gasser, M. E. Sainio, and A. Svarc, "Nucleons with chiral loops," *Nuclear Physics B*, vol. 307, no. 4, pp. 779–853, 1988, ISSN: 0550-3213. DOI: https://doi.org/10.1016/0550-3213(88)90108-3.

[31] M. S. Sanchez, "Effective field theories of strong-interacting systems in nucleon scattering and heavy-quark bound states," Ph.D. dissertation, Université Paris-Saclay, https://tel.archives-ouvertes.fr/tel-01695540/, 2017.

[32] P. F. Bedaque and U. van Kolck, "Effective field theory for few-nucleon systems," *Annual Review of Nuclear and Particle Science*, vol. 52, no. 1, pp. 339–396, 2002. DOI: 10.1146/annurev.nucl.52.050102.090637.

[33] J. R. Taylor, *Scattering Theory: The quantum Theory on Nonrelativistic Collisions*. Wiley, New York, 1972.

[34] J. J. Sakurai and J. Napolitano, *Modern Quantum Mechanics*, 2nd ed. Cambridge University Press, 2017.

[35] E. Epelbaum and J. Gegelia, "Regularization, renormalization and peratization in effective field theory for two nucleons," *The European Physical Journal A*, vol. 41, no. 3, pp. 341–354, 2009-07. DOI: 10.1140/epja/i2009-10833-3.

[36] U. van Kolck. (2020). "The problem of renormalization of chiral nuclear forces." arXiv: 2003.06721 [nucl-th].

[37] M. I. Haftel and F. Tabakin, "Nuclear saturation and the smoothness of nucleon-nucleon potentials," *Nuclear Physics A*, vol. 158, no. 1, pp. 1–42, 1970. DOI: https://doi.org/10.1016/0375-9474(70)90047-3.

[38] E. E. Salpeter and H. A. Bethe, "A relativistic equation for bound-state problems," *Physical Review*, vol. 84, pp. 1232–1242, 6 1951-12. DOI: 10.1103/PhysRev.84.1232.

[39] R. Blankenbecler and R. Sugar, "Linear integral equations for relativistic multichannel scattering," *Physical Review*, vol. 142, pp. 1051–1059, 4 1966-02.

[40] K. Erkelenz, R. Alzetta, and K. Holinde, "Momentum space calculations and helicity formalism in nuclear physics," *Nuclear Physics A*, vol. 176, no. 2, pp. 413–432, 1971. DOI: https://doi.org/10.1016/0375-9474(71)90279-X.

[41] S. B. Miller, "Nucleon-nucleon scattering in a wave-packet formalism," Licentiate Thesis, Chalmers University of Technology, https://research.chalmers.se/publication/517065, 2020.

[42] J. A. Melendez, S. Wesolowski, and R. J. Furnstahl, "Bayesian truncation errors in chiral effective field theory: Nucleon-nucleon observables," *Physical Review C*, vol. 96, no. 2, 2017-08. DOI: 10.1103/physrevc.96.024003.

[43] E. Epelbaum, H. Krebs, and U. .-G. MeiSSner, "Improved chiral nucleon-nucleon potential up to next-to-next-to-next-to-leading order," *The European Physical Journal A*, vol. 51, no. 5, 2015-05. DOI: 10.1140/epja/i2015-15053-8.

[44] A. Ekström and S. B. Miller, Private communication (2021).

[45] S. Behnel, R. Bradshaw, C. Citro, L. Dalcin, D. S. Seljebotn, and K. Smith, "Cython: The best of both worlds," *Computing in Science & Engineering*, vol. 13, no. 2, pp. 31–39, 2011.

[46] R. Navarro Pérez, J. E. Amaro, and E. Ruiz Arriola, "Partial-wave analysis of nucleon-nucleon scattering below the pion-production threshold," *Physical Review C*, vol. 88, p. 024 002, 2 2013-08.

[47] R. N. Pérez, J. E. Amaro, and E. R. Arriola, "Coarse-grained potential analysis of neutron-proton and proton-proton scattering below the pion production threshold," *Physical Review C*, vol. 88, p. 064 002, 6 2013-12.

[48] S. Wu and B. Long, "Perturbative nn scattering in chiral effective field theory," *Physical Review C*, vol. 99, no. 2, 2019-02. DOI: 10.1103/physrevc.99.024003.

[49] D. S. Sivia and J. Skilling, *Data Analysis - A Bayesian Tutorial*, 2nd, ser. Oxford Science Publications. Oxford University Press, 2006.

[50] C. Forssén and D. Phillips, *Learning from data: Assigning probabilities*, Accessed: Sep 28, 2020, 2020-09. [Online]. Available: https://github.com/physics-chalmers/tif285.git.

[51] S. Wesolowski, R. J. Furnstahl, J. A. Melendez, and D. R. Phillips, "Exploring bayesian parameter estimation for chiral effective field theory using nucleonnucleon phase shifts," *Journal of Physics G: Nuclear and Particle Physics*, vol. 46, no. 4, p. 045 102, 2019-02. DOI: 10.1088/1361-6471/aaf5fc.

[52] B. H. Daub, V. Henzl, M. A. Kovash, *et al.*, "Measurements of the neutron-proton and neutron-carbon total cross section from 150 to 800 kev," *Physical Review C*, vol. 87, no. 1, 2013-01. DOI: 10.1103/physrevc.87.014005.

[53] J. Clement, P. Stoler, C. Goulding, and R. Fairchild, "Hydrogen and deuterium total neutron cross sections in the mev region," *Nuclear Physics A*, vol. 183, no. 1, pp. 51–59, 1972. DOI: https://doi.org/10.1016/0375-9474(72)90930-X.

[54] P. W. Lisowski, R. E. Shamu, G. F. Auchampaugh, *et al.*, "Search for resonance structure in the np total cross section below 800 mev," *Physical Review Letters*, vol. 49, pp. 255–259, 4 1982-07. DOI: 10.1103/PhysRevLett.49.255.

[55] D. Foreman-Mackey, D. W. Hogg, D. Lang, and J. Goodman, "Emcee: The MCMC hammer," *Publications of the Astronomical Society of the Pacific*, vol. 125, no. 925, pp. 306–312, 2013.

[56] B. D. Carlsson, A. Ekström, C. Forssén, *et al.*, "Uncertainty analysis and order-by-order optimization of chiral nuclear interactions," *Physical Review X*, vol. 6, no. 1, 2016-02. DOI: 10.1103/physrevx.6.011019.

[57] D. Foreman-Mackey, "Corner.py: Scatterplot matrices in python," *The Journal of Open Source Software*, vol. 1, no. 2, p. 24, 2016-06. DOI: 10.21105/joss.00024.

[58] I. Svensson, A. Ekström, and C. Forssén. (2021). "Bayesian parameter estimation in χEFT using hamiltonian monte carlo." In preparation.

[59] E. M. Henley and A. Garcia, *Subatomic Physics*, 3rd. World Scientific, 2007. DOI: 10.1142/6263.

[60] S. Wesolowski, N. Klco, R. J. Furnstahl, D. R. Phillips, and A. Thapaliya, "Bayesian parameter estimation for effective field theories," *Journal of Physics G: Nuclear and Particle Physics*, vol. 43, no. 7, p. 074 001, 2016.

[61] S. Wesolowski, I. Svensson, A. Ekström, *et al.* (2021). "Fast rigorous constraints on chiral three-nucleon forces from few-body observables." arXiv: 2104.04441 [nucl-th].

[62] A. Ekström, G. Baardsen, C. Forssén, *et al.*, "Optimized chiral nucleon-nucleon interaction at next-to-next-to-leading order," *Physical Review Letters*, vol. 110, p. 192 502, 19 2013-05. DOI: 10.1103/PhysRevLett.110.192502.

A

Conventions

The conventions used in Part I of this thesis will largely follow those of the the book by Michel E. Peskin and Daniel V. Schröder Ref. [11].

A.1 General

Greek indices $\mu, \nu, \rho, \sigma, ...$ is often used as Lorentz indices and take values 0,...,3. Latin indices $i, j, k, l, ...$ are used for general purpose. Latin indices $a, b, c, d, ...$ are mostly used as indices enumerating elements in Lie algebras.

Vectors in euclidean three-dimensional space are denoted by a bold font, e.g. $\boldsymbol{k}$. Unit vectors in some direction $\boldsymbol{p}$ are denoted by $\hat{\boldsymbol{p}} = \boldsymbol{p}/|\boldsymbol{p}|$. Where no confusion is possible, the modulus of a vector will written with the same name but not bold e.g. $k = |\boldsymbol{k}|$.

If nothing else is stated, units where $c = \hbar = 1$ are used.

A.2 Relativity

The mostly minus metric is used

$$g_{\mu\nu} = g^{\mu\nu} = \begin{pmatrix} 1 & 0 & 0 & 0 \\ 0 & -1 & 0 & 0 \\ 0 & 0 & -1 & 0 \\ 0 & 0 & 0 & -1 \end{pmatrix}. \tag{A.1}$$

The convention for writing Lorentz vectors is

$$x^\mu = (x^0, \boldsymbol{x}), \quad g_{\mu\nu}x^\nu = (x^0, -\boldsymbol{x}), \tag{A.2}$$

which, under Lorentz transformations, transform according to

$$x'_\nu = \Lambda_\nu{}^\mu x_\mu. \tag{A.3}$$

For a massive particle with $p^\mu = (p^0, \boldsymbol{p}) \equiv (E, \boldsymbol{p})$, the mass-shell relation reads

$$p^2 = E^2 - \boldsymbol{p}^2 = m^2.$$

The derivative is often abbreviated according to

$$\frac{\partial}{\partial x^\mu} = \partial_\mu = (\partial_0, \boldsymbol{\nabla}) .$$

The quantum mechanical momentum operator has the form

$$p^\mu = i\partial^\mu,$$

which gives the plane wave e^{-ikx} momentum k^μ.

A.2.1 Gamma Matrices

The clifford algebra for the gamma matrices read

$$\{\gamma^\mu, \gamma^\nu\} = 2g^{\mu\nu}\mathrm{id}, \tag{A.4}$$

where id is the identity in Dirac space. The representation used is the *Weyl* or *chiral representation* of the gamma matrices which in 2×2 block form reads

$$\gamma^0 = \begin{pmatrix} 0 & 1 \\ 1 & 0 \end{pmatrix}, \quad \gamma^i = \begin{pmatrix} 0 & \sigma^i \\ -\sigma^i & 0 \end{pmatrix}, \tag{A.5}$$

where the *Pauli matrices* σ^i take the form

$$\sigma^1 = \begin{pmatrix} 0 & 1 \\ 1 & 0 \end{pmatrix}, \ \sigma^2 = \begin{pmatrix} 0 & -i \\ i & 0 \end{pmatrix}, \ \sigma^3 = \begin{pmatrix} 1 & 0 \\ 0 & -1 \end{pmatrix}. \tag{A.6}$$

The matrix $\gamma^5 \equiv i\gamma^0\gamma^1\gamma^2\gamma^3$ satisfies the properties

$$\left(\gamma^5\right)^\dagger = \gamma^5, \tag{A.7}$$

$$\left(\gamma^5\right)^2 = \mathrm{id}, \tag{A.8}$$

$$\{\gamma^\mu, \gamma^5\} = 0. \tag{A.9}$$

In the Weyl representation γ^5 reads, in 2×2 block form,

$$\gamma^5 = \begin{pmatrix} -1 & 0 \\ 0 & 1 \end{pmatrix}. \tag{A.10}$$

A.3 Fourier Transforms

The plane wave e^{-ikx} has momentum k^μ, and the Fourier transforms look like

$$f(x) = \int \frac{d^4k}{(2\pi)^4}\, e^{-ikx} f(k) \tag{A.11}$$

$$f(k) = \int d^4x\, e^{+ikx} f(x) \tag{A.12}$$

which gives the delta function

$$\int d^4x\, e^{ikx} = (2\pi)^4 \delta^{(4)}(k). \tag{A.13}$$

There is no special notation used for the Fourier transform of a function, but it should be clear from the context where p, q and k are almost exclusively used to denote momentum and x, and r denotes position.

A.4 Quantum Field Theory

In our conventions the free scalar field Lagrangian reads

$$\mathcal{L}_{\text{Scalar}} = \frac{1}{2}(\partial_\mu \phi)^2 - \frac{1}{2}m^2\phi^2,$$

which gives the Feynman propagator in momentum space

$$D_\phi(p) = \frac{i}{p^2 - m^2 + i\epsilon}$$

The Lagrangian for the free Dirac field ψ looks like

$$\mathcal{L}_{\text{Dirac}} = \bar{\psi}(i\gamma^\mu \partial_\mu - m)\psi, \tag{A.14}$$

where the *Feynman slash notation* $\not{\partial} \equiv \gamma^\mu \partial_\mu$ is often used. The Dirac adjoint is defined as $\bar{\psi} \equiv \psi^\dagger \gamma^0$. The Feynman propagator for the Dirac field in momentum space reads

$$D_\psi(p) = \frac{i(\not{p} + m)}{p^2 - m^2 + i\epsilon}.$$

B

Proof of Goldstone's Theorem

In this appendix the proof of Goldstone's, theorem stated in Section 2.5, will be given.

B.1 Proof of Goldstone's Theorem at Classical Level

We will first consider the proof of Goldstonets theorem for a classical scalar field theory. The classical proof can then be extended to a quantum theory, which includes quantum corrections, by using the *effective action* formalism, see Ref. [11].

Consider a classical theory of N scalar fields, $\phi^i(x)$, $(i = 1, \ldots, N)$, with Lagrangian

$$\mathcal{L}(\phi) = \mathcal{L}_{kin}(\phi) - V(\phi). \tag{B.1}$$

Assume that ϕ_0^i minimizes the potential, V, so that

$$\frac{\partial}{\partial \phi^i} V \Big|_{\phi^i(x)=\phi_0^i} = 0. \tag{B.2}$$

By expanding V around ϕ_0^i one can identify the mass matrix, m_{ij}^2,

$$V(\phi) = V(\phi_0) + \frac{1}{2}(\phi - \phi_0)^i (\phi - \phi_0)^j \frac{\partial^2}{\partial \phi^i \partial \phi^j} V \Big|_{\phi_0^i} + ... \tag{B.3}$$

which is

$$m_{ij}^2 = \frac{\partial^2}{\partial \phi^i \partial \phi^j} V \Big|_{\phi_0^i}. \tag{B.4}$$

Since the partial derivatives commute (for reasonable potentials) the mass matrix is symmetric, whose eigenvalues are the masses of the fields. We also know that the eigenvalues cannot be negative, since we assume that ϕ_0^i is a minimum.

Since $\mathcal{L}_{\text{kin}}$ vanish for constant fields, $V(\phi)$ must be invariant if $\mathcal{L}$ is invariant. Consider constant fields ϕ^i and take some group element

$$g(\alpha) = \exp(i\alpha^a T_{ij}^a) \in G, \tag{B.5}$$

where α^a are parameters and T^a are the generators of G. Invariance of the potential under the group G is the condition $V(g\phi) = V(\phi)$, for all ϕ and g. This means in particular that if we differentiate both sides w.r.t. α^a, we get

$$\frac{d}{d\alpha^a} V(g(\alpha)\phi) = 0 \implies \frac{\partial V}{\partial \phi^i} i T^a_{ij} \phi^j = 0 \tag{B.6}$$

Now, take a derivative of the above expression with respect to ϕ^j

$$\frac{\partial^2 V}{\partial \phi^j \partial \phi^i} T^a_{ij} \phi^i + \frac{\partial V}{\partial \phi^i} T^a_{ij} = 0. \tag{B.7}$$

Evaluating this at $\phi^i = \phi^i_0$ and using that ϕ^i_0 is a minimum gives

$$\frac{\partial^2 V}{\partial \phi^j \partial \phi^i} T^a_{ij} \phi^i_0 = 0 \iff m^2_{ij} T^a_{ij} \phi^j_0 = 0 \tag{B.8}$$

Now, for the broken generators not leaving the vacuum invariant, i.e. $\{\hat{T}^a \mid \hat{T}^a_{ij}\phi^j_0 \neq 0\}$, there must exist a zero eigenvalue in m^2_{ij} since it has to annihilate a non-zero vector $T^a_{ij}\phi^j$.

C

Extra Figures

C.1 Neutron-Proton Phase Shifts in MWPC

Fig. C.1 shows the cutoff dependence of LECs, which is the same as Fig. 5.4 but for a larger variety of cutoffs.

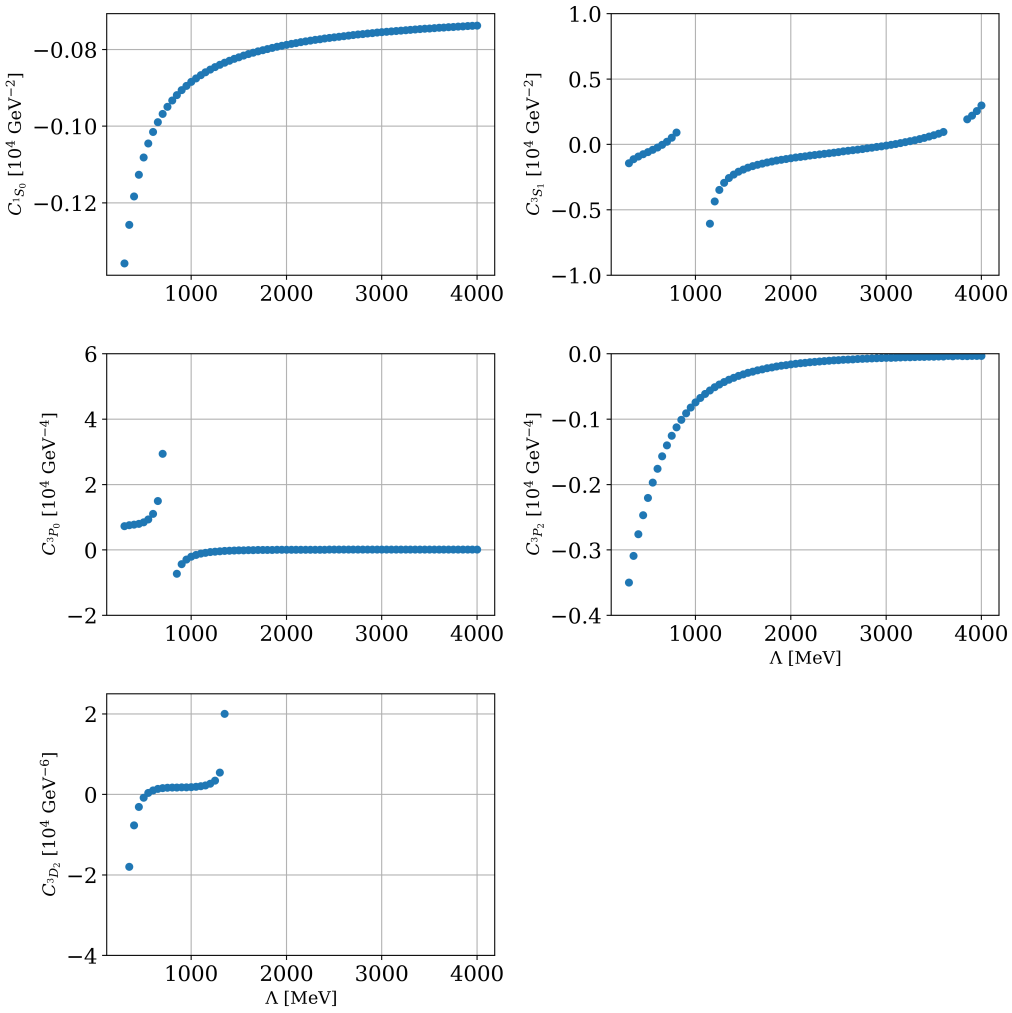

Figure C.1: This figure shows the cutoff dependence of LECs. The regions where no dots appear, the algorithm for finding the optimal LEC does not converge.

C.2 Bayesian Inference of LECs

Some extra figures that show the posterior pdf for the LECs are shown here. These figures are obtained in exactly the same was as Fig. 6.2, but for varying cutoff. Figs. C.2, C.3 and C.4 show the posterior pdf for $\Lambda = 350$ MeV, $\Lambda = 550$ MeV and $\Lambda = 650$ MeV, respectively.

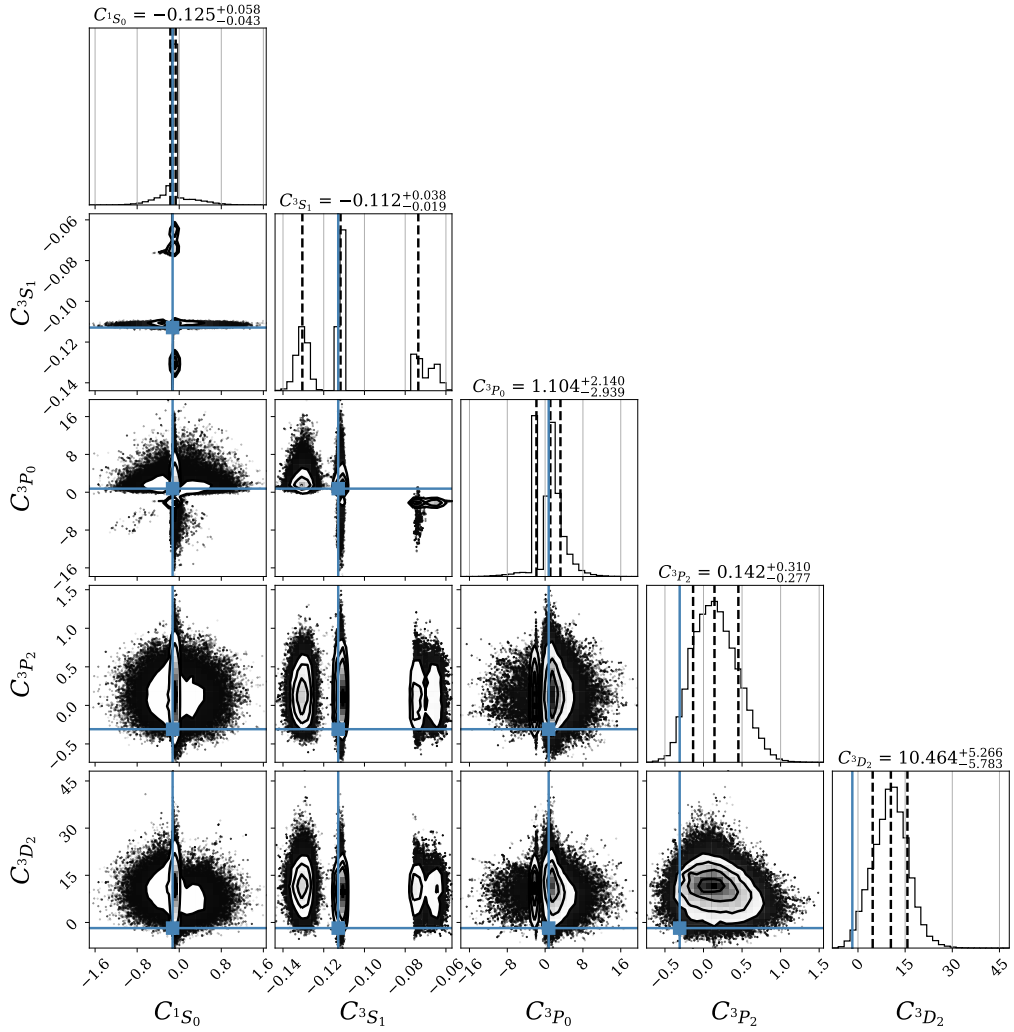

Figure C.2: Corner plot [57] of the joint posterior pdf for the LECs. The units are as in Eq. (5.3) and $\Lambda = 350$ MeV. The blue square indicates the LEC values fitted to the phase shifts in Chapter 5, as also shown in Table 5.2. The dashed black lines indicate the median and 68 % DoB regions for each individual LEC, even though they are not that informative due to a high degree of multi-modality.

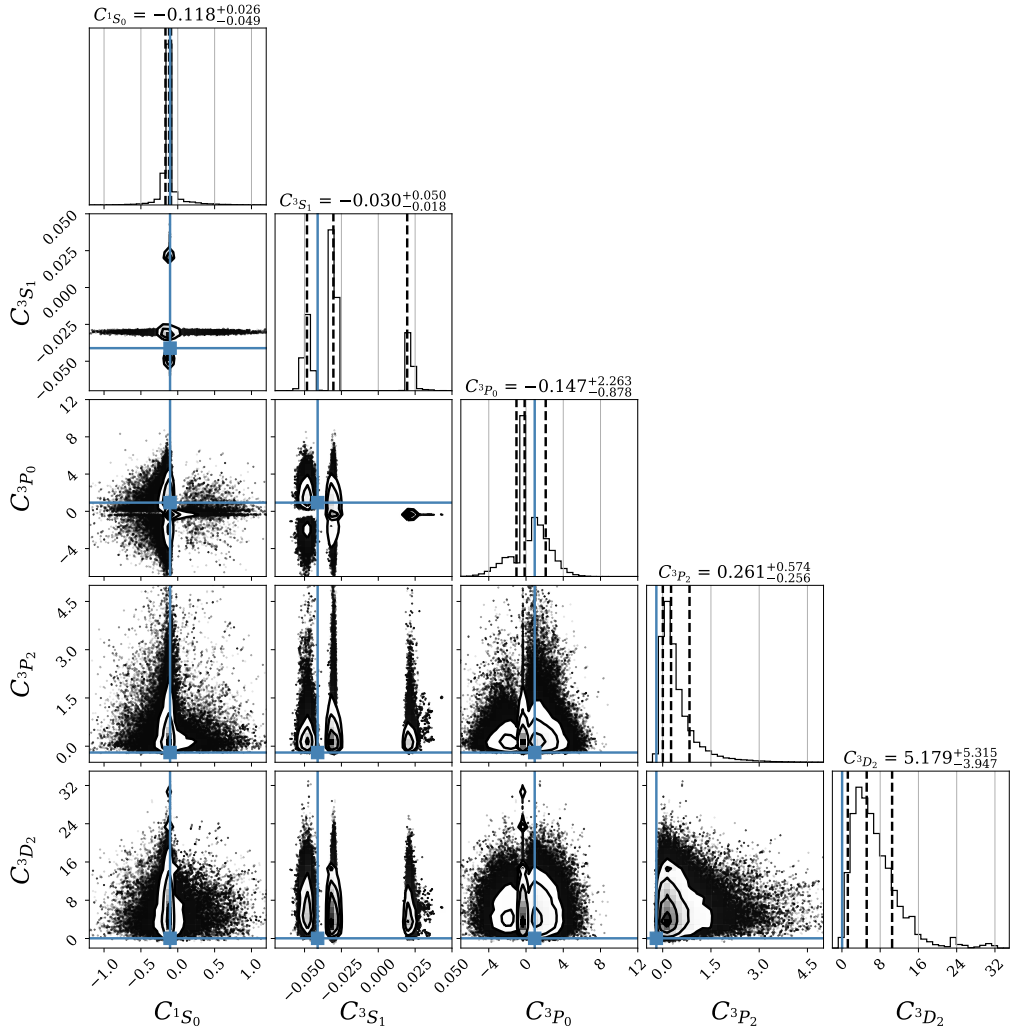

Figure C.3: Same pdf as in Fig. C.2 but with the cutoff $\Lambda = 550$ MeV.

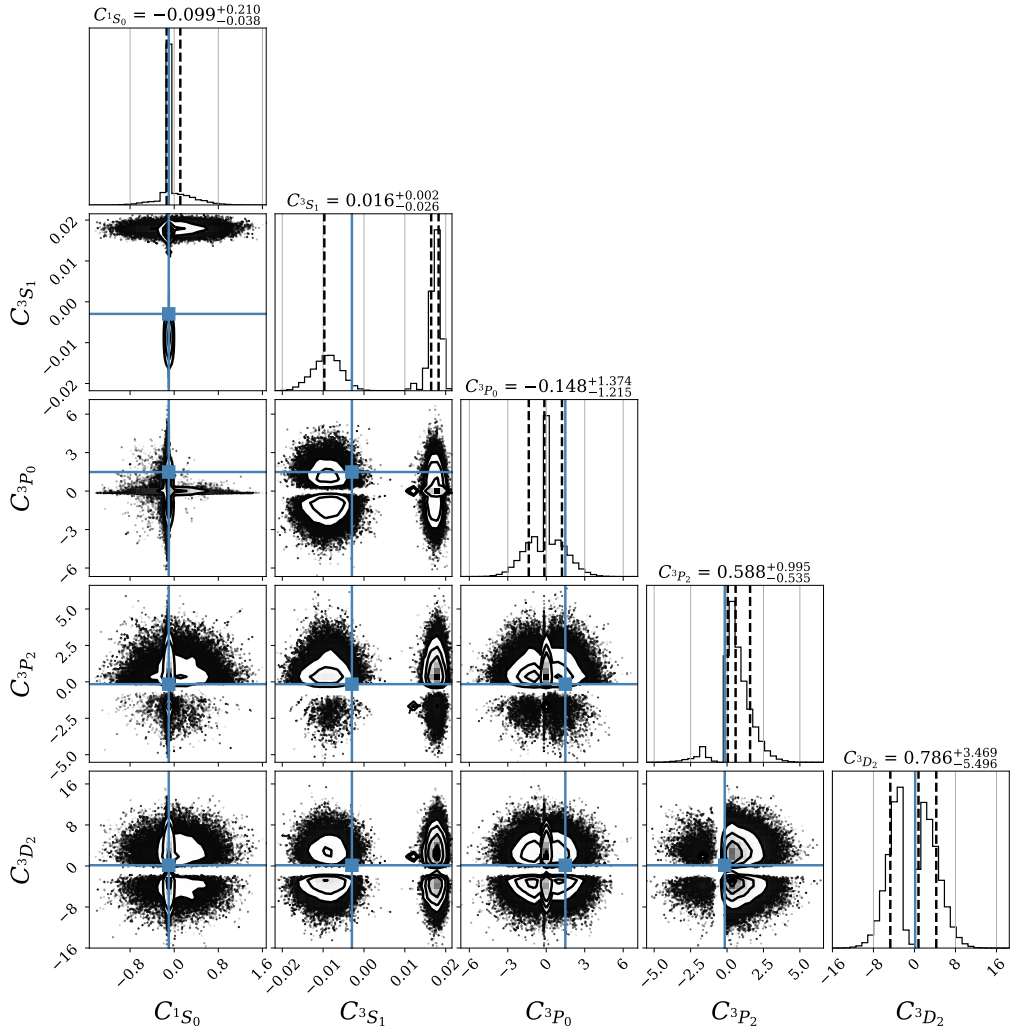

Figure C.4: Same pdf as in Fig. C.2 but with the cutoff $\Lambda = 650$ MeV.

DEPARTMENT OF PHYSICS
CHALMERS UNIVERSITY OF TECHNOLOGY
Gothenburg, Sweden 2021
www.chalmers.se

CHALMERS
UNIVERSITY OF TECHNOLOGY